THESIS APPROVAL

The abstract and thesis of Robin Rachelle Johnston for the Master of Science in Geology presented February 12, 2004, and accepted by the thesis committee and the department.

COMMITTEE APPROVALS: ______________________________

Andrew G. Fountain, Chair

____

Christina L. Hulbe

____

Martin J. Streck

____

Aslam Khalil
Representative of the Office of Graduate Studies

DEPARTMENTAL APPROVAL: ______________________________

Michael L. Cummings, Chair
Department of Geology

ABSTRACT

An abstract of the thesis of Robin Rachelle Johnston for the Master of Science in Geology presented February 12, 2004

Title: Channel Morphology and Surface Energy Balance on Taylor Glacier, Taylor Valley, Antarctica

Deeply-incised channels on Taylor Glacier in Taylor Valley, Antarctica initiate as medial moraines traced tens of kilometers up-glacier, are aligned with the direction of flow, and at their most developed occupy about 40% of the ablation zone in the lower reaches of the glacier. Development of the South Channel occurs in three stages. The first stage, the *1st Steady State*, is characterized by rather uniform development, where the channel widens at much less than 0.1 m yr^{-1} and deepens at much less than 0.01 m yr^{-1}, maintaining a width to depth ratio of about 8. The second stage, the *Transition Phase*, is characterized by dramatic widening channel (from 10 to 110 m) and deepening (from 2 to 24 m). During this stage, the peak rate of widening is about 1.5 m yr^{-1} and the channel is about 25 times as wide as it is deep. The third stage of channel development, the *2nd Steady State*, is characterized by a steady decrease in the rate of channel deepening and a leveling off of the width to depth ratio as the channel ceases to

widen. Eventually, the channel reaches a new near equilibrium state of continued uniform development where the width to depth ratio is about 4.

The microclimate within the channels differs significantly from conditions on the adjacent glacier surface. The channels are warmer by 1.7°C, have wind speeds reduced by 2.4 m s^{-1}, and the net shortwave radiation is greater by about 14 W m^{-2} compared to the glacier surface. As a result, melt makes up a much higher percentage of the total ablation within the channels than it does on the glacier surface – as much as 75% and perhaps up to 99% under extremely low wind regimes, compared to about 45%. While the altered microclimate within the channels drives their rapid development during the *Transition Phase*, the relationship between average wall slopes and solar angles may represent the channels coming into equilibrium with the solar regime in the valley.

CHANNEL MORPHOLOGY AND SURFACE ENERGY BALANCE ON TAYLOR GLACIER, TAYLOR VALLEY, ANTARCTICA

by

ROBIN RACHELLE JOHNSTON

A thesis submitted in partial fulfillment of the
requirements for the degree of

MASTER OF SCIENCE
in
GEOLOGY

Portland State University
2004

DEDICATION

Dedicated with enormous gratitude to my dear sister and friend, Kim Kathline Johnston - who teaches much to many - for her extraordinary love and untiring support throughout time. Sis, thank you for taking this journey with me. A grand journey it has been, shaped and colored by a multitude of nobulets and rainwedges. May we forever be able to recognize them in our world, and may they be abundant.

I love you so much.

ACKNOWLEDGEMENTS

I owe much thanks to many people: my advisor, Andrew Fountain, for making my graduate studies so interesting; my committee members, Christina Hulbe, Martin Streck, and Aslam Khalil, for their insight; Thomas Nylen, for being a great field partner and office mate; and the entire staff of the Geology Department, all of whom strive for excellence. There are others to thank as well: Karen Lewis, for sharing her knowledge; Jennifer Horsman and Chris Jaros, for their efforts to provide me with aerial photographs of Taylor Valley; Rae Spain for her superb operations of Lake Hoare Camp and her friendship; Kathy Welsh, for making being at McMurdo all the more interesting; the operation controllers and pilots at McMurdo HeloOps; and Jeff Scanniello, Chuck Kurnik, Dennis Kenley, Forrest McCarthy, Bill McCormick, and many others who helped with field support in Taylor Valley.

There isn't enough thanks in the world for the friendship and support of William Schryver, the man of a thousand pertinent questions. To my good friends Michelle Cunico-Johnson, Julie Griswold, Meg Lunney, Christina Hulbe, and Nancy Erikkson – I do, and shall, miss sharing time with you daily. I've made many other friends along the way for whom I'm grateful. I send special thanks to Murphy Johnston for his fuzzy, warm companionship. And thank you Kim, for everything.

The National Science Foundation (NSF) provided funding for this work as part of the NSF Long-Term Ecological Research (LTER) program through grant number OPP-9810219. It was my good fortunate to be involved in this incredible project.

Table of Contents

List of Figures

List of Tables

1 INTRODUCTION

The National Science Foundation (NSF) established the Long-Term Ecological Research (LTER) network in 1980 to improve understanding of the basic properties of Earth's ecosystems and the factors causing changes in these systems through long-term field studies (LTER, 2001). The twenty-four sites in the network include diverse ecosystems such as rainforests, cold deserts, marine ecosystems, and urban landscapes. Twenty-one sites are located in the United States, one in Puerto Rico, and two in Antarctica (LTER, 2001). Of these two, the Palmer Station site on the Antarctic Peninsula focuses on polar marine ecosystems and the McMurdo Dry Valleys (MCM-LTER) site near the Ross Sea focuses on a polar desert ecosystem The work presented here was conducted in the MCM-LTER.

The McMurdo Dry Valleys (MCM) (~ 77° 30' S, 162° E) cover roughly 4800 km^2 and are the largest relatively ice-free regions of Antarctica (Figure 1.1), about 4% of the continent (Drewry et al., 1982). The three main valleys that comprise the heart of the region are Victoria, Wright, and Taylor valleys. They are generally northeast-southwest trending valleys of exposed bedrock, sand, and debris with minor soil development, and are flanked by mountains up to 2200 meters (m) in elevation. Polar alpine glaciers descend from the mountains, and outlet glaciers flow into the valleys from the East Antarctic Ice Sheet. Perennially ice-covered lakes exist at all three valley floors: Lake Vida in Victoria Valley, Lake Vanda in Wright Valley, and lakes Fryxell, Hoare, and Bonney in Taylor Valley.

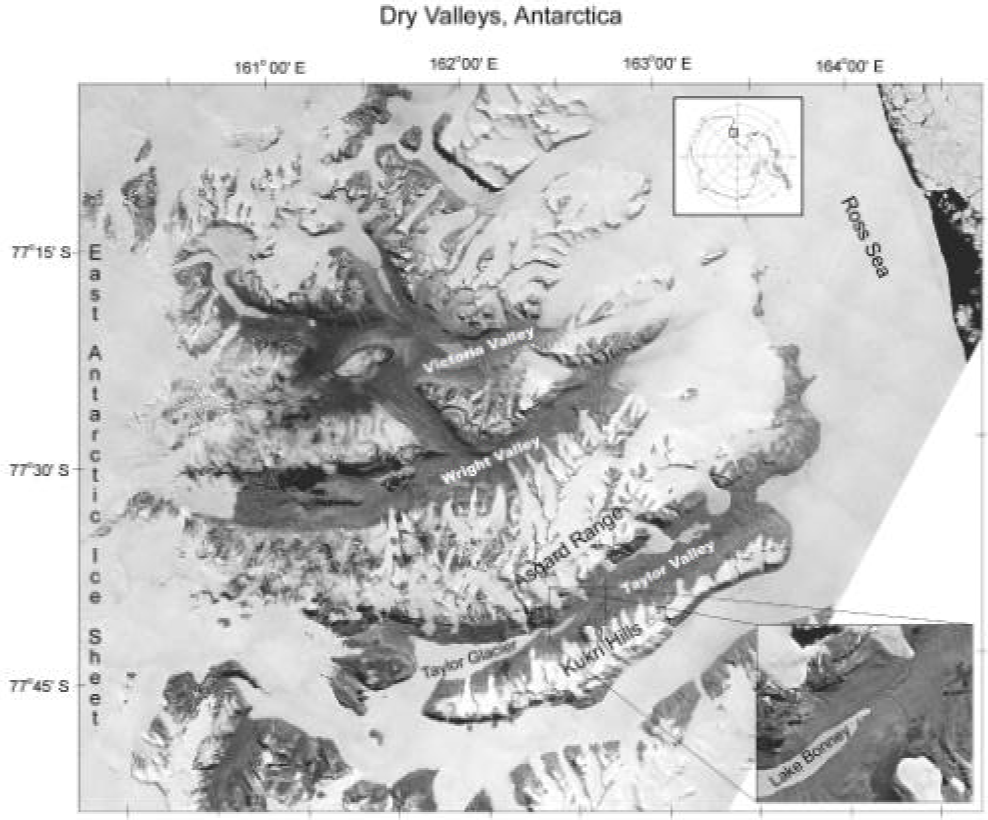

Figure 1.1 – Satellite image of the McMurdo Dry Valleys (NSF, 1999). Upper inset shows location of larger image.

The MCM-LTER site is considered an end-member site, in that it is the coldest and driest site within the LTER network, and life at the MCM site approaches its environmental limits (NSF, 1999). Life in the valleys consists of microorganisms, lichens, and mosses that inhabit the rocks and lakes. No higher plants or animals exist in the valleys. In fact, the top predator is the nematode, a microscopic worm-like creature that inhabits the soil (Freckman and Virginia, 1998). The delicate balance between the availability of liquid water and biologic productivity make dry valley ecosystems sensitive indicators of global environmental change (Doran, 2002).

The main objective of the MCM-LTER is to define physical controls on the structure and function of valley ecosystems. The project is a collaboration between Ohio State University, the University of Colorado, Montana State University, Colorado State University, Dartmouth College, and Portland State University. Portland State University's role in the MCM-LTER is to define the controls on glacial meltwater production in the valleys. The hydrologic regime in the McMurdo Dry Valleys of Antarctica largely controls the distribution of life in this polar desert (Moorhead and Priscu, 1998) and because precipitation in the valleys is severely limited (Keys, 1980), glacial melt is the primary hydrologic variable.

I believe that channels on Taylor Glacier, unlike stream channels on ice-free terrain and most glacier surfaces, do not merely route water generated elsewhere, but actually produce the water they carry. Meltwater reaching Lake Bonney - the proglacial lake at the terminus of Taylor Glacier - is measured at gauging stations on streams feeding the lake. However, deeply incised channels in the lower ablation zone of Taylor Glacier (Figure 1.2) discharge directly to Lake Bonney, and the water within

Figure 1.2 -Aerial view looking up-glacier at the channels on Taylor Glacier. The vertical terminus cliff in the foreground is ~ 20 m high.

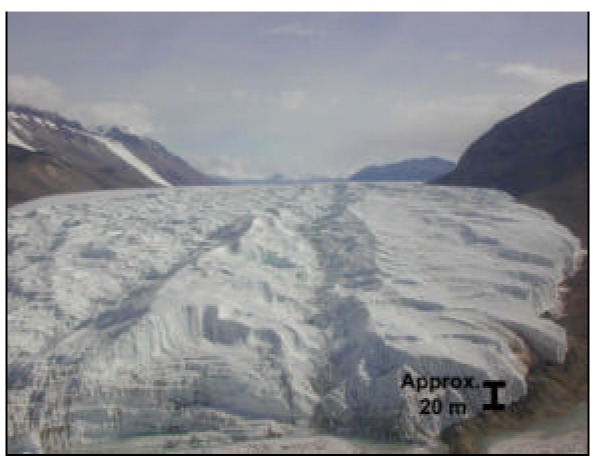

these channels is not monitored. Knowledge of how these channels form, and the processes that govern their morphology, is essential to understanding water flow from this glacier, and of other polar glaciers with similar surface morphologies.

The aims of the thesis are to characterize channel geometry, determine the rate of channel development, model the surface energy balance to differentiate between melt and sublimation within the channels, and to estimate the direct run-off from Taylor Glacier to Lake Bonney. I hypothesize that as the glacier surface flows to lower elevations, and therefore to warmer air temperatures, the shallow channels rapidly enlarge due to a microclimate in the channels. To test my hypothesis, I work through a set of objectives: examining large-scale surface features on glaciers in Taylor Valley in an effort to place the channels on Taylor Glacier into context (Chapter 2); measuring channel morphology to determine geometric changes of the channels and their rate of development, as well as measuring meteorological differences between surface and channel bottom (Chapter 3); and evaluating ablation differences between the surface by calculating the energy balance for each setting using the meteorological measurements (Chapter 4). Results of this work are important to understanding the spatial variability of meltwater production and the hydrologic cycle in the valleys.

1.1 Geographic Setting

Taylor Valley is the main study site of the MCM-LTER project. The climate in Taylor Valley is that of a polar desert – cold, windy, and dry. The mean annual air temperature and wind speed are -17.8°C and 3.4 m s^{-1}, respectively, and the mean annual relative humidity is 64% (Doran, 2002). The average annual precipitation at the valley bottom, occurring as snow, is <10 cm water equivalent (Keys, 1980); (Bromley, 1985). The valley is ~ 35 km long from the edge of McMurdo Sound in the east to the terminus of Taylor Glacier, which is the outlet glacier flowing into the valley from the East Antarctic Ice Sheet in the west (Figure 1.1). The valley is flanked to the north by the Asgard Range and to the south by the Kukri Hills. Maximum elevation in these mountains is ~ 2200 m. Numerous alpine glaciers originate in the mountains but only the largest reach the valley floor (Figure 1.3).

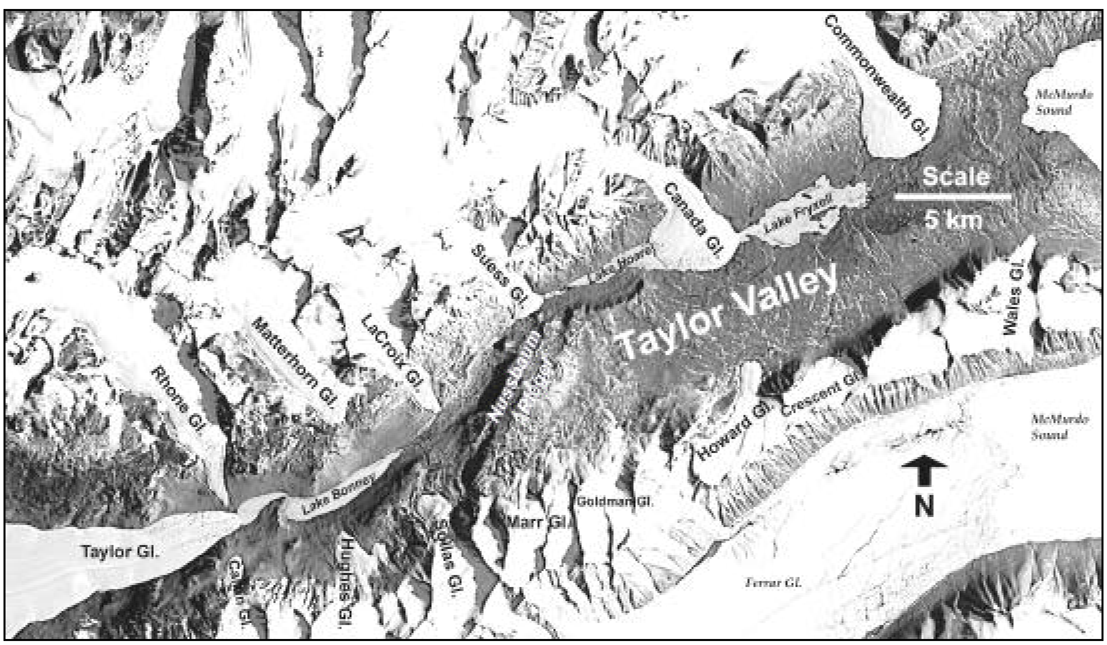

Figure 1.3 - Glaciers and lakes in Taylor Valley.

1.2 Glacial Characteristics

The glaciers of the McMurdo Dry Valleys are polar glaciers, or “cold” glaciers – the ice is cooler than its pressure-dependent melt temperature throughout its mass. This contrasts with temperate glaciers, where the entire ice mass warms to the melt temperature at some time during the year. The thermal regime is important. Polar glaciers are frozen to the substrate and flow only through internal deformation. The result is very slow ice flow, generally two orders of magnitude slower than in temperate settings. Without basal meltwater, basal erosion and valley modification are also slow.

The annual mass balance of a glacier is reflected in the equilibrium line altitude (ELA) – the elevation on a glacier between the accumulation zone (zone of net mass gain) and the ablation zone (zone of net mass loss) – and the ELA is a reflection of the local climate. Spatial variation in the climate of Taylor Valley is reflected in ELA and snowfall trends in the valley (Fountain et al., 1999b). The average ELA for glaciers in the valley, from the coast to 15 km inland, is about 450 m. From about 20 to 35 km inland the average ELA is about 1150 m. Therefore, the average ELA rises about 700 m over a distance of about 5 km. The shift in the ELA may in part be controlled by the Nussbaum Riegel, which bisects the valley at about 20 km inland (Fountain et al., 1999b) (Figure 1.4). The Nussbaum Riegel may act to contain coastal winds to the down-valley side of the riegel and continental katabatic winds to the up-valley side of the riegel. Additionally, snow depth decreases with distance inland (Figure 1.4); thus, the riegel may suppress precipitation-bearing air masses from reaching the up-valley regions. Therefore, glacier distribution throughout the valley is a result of this spatial change in climate and topographic constraints.

Ablation is mass loss in all its forms. In the dry valleys, sublimation accounts for 40-80%, melt for 20-60%, and calving for less than 5% of mass loss (Fountain et al., 1998; Lewis et al., 1998). We measure the annual mass exchange on glaciers using a network of poles called ablation stakes drilled into the glacier. Mass accumulation is reflected as stakes become shorter (buried) with time. Ablation is reflected in the lengthening of the stakes as ice is lost at the surface. Mass balance studies on glaciers in the dry valleys indicate that the accumulation zone gains about 10-30 cm of snow and the ablation zone loses of about 6-15 cm of ice annually (Fountain et al., 1998). These rates are similar to those measured by Chinn on Wright Glacier in Wright Valley (1980).

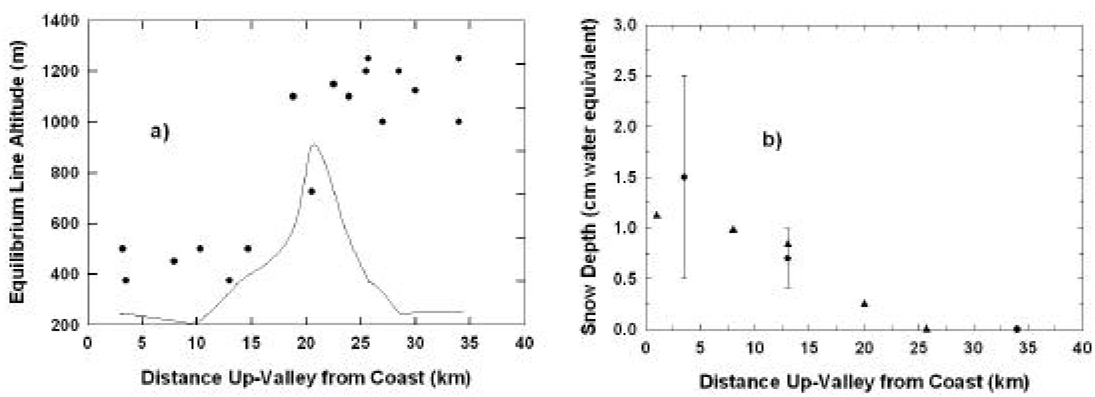

Figure 1.4 – a) Glacier ELA with increasing distance from the coast in Taylor Valley. The black dots are the ELA's on different glaciers in the valley and the solid black line is the mid-valley altitude profile showing the location and elevation of the Nussbaum Riegel (Fountain et al., 1999a). b) Snow depth with distance from the coast in Taylor Valley. Triangles are snow depth on the valley floor after a snowfall in January 1997. Circles are snow accumulation on 3 glaciers from Nov. 1996 to Jan. 1997 between 200 and 300 m elevation, with bars representing the range of snow depths within the elevation range on the glaciers (Fountain et al., 1999a).

The terminal walls of the glaciers in the dry valleys tend to be ~ 20 m high and nearly vertical. Several processes produce this geometry (Fountain et al., 1998): ice advection exceeding ablation in advancing glaciers, faster ice flow at the upper surface than at the base, and the low sun angle, which leads to an increase in ablation rates on vertical walls compared to the horizontal surfaces.

1.3 Glacial History

Glaciers have existed in Taylor Valley for at least the last 3.5 million years (Hall et al., 1993; Wilch et al., 1993) with variations in climate controlling their extent. Taylor Valley is affected by the behavior of both the East Antarctic Ice Sheet, which discharges into the head of the valley, and the Ross Ice Shelf, at the downstream end of the valley (Denton et al., 1989; Hall et al., 1993; and Hendy et al., 1979). Expansion of the East Antarctic Ice Sheet (EAIS) ~100,000 years ago resulted in the advance of Taylor Glacier down-valley to Lake Fryxell (Figure 1.3). By ~ 70,000 years ago, Taylor Glacier retreated to its present location in the valley. Between 40,000 and 7,000 years ago, the Ross Ice Shelf entered Taylor Valley multiple times, which resulted in the formation of Lake Washburn – a lake that once filled the valley up to 300 m in elevation (Denton et al., 1989). This lake drained with the last retreat of the Ross Ice Shelf ~ 7,000 years ago. The three main present-day lakes in Taylor Valley – lakes Bonney, Hoare, and Fryxell – are remnants of Lake Washburn. The last retreat of the ice shelf left a moraine that now blocks stream flow from the valleys into McMurdo Sound, creating the enclosed Lake Fryxell. The alpine glaciers are relatively stable features and have retained their approximate positions since the Pliocene (Hall et al., 1993; Wilch et al., 1993).

2 SURFACE FEATURES AND DEBRIS DISTRIBUTION ON GLACIERS IN TAYLOR VALLEY

2.1 Surface Features

Several surface morphologies exist on the glaciers in Taylor Valley. Surface morphology is determined by both the flow of the glacier over its bed and by surface processes. Some regions of the glacier surfaces are relatively smooth (Figure 2.1, a).

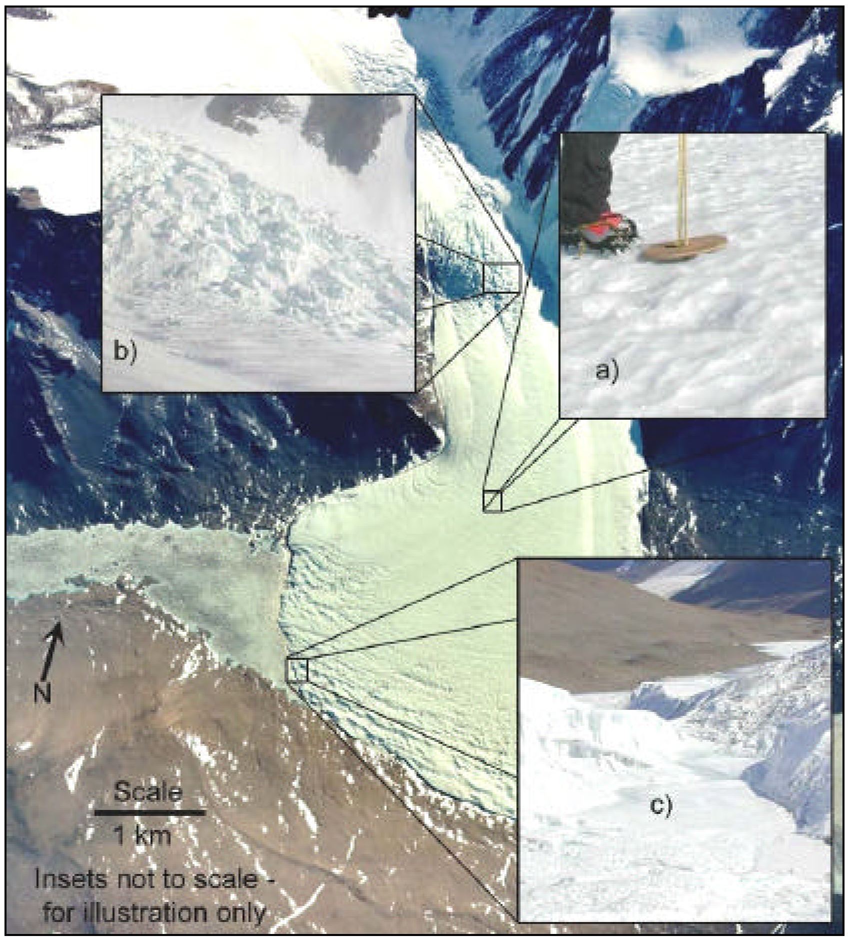

Figure 2.1 – Examples of some glacier surface features, using Canada Glacier as an example. Insets are for illustration only and not to scale – a) relatively smooth region such as the *Non-descript* classification, b) topographically controlled ice falls such as the *Topo* classification, and c) a 10's of meters wide channel-like feature such as the *Aligned* or *Transverse* classification.

Other features such as crevasses, ogives, and icefalls are, in part, topographically controlled (Figure 2.1, b). Still other features are channel-like (Figure 2.1, c), and oriented either transverse or parallel to the direction of ice flow. The topographically controlled and the channel-like features are clearly evident in aerial photographs. I analyzed the glacial surfaces in Taylor Valley using LTER aerial photographs of 600 dots per inch resolution and 1:20,000 scale, taken at an altitude of roughly 4500 m above sea level (LTER, 2001). The photographs were examined in Adobe Photoshop, and the patterns of surface roughness were classified based on surface texture and orientation relative to ice flow. Figures 2.2 – 2.15 show the individual valley glaciers overlain with the classification system. I classified five surface types:

1) *Aligned* – These are features oriented parallel to ice flow direction. Aligned features can be either long, incised channel-like features (as on Taylor Glacier, Figure 2.2), or they may appear simply as linear discolorations on the glacier surface without having any distinctive surface morphology, such as on Commonwealth (Figure 2.3), Sollas (Figure 2.4), and Howard (Figure 2.5) glaciers.

2) *Transverse* – These are channel-like features oriented transverse to the ice flow direction. The southwest corner of Canada Glacier (Figure 2.6) is the best example of such a feature. The only other glacier in the valley that exhibits this feature is a small section of the central terminus of Suess Glacier (Figure 2.7).

3) *Mottled* – These features look like blotchy patches on the glacier surface. They do not exhibit any particular relationship to flow direction and are common to nearly all glaciers. They can either be relatively smooth surfaces, such as Hughes

(Figure 2.8) and Sollas (Figure 2.4) glaciers, or can exhibit minor surface roughness, such as portions of Suess Glacier (Figure 2.7).

4) *Topo* – These are icefalls, ogives, and crevasses. Icefalls occur when ice flows rapidly over steep region of the bedrock, resulting in extreme longitudinal extension and fracture (Benn and Evans, 1998). In general, crevasses propagate in the direction of the least comprehensive principal stress (Meier, 1960; Nye, 1952). Ogives (convex downflow arcuate bands or waves) generally form down-glacier of icefalls (Nye, 1958; Waddington, 1986). Good examples of this surface feature are seen on Suess (Figure 2.7), LaCroix (Figure 2.9), and Rhone (Figure 2.10) glaciers.

5) *Non-descript* – This category contains any remaining surface area, where no specific features are present. This classification dominates Calkin (Figure 2.11), Marr (Figure 2.12), Goldman (Figure 2.13), Crescent (Figure 2.14), and Wales (Figure 2.15) glaciers. This surface type is, in essence, a special case of the *Topo* classification, in which the subglacial topography is relatively smooth.

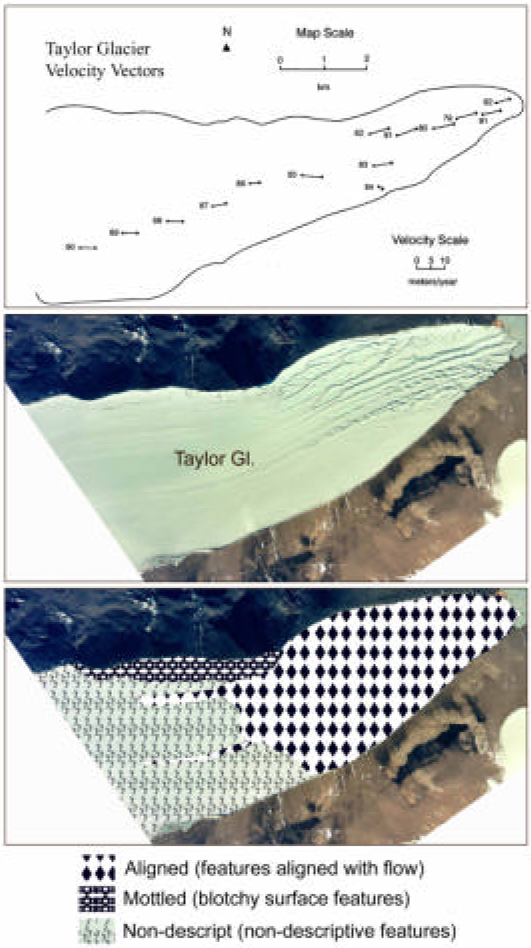

Figure 2.2 - Surface classification and flow vectors for Taylor Glacier. Ice flow vectors supplied by Karen Lewis through the MCM-LTER.

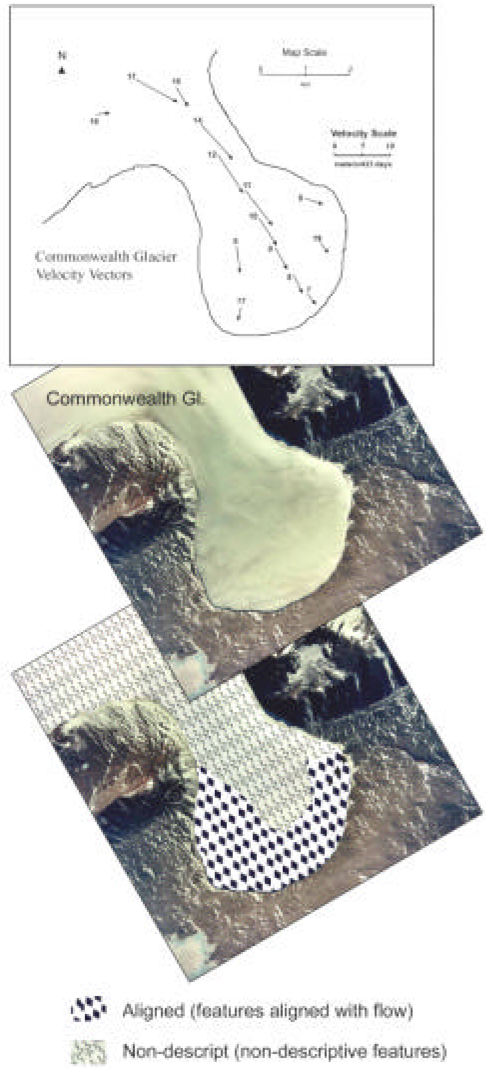

Figure 2.3 - Surface classification and flow vectors for Commonwealth Glacier. Ice flow vectors supplied by Karen Lewis through the MCM-LTER.

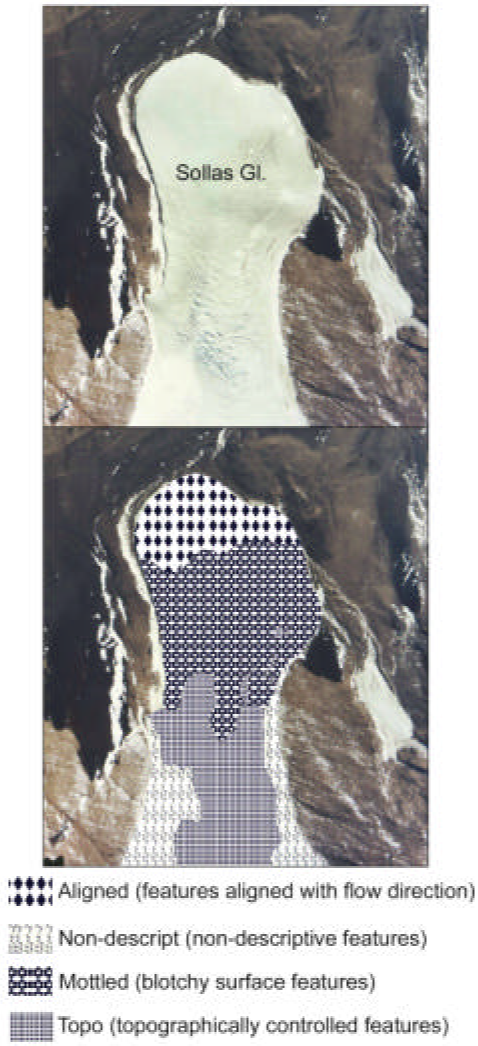

Figure 2.4 - Surface classification for Sollas Glacier.

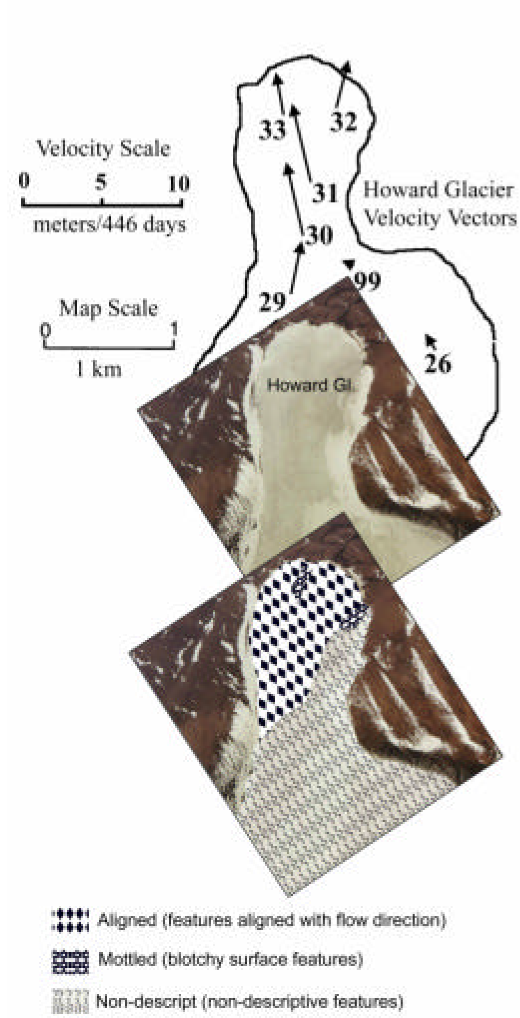

Figure 2.5 - Surface classification and flow vectors for Howard Glacier. Ice flow vectors supplied by Karen Lewis through the MCM-LTER.

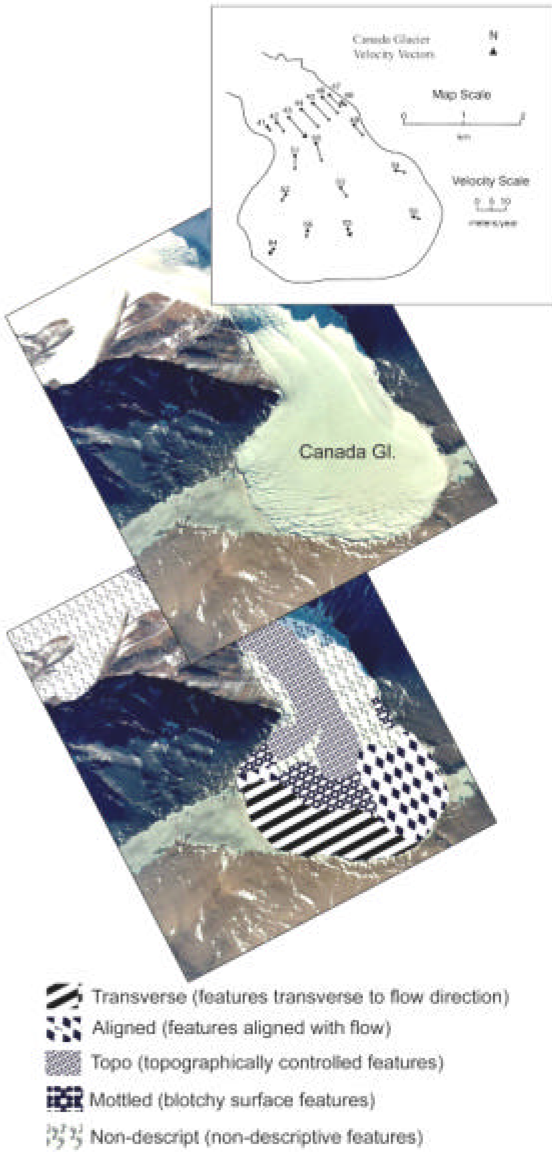

Figure 2.6 - Surface classification and flow vectors for Canada Glacier. Ice flow vectors supplied by Karen Lewis through the MCM-LTER.

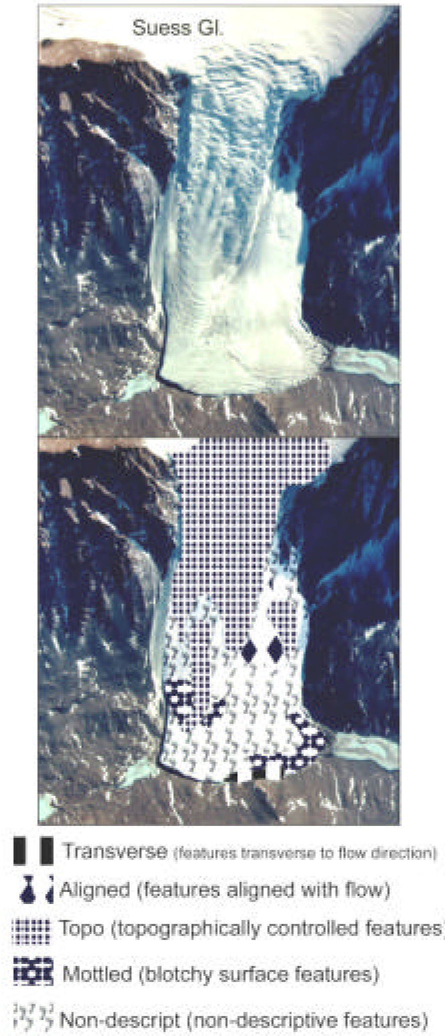

Figure 2.7 - Surface classification for Suess Glacier.

Figure 2.8 - Surface classification for Hughes Glacier.

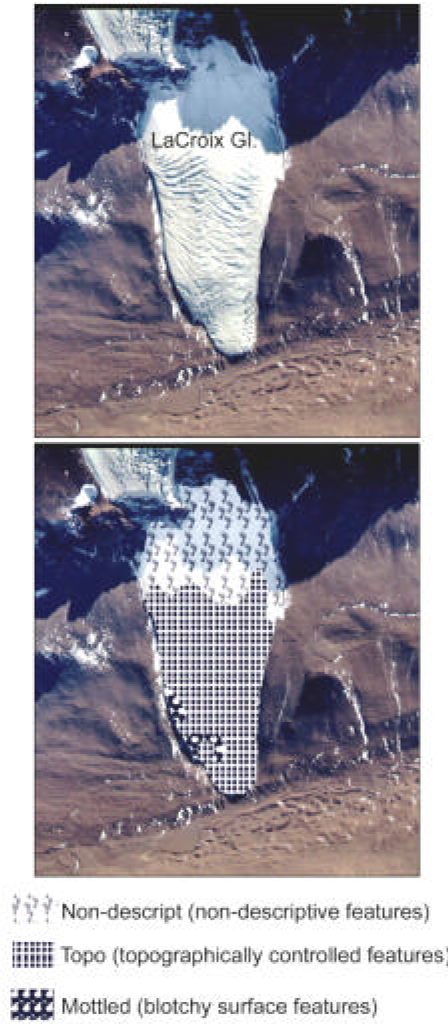

Figure 2.9 - Surface classification for LaCroix Glacier.

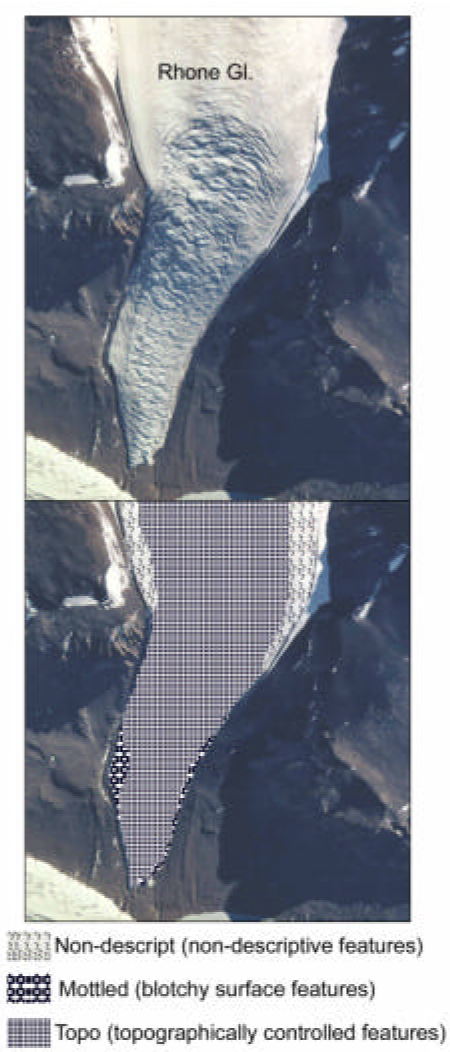

Figure 2.10 - Surface classification for Rhone Glacier.

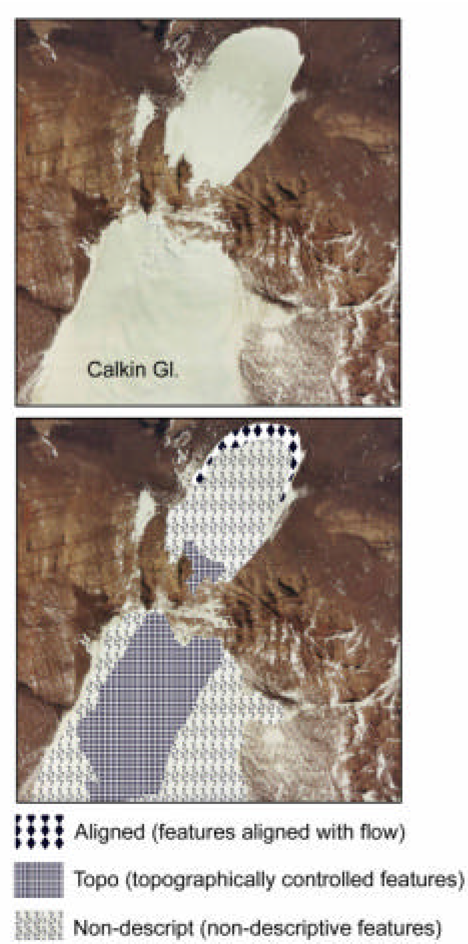

Figure 2.11 - Surface classification for Calkin Glacier.

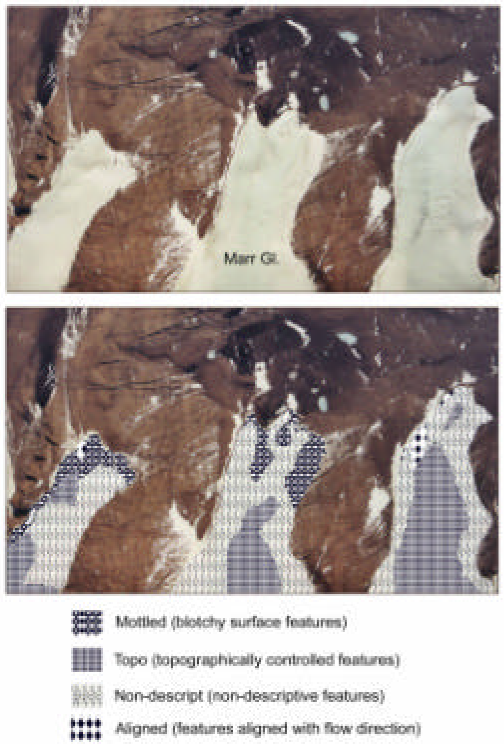

Figure 2.12 - Surface classification for Marr Glacier.

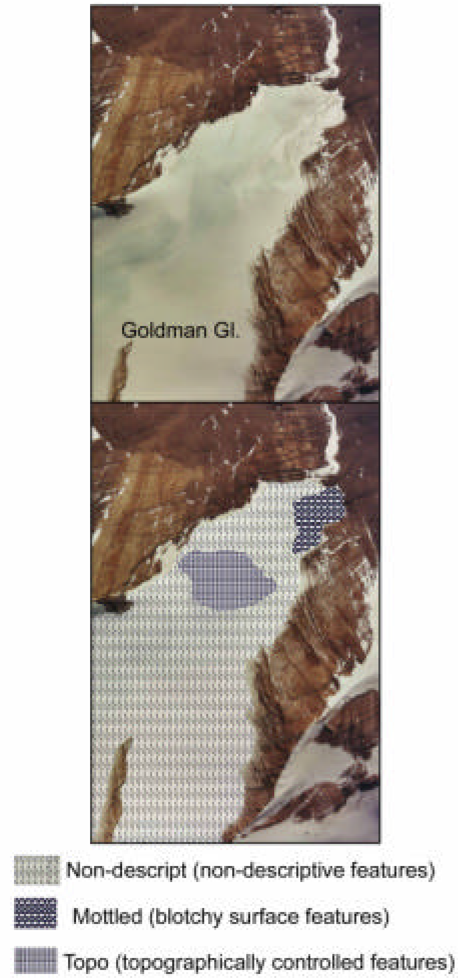

Figure 2.13 - Surface classification for Goldman Glacier.

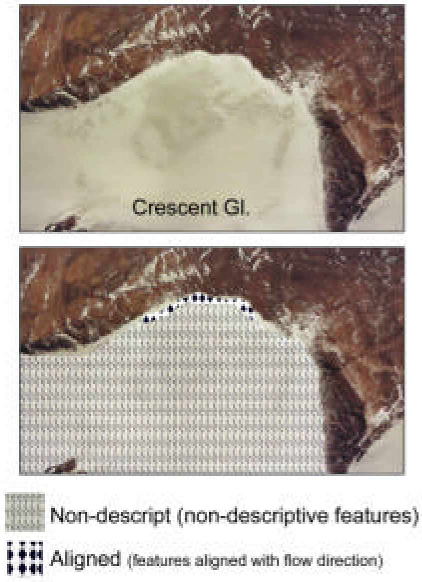

Figure 2.14 – Surface classification for Crescent Glacier.

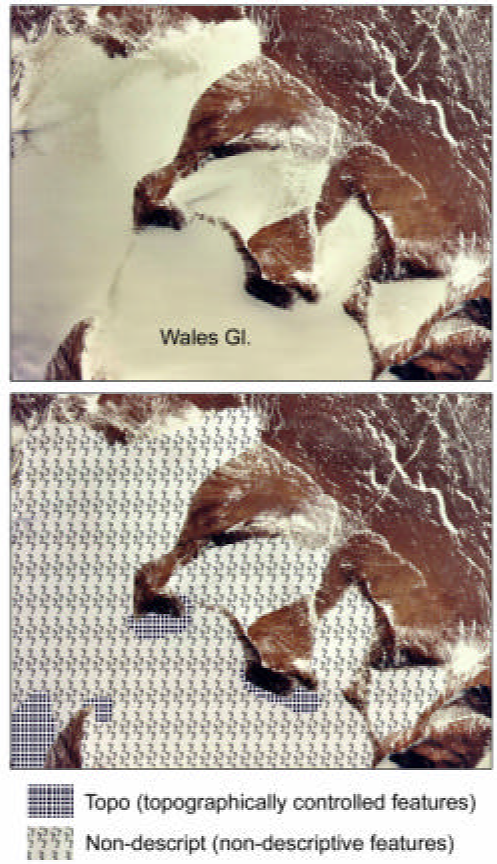

Figure 2.15 – Surface classification for Wales Glacier.

To see the valley-wide distribution of surface features, the pattern-coded images of the individual glaciers were draped over a satellite image of the valley (Figure 2.16). The *Topo* features are found in and down slope of steeply inclined topography (e.g., icefalls, ogives). This feature occurs on nearly all glaciers flowing from the mountain ranges flanking both sides of the valley. The *Mottled* and *Non-descript* features are found in regions of relatively low relief. While there are small areas of *Aligned* on regions of the glaciers in the upper reaches of the valley walls, the largest regions of *Aligned*, as well as *Transverse,* features are at or near the valley floor. While the *Topo, Mottled,* and *Non-descript* features are all interesting in their own right and worthy of discussion, it is the *Aligned* and *Transverse* classifications that are of particular interest to my project.

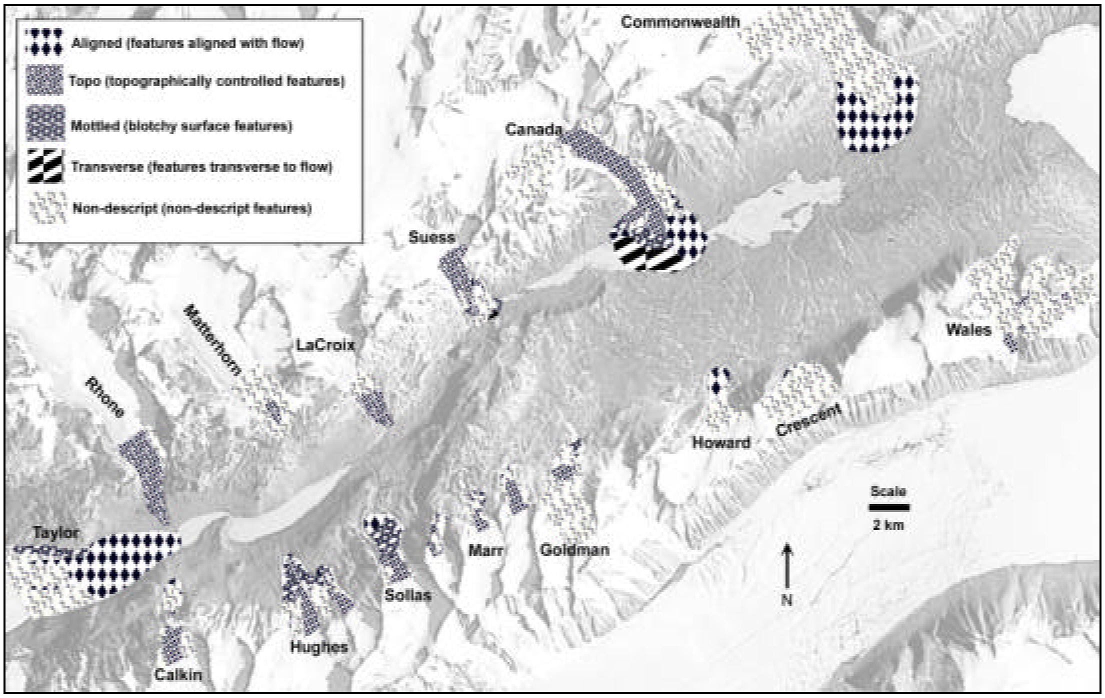

Figure 2.16 - Pattern-coded images of individual glaciers draped over the satellite image of Taylor Valley.

2.2 Aligned and Transverse Features

Commonwealth, Canada, and Taylor glaciers all exhibit large regions of *Aligned* features (Figure 2.16). There is also a large region of *Transverse* features on Canada Glacier and a smaller region of *Transverse* at the center terminus of Suess Glacier. The regions are all located in the lower elevations of the ablation zone. All of the *Transverse* regions, and the large *Aligned* regions on Taylor and Canada glaciers, have a distinct, deeply-incised morphology.

Aligned features are more defined on Canada than on Commonwealth Glacier, but these features are most well-defined on Taylor Glacier (Figures 2.17 – 2.19). The Taylor Glacier *Aligned* features are very distinct channel-like, and oriented with the direction of flow. The *Transverse* features on Canada Glacier (Figure 2.20), also distinct and channel-like, are oriented oblique to flow direction. By visual estimation, the deeply-incised *Aligned* or *Transverse* features cover about 40% of the lower ablation zone on Taylor Glacier, 30% on Canada Glacier, and 5% on Suess Glacier. Assuming that all melt originates in the ablation zone, and considering that ablation rates are higher on inclined walls than on horizontal surfaces (discussed in subsequent chapters), the occurrence of these deeply-incised features in the lower ablation zone may, cumulatively, play an important role in the generation and evacuation of meltwater from valley glaciers and thus in regional hydrology.

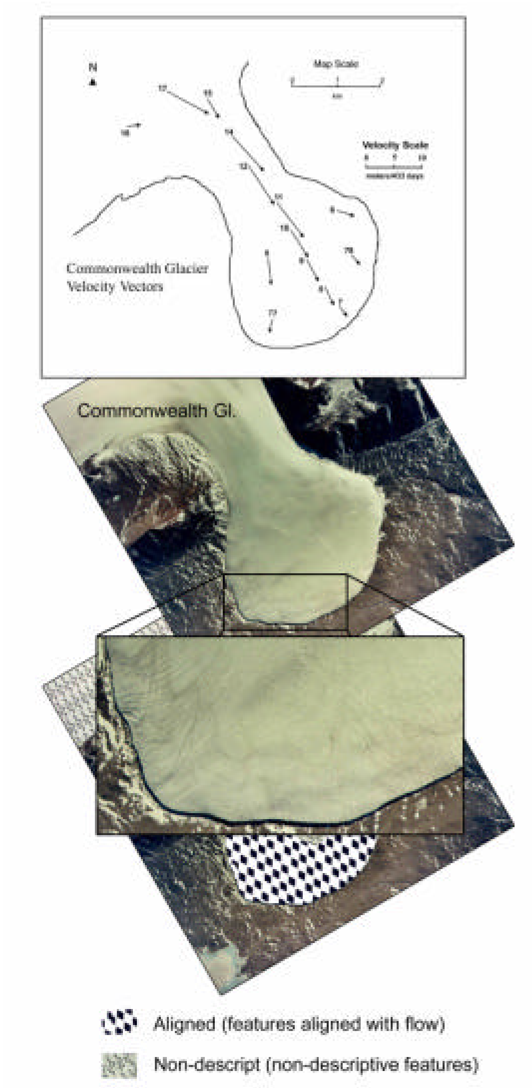

Figure 2.17 – The *Aligned* features of Commonwealth Glacier.

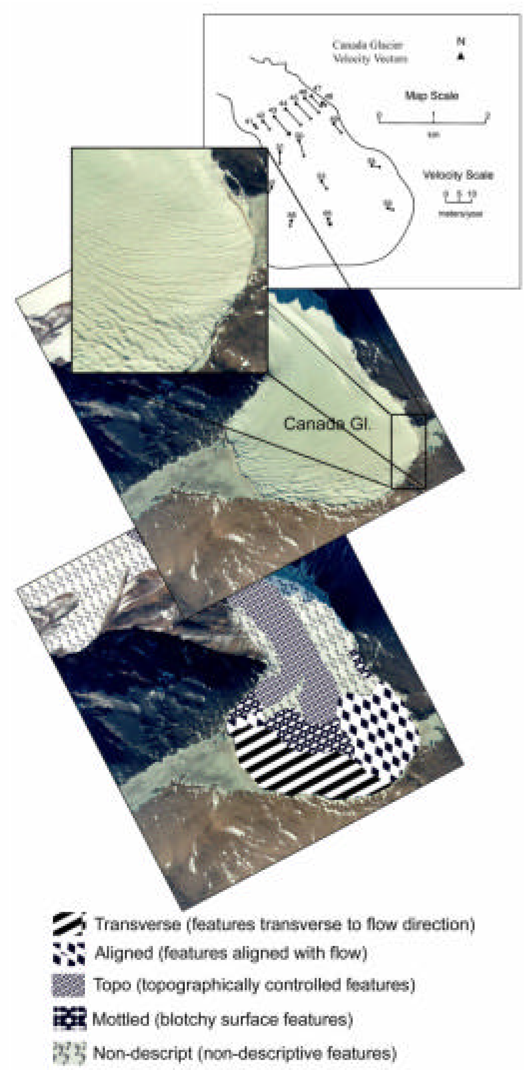

Figure 2.18 – The *Aligned* features on Canada Glacier.

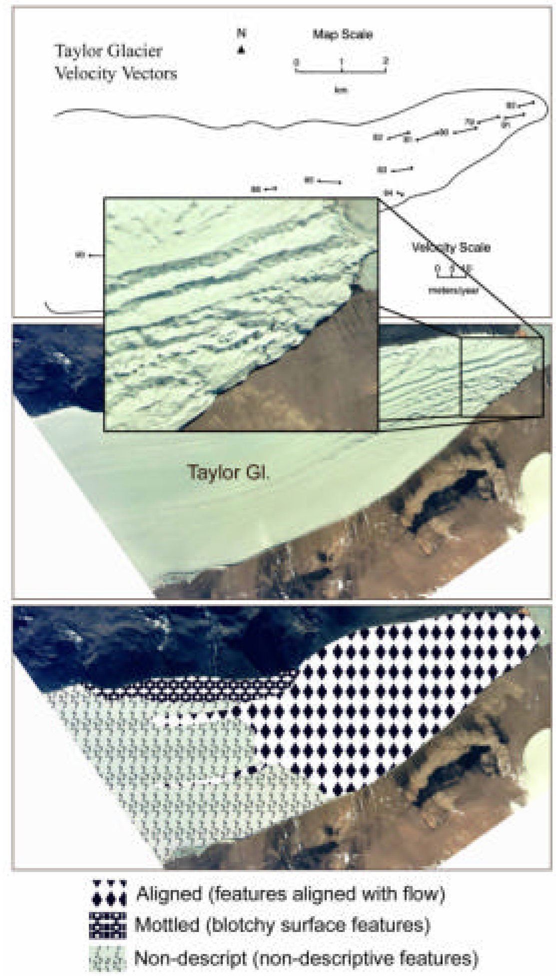

Figure 2.19 – The *Aligned* features on Taylor Glacier.

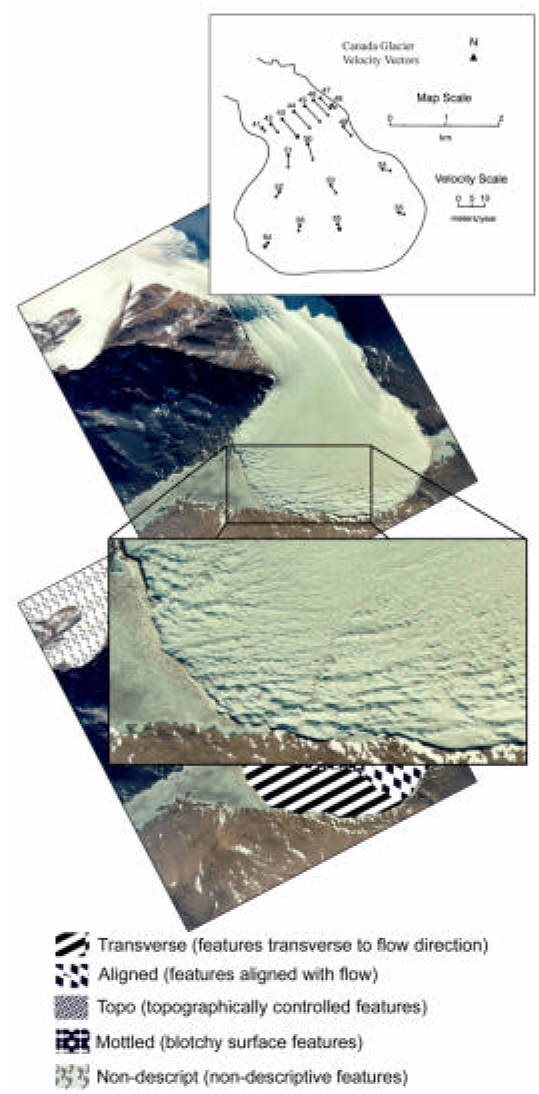

Figure 2.20 – The *Transverse* features on Canada Glacier.

2.3 Sediment Distribution

A small *Mottled* region is located in the east corner of Suess Glacier (Figure 2.21). The region does not have channel-like features, but it does exhibit surface roughness. What is distinct about this region of Suess Glacier is that it is mantled with rock debris (sediment) that clearly affects the morphology of the surface.

Figure 2.21 - East side of Suess Glacier showing the sediment content in the Mottled zone.

Sediment has a lower albedo than the ice it lies on and absorbs more solar radiation than the ice. Concentrations of debris as low as 13 g m^{-2} can reduce glacier albedo by greater than 6% (Lewis, 2001). Greater energy absorption by the sediment and can lead to increased glacier melt. However, a mantle of debris can also insulate the surface. The difference lies in the thickness of the debris layer (Ostrem, 1959). Investigations on debris-mantled regions of Isfallsglaciären, North Sweden, showed that ablation rates sharply increased (Figure 2.22) with debris thickness up to ~ 1 cm and decreased at thicknesses greater than ~1 cm. At about 2 cm thickness, the rate of ablation is similar to that of clean ice. The ablation rate decreased to nearly zero at

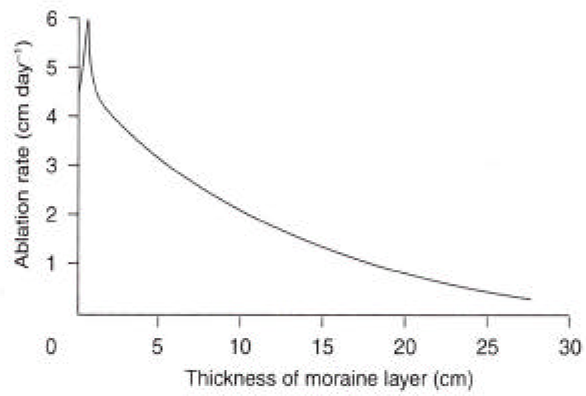

Figure 2.22 - Effects of debris mantle thickness on ablation rates on Isfallsglaciären, North Sweden. (Benn and Evans, 1998 from Østrem, 1959)

about 25 cm debris thickness. This indicates that debris thicker than roughly 25 cm insulates the ice from ablation. A clear example of debris acting as an insulator occurs in Beacon Valley, Antarctica, where ice possibly as old as late Miocene survives below a 20–100 cm mantle of debris (Marchant et al., 2002; Schafer et al., 2000). Similar preservation of glacier ice is observed in numerous rock glaciers in Antarctica and elsewhere (Nakawo et al., 2000). Without exception, debris is present on glacier surfaces in the study area that have any kind of surface roughness, as observed on regions of Suess (Figure 2.23, a), Commonwealth (b), and Canada glaciers (c). Sediment is transported to the glaciers in a number of ways: as wind-blown debris, by avalanche, or as moraines.

The channels on Taylor Glacier result from medial moraines whose path can be traced tens of km up-glacier from the terminus. This origin is demonstrated in aerial photography, satellite imagery, topographic maps of the region, and field observations. My thesis focuses on two of these channels, which I have termed the North and South channels (Figure 2.24). The North Channel can be traced back to

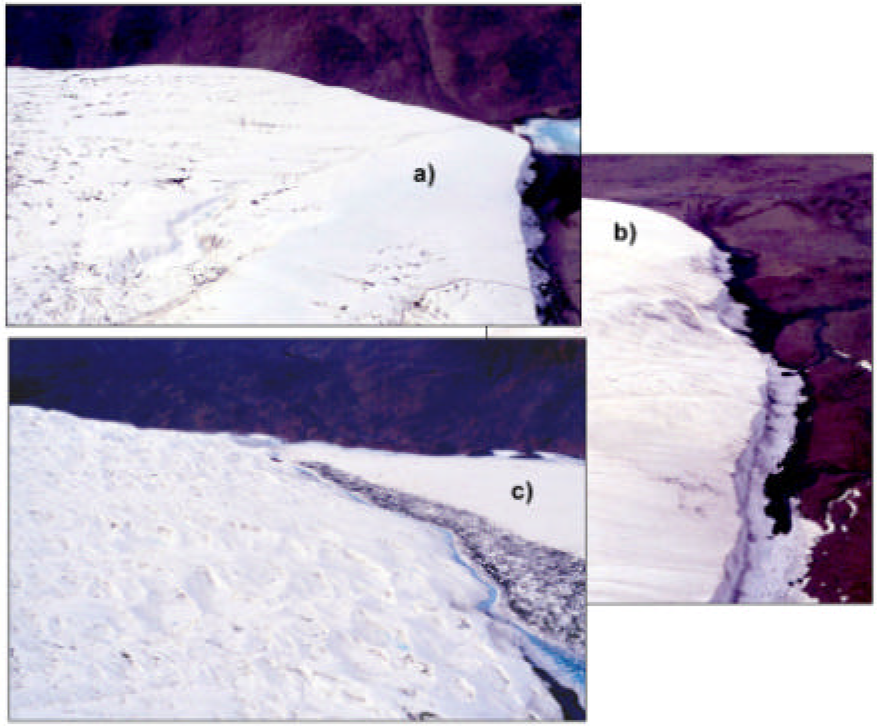

Figure 2.23 – Sediment on a) the west side of Suess, b) the west side of Commonwealth, and c) the west side of Canada glaciers.

a debris-laden region of icefall near Finger Mountain, roughly 45 km up-glacier from the snout of Taylor Glacier. The South Channel can be traced back to a medial moraine resulting from the confluence of Taylor and Ferrar glaciers at Knobhead, roughly 28 km up-glacier from Taylor Glacier snout. The medial moraines are primarily comprised of large, sporadically distributed blocks with minor amounts of sand and cobble sized debris (Figure 2.25). These medial moraines were described by Taylor (1916) as consisting of “a block here, another 20 feet off, a third somewhat further, and so on along a line” down the glacier.

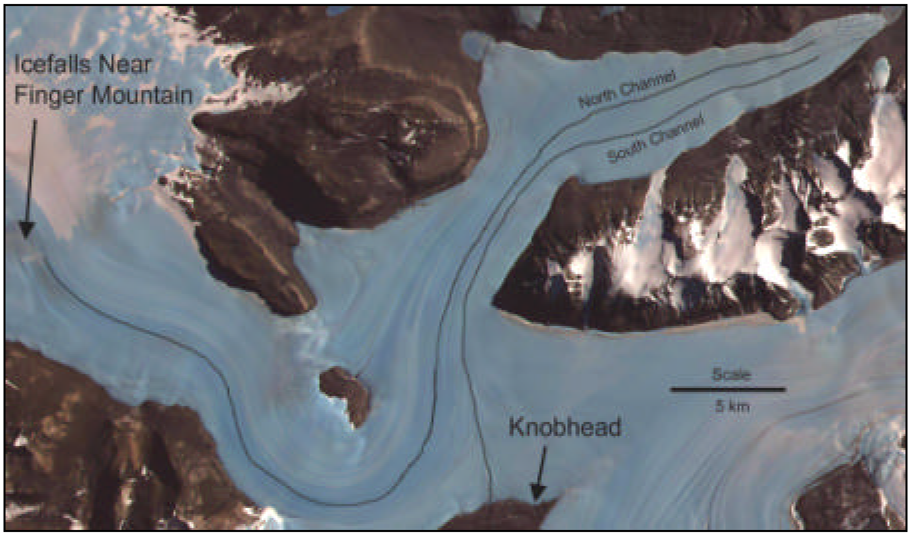

Figure 2.24 - Taylor Glacier with lines added to emphasize the debris source for the North and South Channels.

Figure 2.25 - An example of the boulders that comprise the medial moraines on Taylor Glacier (background) and an ablation well that has developed around one of the boulders (foreground) due to the emission of longwave radiation. The foreground boulder is roughly 2 meters across.

3 CHANNEL MORPHOLOGY AND METEOROLOGICAL MEASUREMENTS

The oldest available aerial photographs of Taylor Glacier were taken in 1961. Comparison of these images with the most recent aerial photographs indicates that the channels on the glacier have changed little between 1961 and 2001. The earliest written account of the channels are from Scott (1905), who described the channels in the lower ablation zone of Taylor Glacier in a December 18, 1903, narrative of their journey down the length of the glacier, "[T]he ice grew so disturbed that we were obliged to rope ourselves together and proceed with caution." Griffith Taylor (1916) described the channels in a February 11, 1911, account stating, "[T]he center of the glacier was cut up by surface streams into asymmetric gullies".

Melt from these channels flows to Lake Bonney, the proglacial lake at the terminus of Taylor Glacier, and one of the largest lakes in Taylor Valley. This chapter examines the morphology of the channels as a preliminarily step to energy balance modeling within the channel and at the glacier surface. Detailed channel measurements were made in January 2000 and January 2001, and focused on the two deeply-incised North and South channels (Figure 3.1).

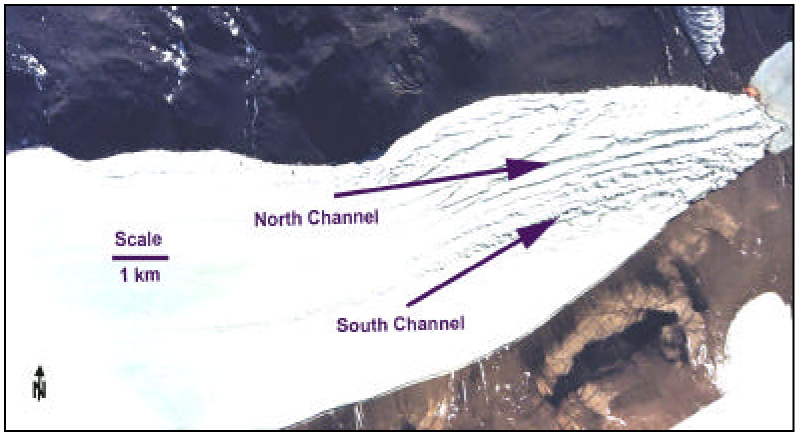

Figure 3.1 – Aerial photograph of Taylor Glacier showing the locations of the North and South Channels (MCM-LTER, 2001).

3.1 Channel Geometry

Cross-sections were surveyed on both channels and a longitudinal profile was measured on the North Channel to characterize channel geometry. Bamboo poles drilled into the ice defined end-points for each cross-section and a Trimble GPS was used to locate their positions. GPS errors were ± 3.2 cm in the horizontal and ± 4.2 cm in the vertical. The cross-sections were surveyed with a Topcon 301D Total Station with errors of ± 3.0 cm in the vertical and horizontal. Albedo readings (discussed later) were recorded at cross-section points. Thirteen and fifteen cross-sections were surveyed on the South and North channels, respectively (Figure 3.2; Appendices 7.1 and 7.2). A fourteenth cross-section (South Channel cross-section 7) was later interpolated to fill a gap in the survey data. A kinematic GPS survey was conducted along the floor of the North Channel and on the glacier surface along the North Channel periphery to define the slopes of the channel floor and the glacier

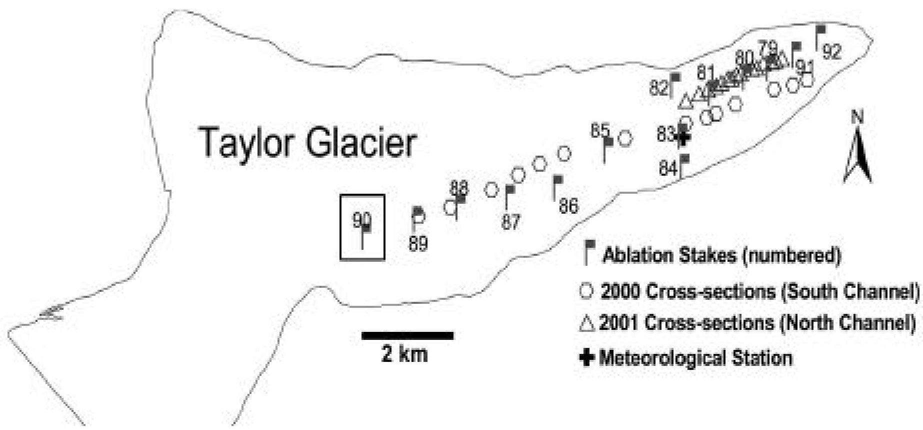

Figure 3.2 - Location of ablation stakes (flags), cross-sections (hexagons and triangles), and the meteorological station on Taylor Glacier (the cross located at stake 83). Stake 90 (boxed) is the datum for all distances down-glacier.

surface. The floor survey began near the glacier terminus and proceeded up-glacier along the channel floor to the highest cross-section, then continued down-glacier along the periphery back to the start position. The sample interval was 5 seconds and the GPS errors are the same as for the cross-sections. The cross-section survey for the North Channel began roughly 4 km down-glacier from start of the South Channel survey. Shortening the survey of the North Channel conserved time, and was warranted because the geometry up-glacier from the survey start was very similar to the South Channel. All down-glacier distances reported in the manuscript are with respect to ablation stake 90 (Figure 3.2).

3.1.1 Observations

Up-glacier, the channels are relatively narrow and shallow but toward the glacier terminus they become great chasms, impossible to maneuver without safety equipment (Figure 3.3). The two channels begin to widen at about the same location ~ 7 km down-glacier from stake 90 (Figure 3.4). The width of the North Channel

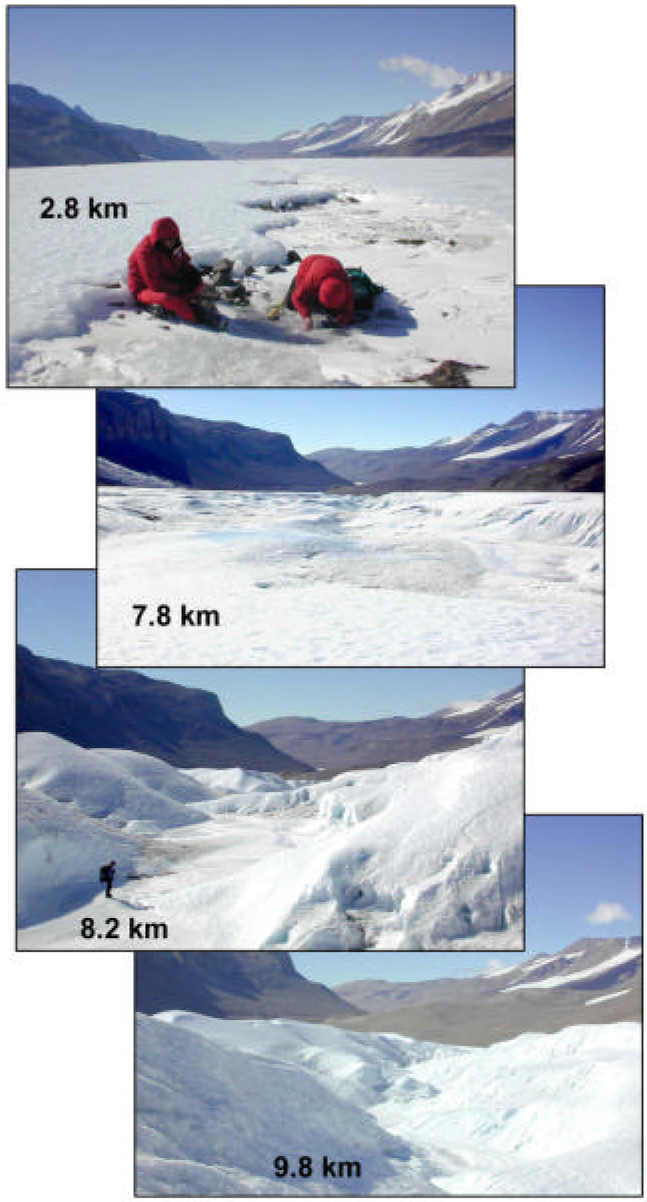

Figure 3.3 – Progression of South Channel development with distance down-glacier. Note the morainal material in the top channel.

increases from 10 to 110 m over 2 km and the width of the South Channel increases from 10 to 120 m over about 0.5 km. The channels also both begin to deepen at about the same location ~ 7 km down-glacier from stake 90 (Figure 3.4), and deepen from

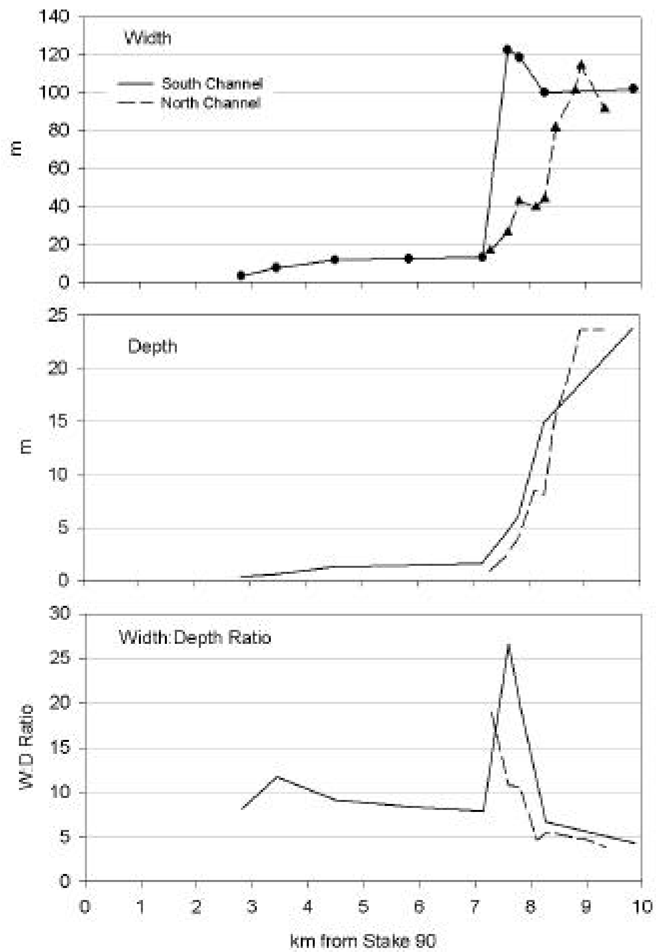

Figure 3.4 - Width, depth, and width to depth ratio of the North and South Channels. Symbols have been added for reference to selected cross-section location.

only a few meters to about 24 m over roughly 1.3 and 2.5 km for the North and South channels, respectively. For the first 7 km down-glacier, the ratio of width to depth is relatively constant (about 8) for the South Channel (Figure 3.4) and likely the same for the North Channel. From about 7 to 8 km down-glacier, a region of transition ensues and the width to depth ratio increases dramatically. This is followed by a second relatively constant width to depth ratio (approaching 4) toward the end of the survey.

The time required for channel development can be estimated using the mean surface speed of the glacier. The estimated time of development, with respect to stake 90, for the South Channel is based on average horizontal surface velocity at ablation stakes from November 1995 to January 1997 (Fountain, 2001; Appendix D). Assuming that velocity has been consistent over time, the cumulative time of channel development is about 1486 years - that is, it takes ice at stake 90 roughly 1486 years to flow about 10 km (the end of the survey location). I estimated the rate of change in channel widening and deepening, and in the width to depth ratio (Figure 3.5; Appendix E). During the region of transition, the rate of channel widening peaks at about 1.5 m yr^{-1}, while the peak deepening rate is only about 15 *cm* yr^{-1}, and comes at the end of the region of transition (Figure 3.5) and the start of the 2nd steady state condition. The region of transition lasts about 160 years and occurs over a distance of roughly a kilometer.

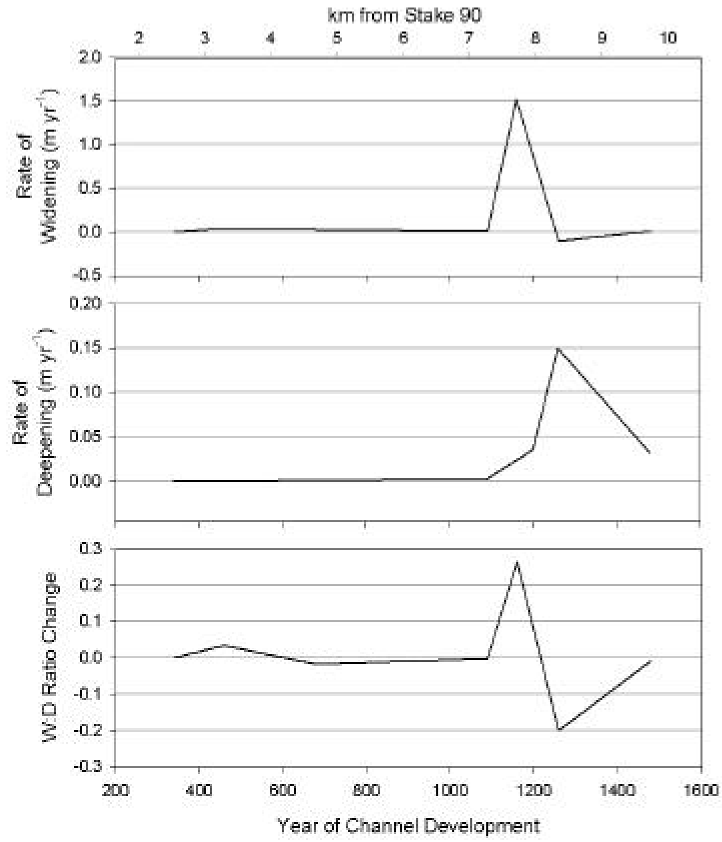

Figure 3.5 - Rate of change in widening, deepening, and width to depth ratio of the South Channel.

There is a slight decrease in the rate of channel development at about 4 km down-glacier from stake 90. Comparing surface velocities with glacier and bed elevations (Figure 3.6), the slight decrease appears to be the result of increased flow speed – and thus reduced residence time – of ice in this zone. The increased flow speed corresponds to a steepening in the slope of the ice surface.

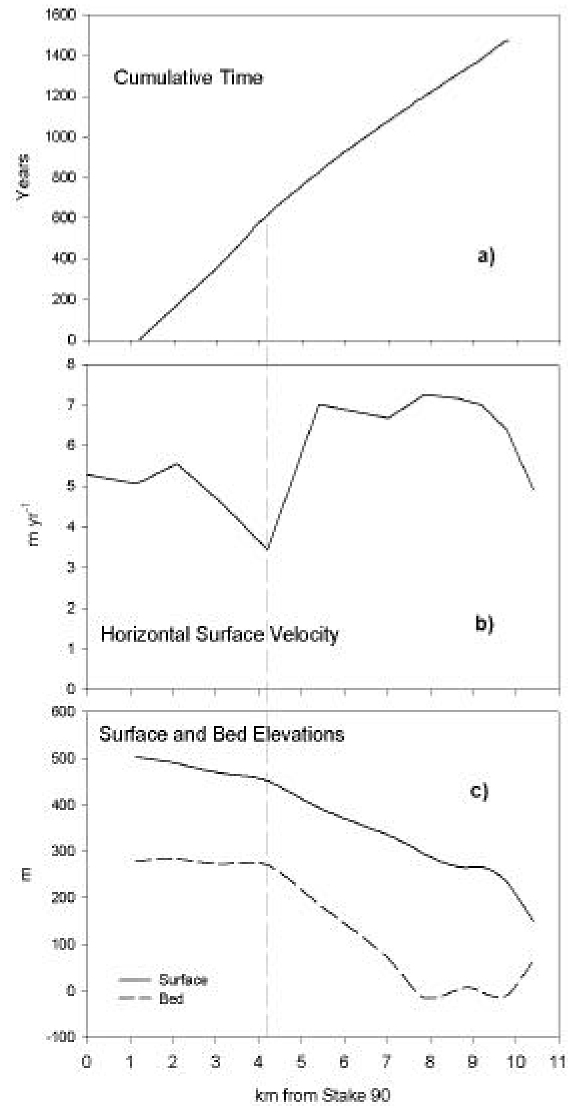

Figure 3.6 - Cumulative time of South Channel development, velocity, and glacier and bed slope. Surface and bed elevation are from ground penetrating radar data (Langevin, 1998).

The average slopes of the north and south-facing walls of the North Channel were calculated using survey points at the periphery and floor of the channel for each cross-section (Figure 3.7). The wall slopes are rather shallow (5°-20° from horizontal) until about 8 km down-glacier. After this point, the slopes increase, and the average *overall* slopes are ~ 25° for the south-facing wall, and ~30° for the north-facing wall.

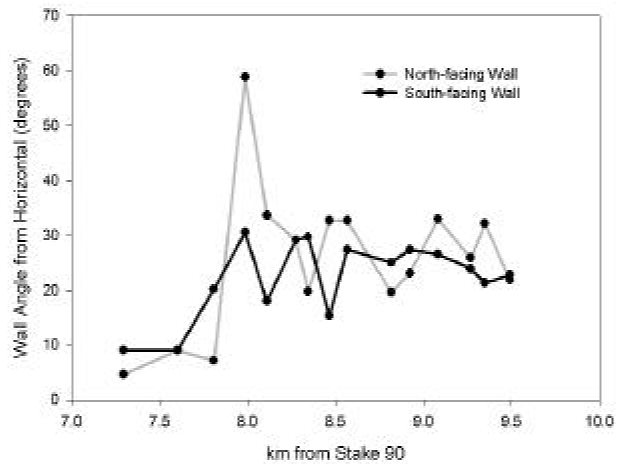

Figure 3.7 – Average horizontal slopes of the north and south-facing walls in the North Channel at each of the 15 cross-sections (black dots). The overall averages of the north-facing and south-facing walls are ~ 30° and ~25°, respectively, after about 8 km down-glacier.

While the *overall* slope of the north-facing wall is ~30°, there are regions of the wall that, unlike the south-facing wall, have very steeply-inclined, stepped regions (Figure 3.8). The slopes of these stepped regions range from 51° to 74° from horizontal, and average 60°.

Figure 3.8 – Steeply-inclined, stepped regions along the north-facing wall of the North Channel.

The average down-glacier channel slope derived from the kinematic GPS survey of the North Channel is small, 0.052 at the periphery and 0.061 at the floor

(Figure 3.9). A change in slope at both the floor and the periphery occurs at ~ 8.75 km. Up-glacier of this point the slopes are 0.041 and 0.049 at the periphery and floor, respectively, and down-glacier they are 0.065 and 0.069. Therefore, the periphery slope increases ~ 59% and the floor slope increases ~40% down-glacier of this point. The channel periphery is relatively smooth until ~ 9.25 km down-glacier, where it

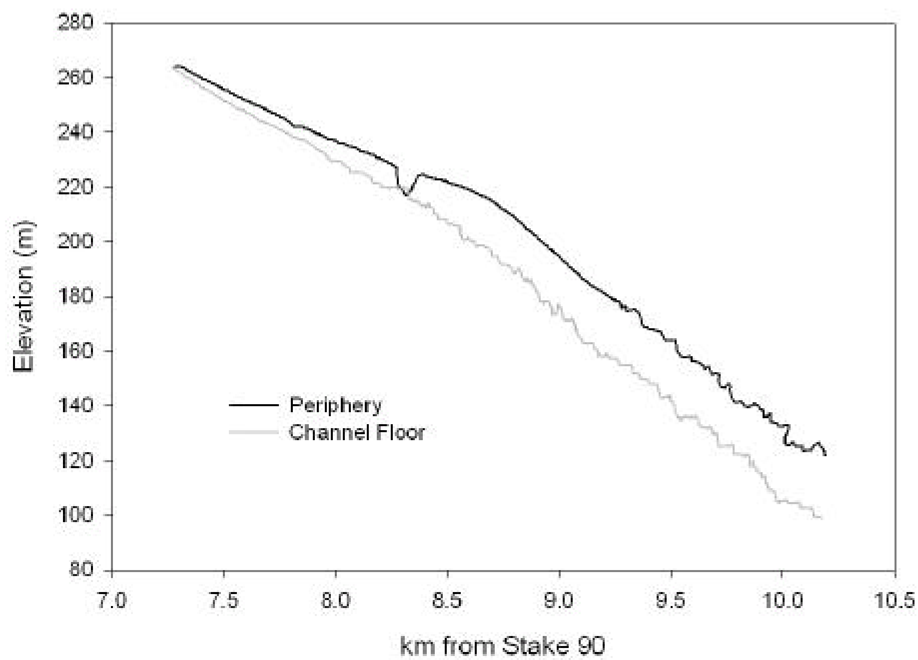

Figure 3.9 - Kinematic survey of the channel periphery and floor. Errors are ±3.2 cm in the horizontal and ±4.2 cm in the vertical.

becomes jagged and knife-like. The channel floor is rougher than the periphery. Its morphology is similar to the pool-and-riffle pattern of a stream. Perennially frozen pools of various sizes are often found at the channel floor. The pools are usually connected by steep, but shallow, streams.

3.2 Albedo

Albedo, the ratio of reflected to incident solar radiation, is an important variable in the surface energy balance because it controls the magnitude of net solar energy absorbed by the ice. The average albedo for dirty ice, clean ice, and dry snow are 21%, 40%, and 74%, respectively (Paterson, 1994). Albedo was measured along the cross-sections, noting if the location was at the surface (periphery), a channel wall, or the channel floor (Figure 3.10) and whether the measurement was made over sediment, ice, or snow. A field-constructed "albedometer" consisted of two LI-COR LI200S pyranometers – one facing up and the other facing down. They were connected to a data logger (Campbell Scientific, Inc.) programmed to display the albedo. The typical error associated with the pyranometers is ± 3% and the total albedo error is about ± 4%.

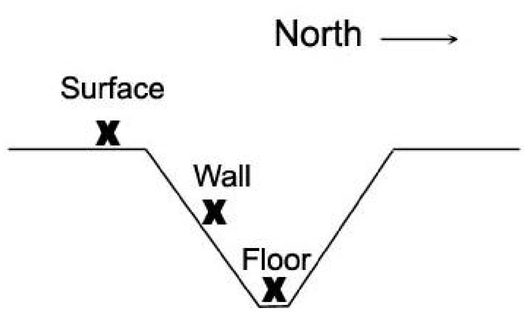

Figure 3.10 – Simplified schematic showing relative location of surface, wall, or floor albedo measurements.

3.2.1 Observations

The albedo data are relatively complete for all cross-section survey points in the South Channel (measured during the 1999-2000 season), but only for the 11 cross-sections farthest up-glacier in the North Channel (measured during the 2000-2001 season) due to instrument malfunction. The albedo is generally greater in the North Channel than in the South Channel (Figure 3.11). This may be due to a colder average air temperature (by ~ 3°) and a greater, although patchy, snow cover in the North Channel during the 2000-2001 season. As expected, the albedo of sediment-covered ice is lower than bare ice, and the albedo of bare ice is lower than that of snow (Figure 3.12). The averages fall within the ranges of albedo measured elsewhere (Paterson, 1994). The average albedo was higher for all locations of the North Channel than the South Channel (Figure 3.13), with the greatest difference between the two channels being at the channel floor. In general, albedo was greater on the north-facing walls than the south-facing walls (Figure 3.14).

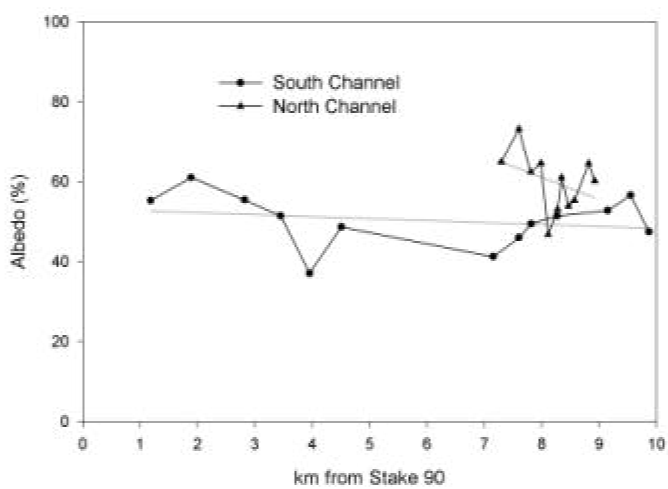

Figure 3.11 - Average albedo at cross-sections 1-6 and 8-14 of the South Channel (dots) and 1-11 of the North Channel (triangles). No albedo was obtained from cross-sections 12-15 in the North Channel. Light gray lines are general trend lines.

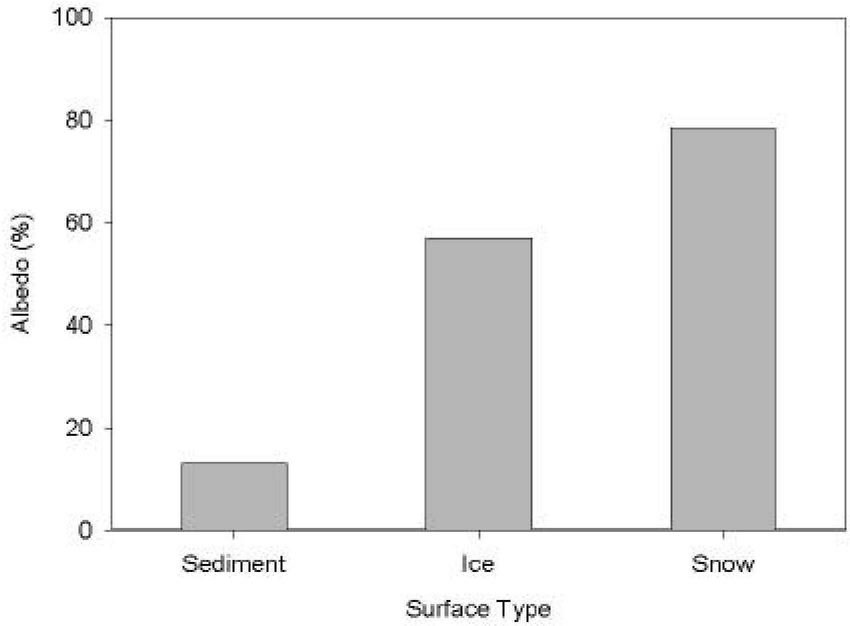

Figure 3.12 - Average albedo of the sediment, snow, and ice surfaces in all cross-sections.

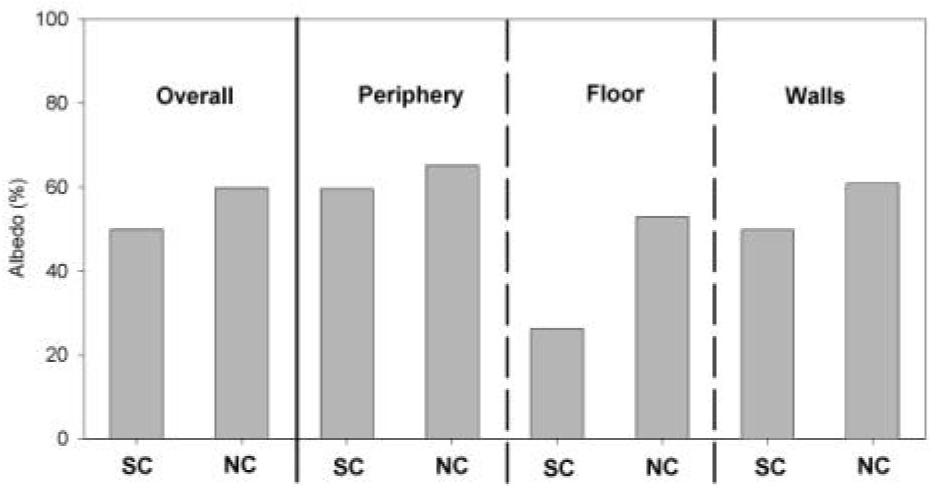

Figure 3.13 - Average overall and periphery, floor, and wall albedo for the channels. SC is the South Channel and NC is the North Channel.

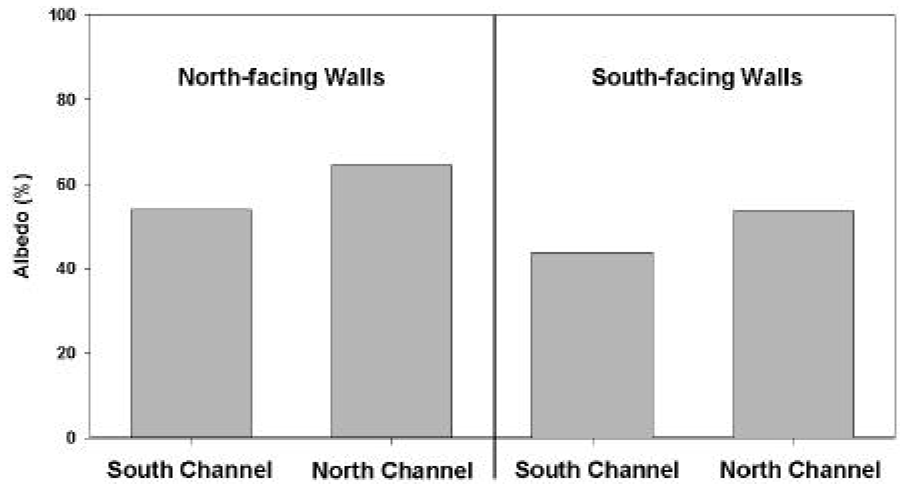

Figure 3.14 – Average albedo on the north and south-facing walls for the North an d South channels.

3.3 Cryoconite Holes

Cryoconite holes are cylinder shaped melt features in the glacier mass that begin to form when sediment becomes trapped in a slight depression on the glacier surface, or from icebound sediment moving upward vertically through the ice column due to emergent ice flow (Fountain et al., Submitted February 2003). Sediment has a lower albedo than the surrounding ice, absorbs more solar energy, warms, and melts into the ice (see McIntyre, 1984; Podgorny and Grenfell, 1996; and Fountain et al., Submitted February 2003).

Cryoconite holes vary in diameter from 1 cm to more than a few meters, and can be more that 50 cm deep. An idealized cross-section of a cryoconite hole is shown in Figure 3.15. A thin layer of sediment covers the base of the hole with a column of water above. In the dry valleys, an ice lid almost always covers the holes (Fountain et al., Submitted February 2003), although cryoconite holes on glaciers in temperate regions of the world apparently don't have ice lids (Wharton Jr. et al., 1985). An air space exists between the ice lid and the water within the hole. The surface expression of these features is a circular patch of darker ice where the ice lid has formed (Figure 3.16). The spatial distribution of cryoconite holes is variable; they can be isolated or

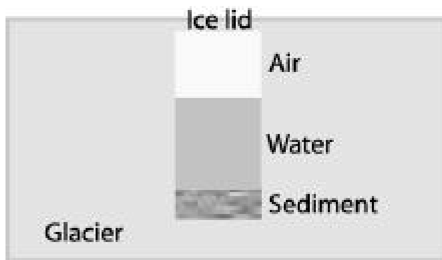

Figure 3.15 - Idealized cryoconite hole schematic showing ice lid, air, water, and sediment at base. Not to scale.

can occur in large numbers on the glacier surface (Figure 3.17).

Field evidence suggests that as the channels on Taylor Glacier develop and the channel walls ablate, cryoconite holes near the channel are scavenged (Figure 3.18 and Figure 3.19). This process flushes water and sediment within the hole to the channel system.

Figure 3.16 - A cryoconite hole on Taylor Glacier, ringed in black to emphasize shape.

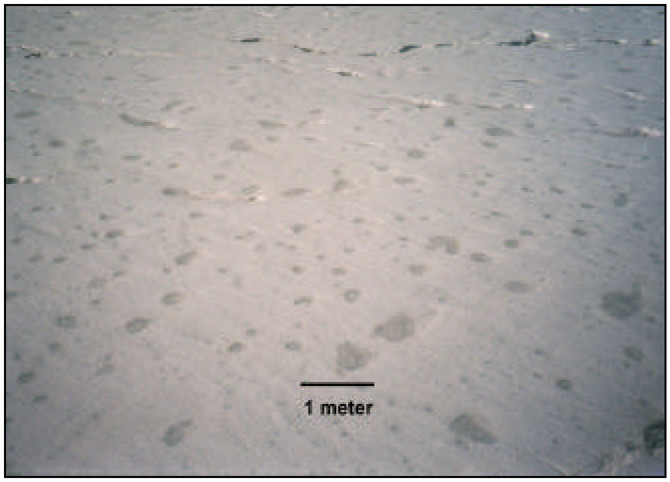

Figure 3.17 - Taylor Glacier surface, densely populated with cryoconite holes

Figure 3.18 - Scavenged cryoconite holes showing the sediment flushed from the hole.

Figure 3.19 – View of a north-facing channel wall, showing many scavenged cryoconite holes, and sediment at the channel floor.

To define the spatial and temporal changes in cryoconite hole concentration down-glacier, as well as estimate the sediment flux to the channels, I measured the number and diameter of cryoconite holes greater than 1 cm in a 2.5 m radius circle around the ablation stakes over the two seasons of fieldwork. Data were collected from all stakes during the 1999-2000 season, and all but stakes 82, 81, and 79 during the 2000-2001 season.

3.3.1 Observations

The number of cryoconite holes around the ablation stakes is not consistent between years (Figure 3.20 a). The most extreme example is stake 89, where the number of cryoconite holes increased from 125 in January 2000 to 475 in 2001. The number generally doubled from 2000 to 2001 at stakes 88, 86, and 85, but there was little change at stakes 87, 84, and 83. There were, on average, 213 cryoconite holes in each survey circle, and they covered 3% of the surface area. Despite the fact that cryoconite hole populations at each stake vary from year to year, the fractional area covered by the holes is remarkably similar between years, with the exception of stake 85 (Figure 3.20 b), which is so great because of one hole > 1m in diameter.

To examine the frequency of cryoconite holes by size at each stake, I plotted the relative frequency of 9 diameter size classes: <2.5, 2.5-5, 5-7.5, 7.5-10, 10-20, 20-30, 30-50, 50-70, and > 70 cm. Over 50% of the cryoconite holes for both the 2000 and 2001 seasons were < 2.5 cm in diameter (Figure 3.21), and the number of cryoconite holes per size class decreased with increasing size class. Additionally, for both seasons, the frequency of the smallest holes (<2.5 cm in diameter) tended to decrease with distance down-glacier, while the frequency of the larger holes tended to increase (Figure 3.22).

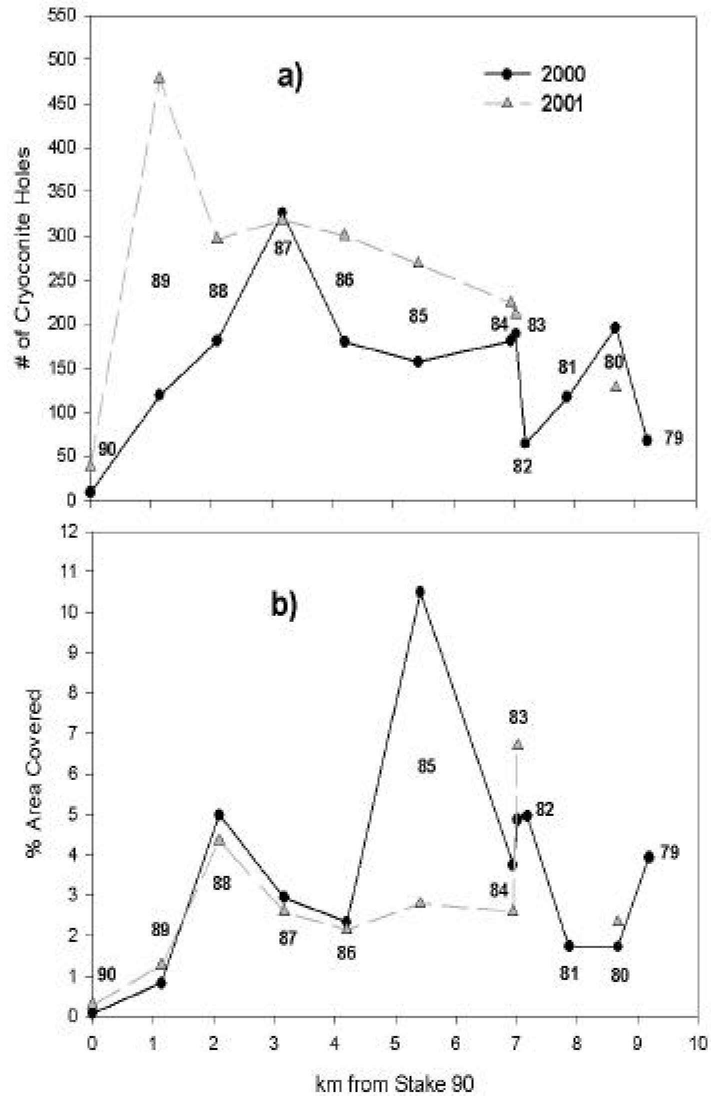

Figure 3.20 - a) Number of cryoconite holes in a 2.5 m radius circle around ablation stakes. Numbers within the graph are the ablation stakes. Data were not collected from ablation stakes 82, 81, and 79 during the 2000-01 field season. b) Total percent of area in 2.5 m radius circle around stakes covered with cryoconite holes.

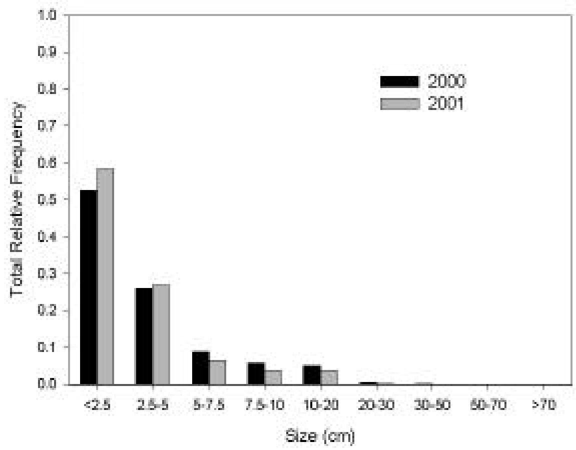

Figure 3.21 - Total relative frequency for each cryoconite hole diameter class size.

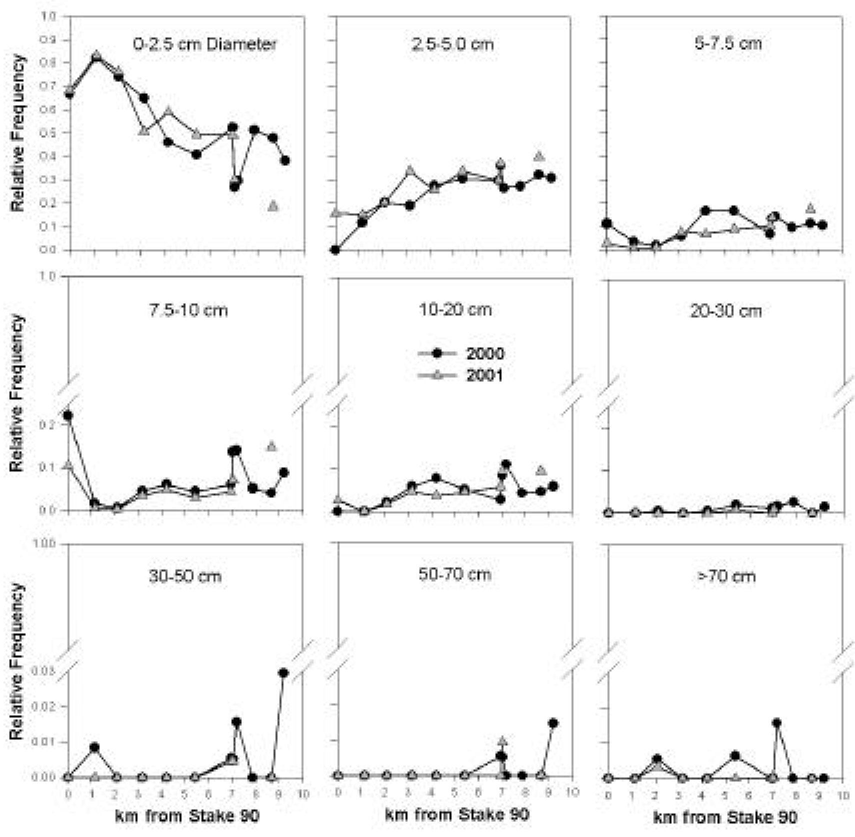

Figure 3.22 - Relative frequency of cryoconite hole diameter class sizes <2.5, 2.5-5, 5-7.5, 7.5-10, 10-20, 20-30, 50-70, and > 70 cm. Black circles are January 2000 data and gray triangles are January 2001 data.

3.4 Surface and Channel Meteorological Data

The meteorological (met) station on Taylor Glacier (77°44′24″ S, 162°07′42″ E, 334 meters above sea level, near ablation stake 83) has been recording temperature, relative humidity, radiation flux, precipitation, and wind speed and direction since the 1994-1995 season (Figure 3.23). Temperature loggers were installed at ablation stakes during the 1999-2000 field season to provide spatial information on temperature

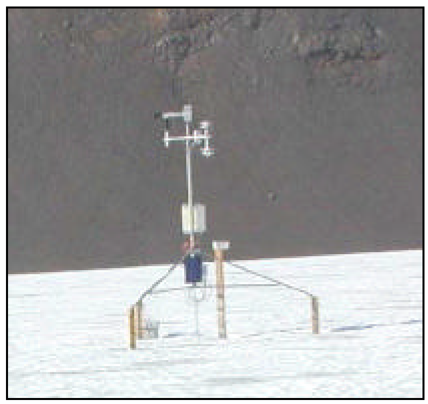

Figure 3.23 – The meteorological station on Taylor Glacier. The station is about 3 m in height.

variations along the longitudinal profile of the glacier. Five Onset StowAway XTI temperature loggers (Onset Computer Corp.) were mounted one meter above the ice surface on bamboo poles near ablation stakes to record temperature hourly. For simplicity, I termed these loggers 98, 86, 83, 80, and 92, in relation to the ablation stakes near which they were placed. The loggers record temperatures over a range of -37°C to 46°C with an error of ± 0.4°C. The period of record for each thermistor is listed in Table 3.1. These data will be used in conjunction with the met station data to characterize temperature variation down-glacier.

Temporary meteorological stations were established along the North Channel during the 2000-2001 field season to provide information on the meteorology in the channels. Data were collected within the channel from November 22, 2000 to January 5, 2001, at a location near cross-section 15. Data were also collected simultaneously in the channel and at the channel periphery from January 6 to 15, 2001, near cross-section 11 (Figure 3.24). Additionally, Karen Lewis supplied meteorological data collected in January 1999 from a temporary station within one of the channels on

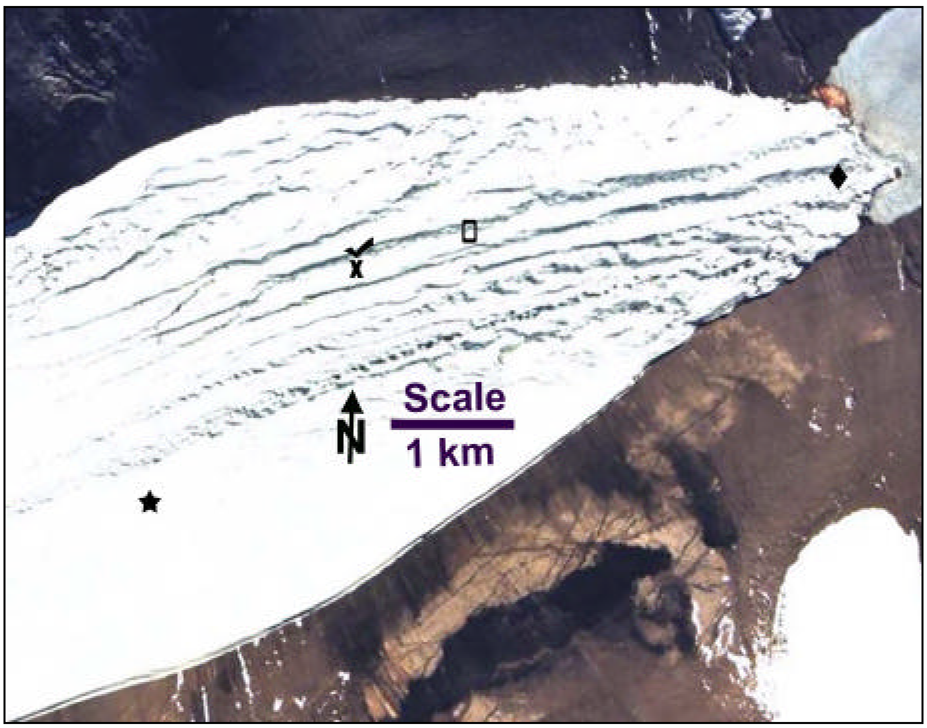

Figure 3.24 - Locations of meteorological stations on Taylor Glacier: star, established station operated 1994 to present; diamond, temporary channel station operated Jan. 18-25, 1999; square, temporary channel station operated Nov. 22, 2000 - Jan. 5, 2001; check and x, simultaneous run of temporary periphery and channel stations operated Jan. 6-15, 2001. See Table 3.1 variables recorded.

Taylor Glacier. Data collected (Table 3.1) included air temperature, wind speed and direction, incoming and outgoing short-wave radiation, and relative humidity.

Table 3.1 - Meteorological instruments, periods of record, and variables recorded on Taylor Glacier. Jan. 18 - 25, 1999 data is from Karen Lewis. The associated errors are different for the loggers and the met stations because the met station temperature data is compiled using the Steinhart-Hart equation, which greatly reduces error (Doran et al., 2002).

Instrument	**Period of Record**	**Variables Recorded and Associated Instrument Error**
Met. Station	Nov. 21, 1994 - Present	Air and ice temperature (±0.02°C), relative humidity (<1%), incoming and outgoing short-wave radiation (±3%), wind speed (±0.3ms^{-1}), wind direction (±3°)
Temp. Station - channel	Jan. 18 - 25, 1999	Air temperature (±0.02°C), relative humidity (<1%), incoming and outgoing short-wave radiation (±3%), wind speed (±0.3ms^{-1}), wind direction (±3°)
Temp. Station - channel	Nov. 22, 2000 - Jan. 5, 2001	
Temp. Station - periphery	Jan. 6 - 15, 2001	
Temp. Station - channel	Jan. 6 - 15, 2001	
Logger 89	Nov. 17, 1999 - Jan. 13, 2000 and Nov. 16, 2000 - Jan. 19, 2001	Air temperature (±0.4°C)
Logger 86	Nov. 17, 1999 - Nov. 16, 2000	
Loggers 83, 80, and 92	Nov. 17, 1999 - Jan. 13, 2000	

3.4.1 Observations

Temperature loggers indicate that the air temperature warms about 3°C over roughly 9.2 km down-glacier (Figure 3.25). The average temperatures over the recording interval were -5.7, -5.3, -4.4, -3.8, and –2.7°C (all ~ ± 2.5°C) at sites, in down-glacier order, 89, 86, 83, 80, and 92, respectively. The corresponding mean lapse rate (rate of decrease in temperature with elevation) is about -0.8°C/100 m (Figure 3.26). However, the lapse rate varied between -0.7°C/100 m and -1.0°C/100 m at adjacent loggers (Figure 3.27). The data logger and met station temperature records were highly correlated, with regression coefficients (r^2) between 0.96 and 0.99 (Table 3.2).

Figure 3.25 - Average air temperature at loggers with distance down-glacier. Bars are standard deviation, and a linear regression line has been added. The numbers reference ablation stakes the loggers were near.

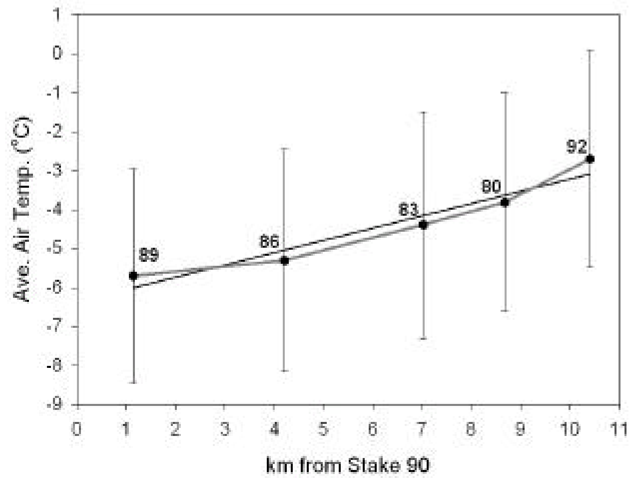

Figure 3.26 – Average air temperature with elevation from logger data, with a linear regression line added (black dashed).

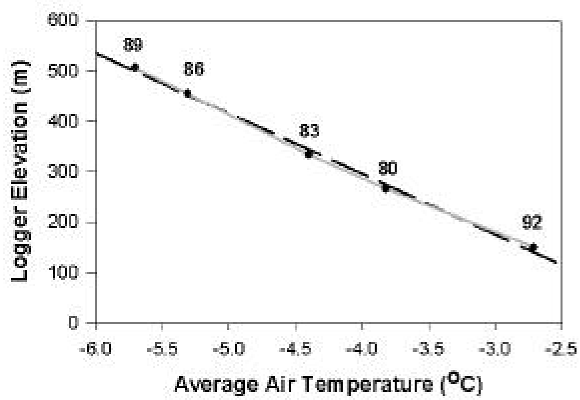

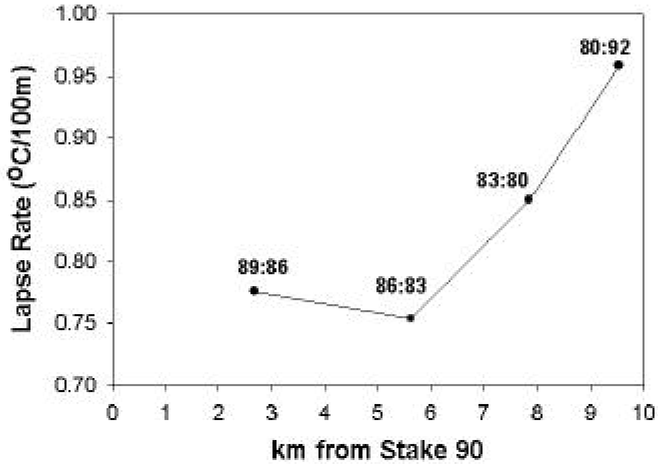

Figure 3.27 - Lapse rate between thermistors with distance down-glacier. The overall lapse rate is 0.85°C/100 m. The points represent the halfway point between thermistors.

Table 3.2 – Summarization of information at and between loggers from Nov. 17, 1999 to Jan. 13, 2000.

Logger	km from 90	Elevation (m)	Ave. Temp (°C)	Temp. Range (°C)	Correlation with met station
89	1.14	506	-5.7	17.9	0.96
86	4.21	455	-5.3	18.4	0.97
83	7.03	334	-4.4	19.9	0.98
80	8.68	266	-3.8	17.6	0.98
92	10.41	150	-2.7	17.8	0.97
Met Station (1m)	7.03	334	-4.3	18.4	

Between Loggers	Distance (km)	Elevation Difference (m)	Temp Difference (°C)	Lapse Rate (°C/100m)	Correlation Coefficient
89 & 86	3.1	51	0.4	0.8	0.97
86 & 83	2.8	121	0.9	0.7	0.98
83 & 80	1.6	68	0.6	0.9	0.99
80 & 92	1.7	116	1.1	1.0	0.99
89 & 92	9.2	356	3.0	0.8	0.96

Only logger 89 recorded data during the second field season (2000-2001). The average temperature was –6.4°C. At the meteorological station it was –5.1 °C. The met station is roughly 6 km down-glacier from and 172 m lower than thermistor 89, which yields a lapse rate of -0.8 °C/100 m, consistent with lapse rate estimates from the temperature records of the previous season. Only logger 86 recorded temperatures over the winter, from mid-January 2000 to mid-November 2001. For the winter months of June, July, and August, the average air temperature at the logger was –24.6°C, 0.2°C warmer than the –24.4°C recorded at the met station. The met station is about 2.8 km down-glacier from stake 86 and is 121 m lower in elevation, corresponding to a reduced winter lapse rate of -0.1°C/100 m, which may be due to weak temperature inversions in winter (Nylen, 2002).

Comparison of Meteorological and Channel Stations

From January 18 to 25, 1999, the channel station was located in a different channel just south of the North Channel (Figure 3.24), roughly 5 km down-glacier from the established met station. The mean air temperature within the channel was warmer than the glacier surface air temperature by 2.1°C and the mean wind speed was reduced by 2.3 m s^{-1} (Figure 3.28). Relative humidity was 5% lower in the channel than it was at the glacier surface. The wind direction is similar for both locations, bimodal – generally up-valley (~80°) and down-valley (~250°). Net shortwave radiation in the channel averaged about 20 W m^{-2} more than the surface.

The radiation peaks were generally greater in the channel but the minima were about the same.

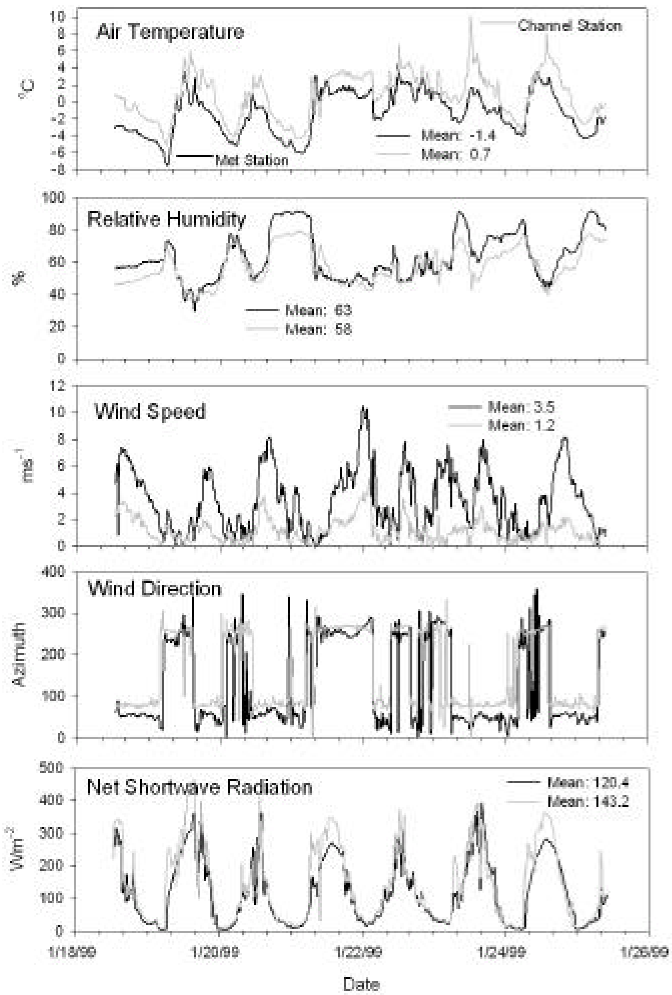

Figure 3.28 - Jan. 18-25, 1999: Air temperature, relative humidity, wind speed and direction, and radiation recorded at the established and a temporary station located in a channel just south of the North Channel, about 5 km down-glacier from the established station. Wind direction is with respect to north.

From November 22, 2000 to January 5, 2001, the temporary station was located within the North Channel, about 3 km down-glacier from the met station. The elevation difference between the met station and the channel at the temporary station location is 193 m. With the lapse rate of -0.8°C/100 m and the average met station temperature of –4.5°C, the temperature in the channel should be about –3.0°C

(±0.02°C). The average air temperature within the channel was –2.8°C (±0.02°C) (Figure 3.29). The average wind speed and relative humidity were reduced by 1.8 m s^{-1} (41%) and 9%, respectively, relative to the station on the glacier surface. At both stations, wind direction was bimodal in the up-and-down-valley directions. Net shortwave radiation was greater by ~ 50 W m^{-2} (28%) in the channel than at the met station.

Figure 3.29- Nov. 22, 2000 to Jan 5, 2001 - Air temperature, relative humidity, and wind speed and direction recorded at the established and temporary stations. The temporary station was located within the North Channel, roughly 3 km down-glacier from the established station. Wind direction is with respect to north.

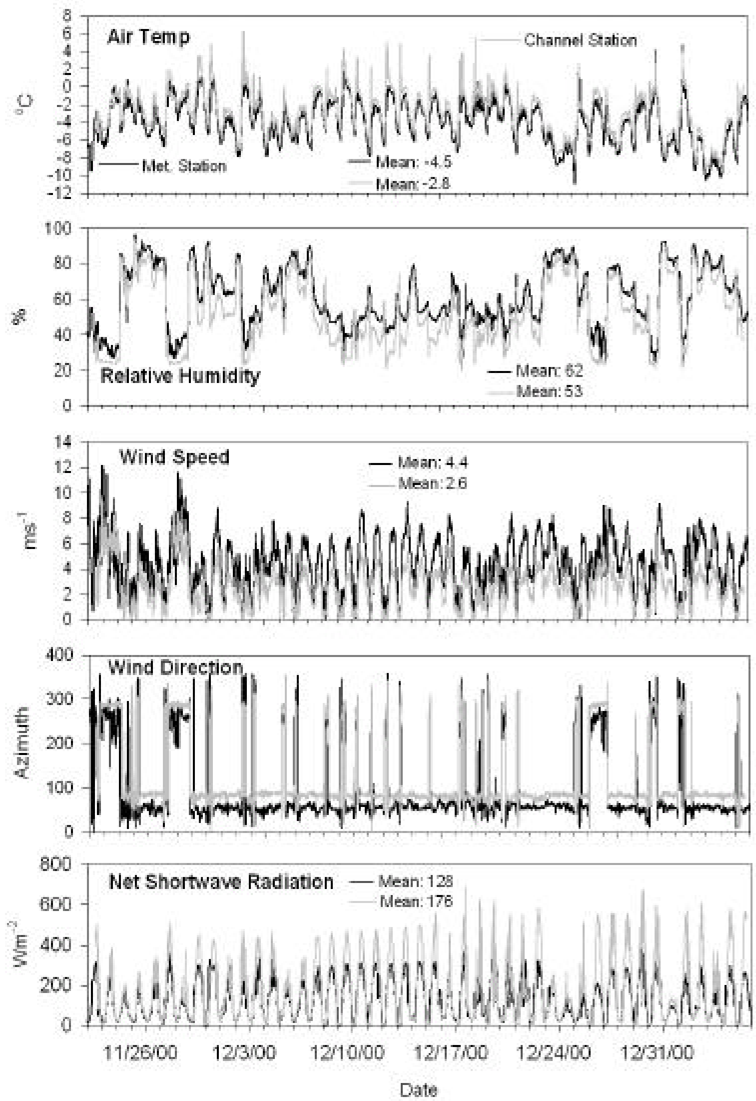

From January 6-15, 2001, two temporary stations were operated simultaneously, one in the North Channel and the other on the glacier surface at the channel periphery (Figure 3.30). The stations were about 2 km down-glacier from the permanent met station. Air temperature was again warmer in the channel, by about 1.3°C (20%), and wind speed was reduced by about 3.1 m s^{-1} (88%). The primary wind direction was

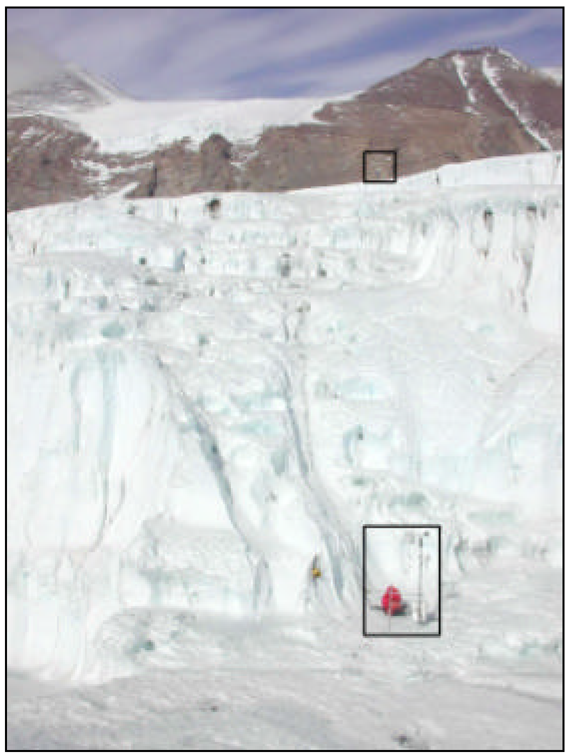

Figure 3.30 – Location of the temporary periphery and channel meteorological stations (outlined in black) near cross-section 11 in the North Channel

up-valley in both locations. However, due to the low wind speed in the channel, wind direction in the channel was more chaotic than at the surface (Figure 3.31). Relative humidity was 5% greater in the channel than at the periphery. Contrary to earlier seasons when net shortwave radiation was greater in the channel, here it was greater at the glacier surface by an average 21 W m^{-2}, which may be attributed to diurnal shading of the channel station. The average hourly values (that is, the average of

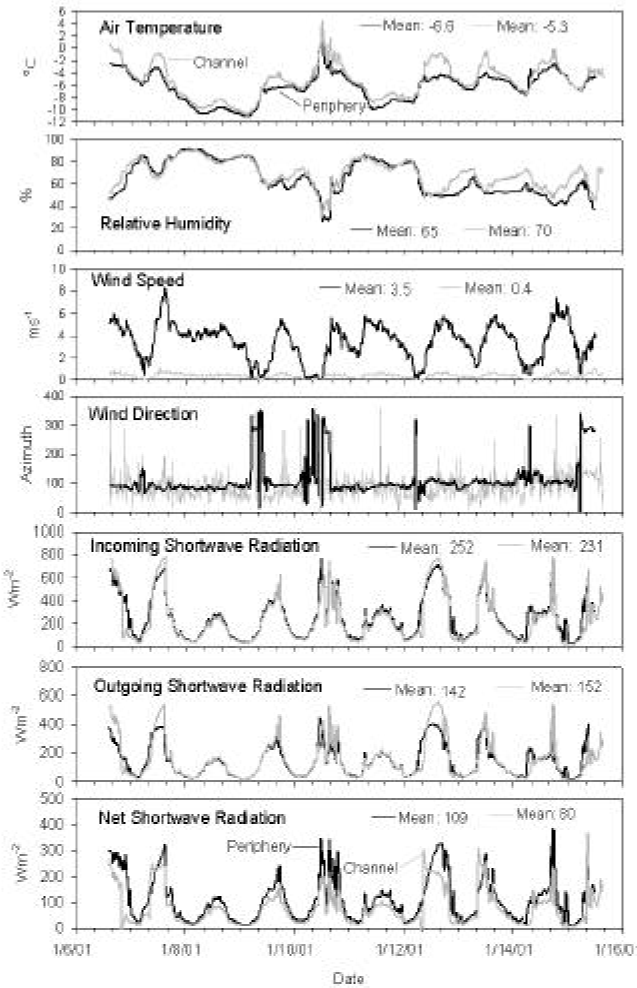

Figure 3.31 - Jan. 6-15, 2001 - Air temperature, relative humidity, wind speed and direction with respect to north, incoming, outgoing, and net shortwave radiation recorded at the temporary stations operated simultaneously and adjacently, at the channel periphery (black) and within the channel (gray).

all 0100, 0200, 0300 hour, etc., records) of incoming and outgoing radiation at the periphery and channel stations over the period of record are shown in Figure 3.32. Indeed, incoming shortwave radiation was smaller at the channel station than the periphery station for nearly all hours of the day, except for those hours when the sun is highest in the sky and incoming radiation is greatest. Outgoing shortwave radiation is greater in the channel during hours of greatest incoming shortwave radiation, and this may be due to reflection off the channel walls.

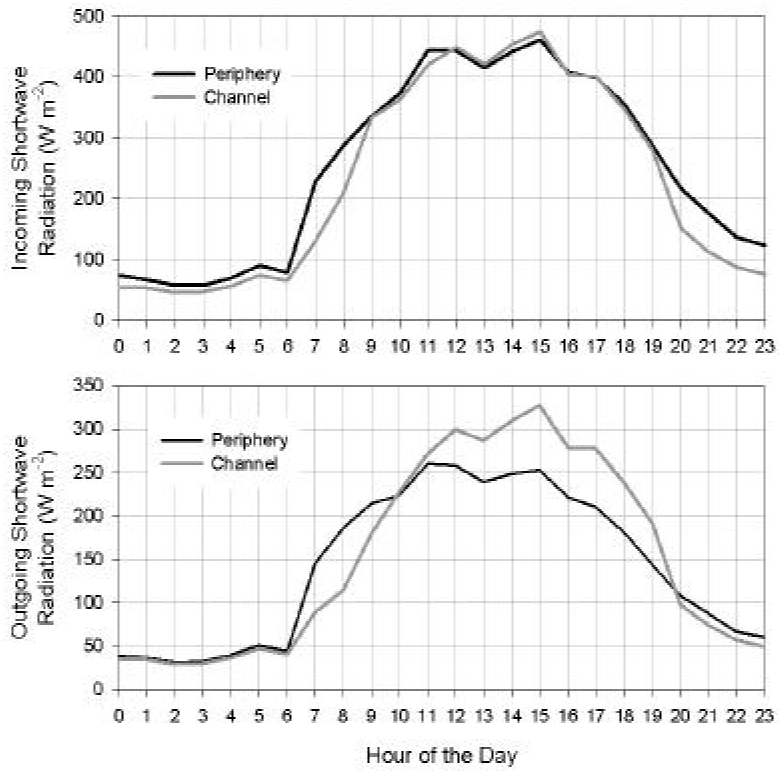

Figure 3.32 – Average per hour incoming and outgoing shortwave radiation at the periphery and channel meteorological stations from Jan. 6-15, 2001.

A great deal of meteorological information from different locations and time periods has been presented in this section. Some of the key findings are summarized in Table 3.3. Considering averages of all the data, a broad generalization can be made about the microclimate in the channels compared to the glacier surface: the channels are warmer by about 1.7°C, wind speed in reduced by about 2.4 m s^{-1}, relative humidity is about the same, and net shortwave radiation is greater in the channel than at the glacier surface.

Table 3.3 – Summary table of average meteorological variables at the surface and in the channels. T is air temperature, WSp is wind speed, RH is relative humidity, and SWnet is net shortwave radiation. For Time Period, t1 is 1/18-25/99, t2 is 11/12/00-1/5/01, and t3 is 1/6-15/01. Surface is either the met station (t1 and t2) or a temporary periphery station (t3). Channel is either the temporary station in the channel 5 km down-glacier from the met station (t1), the one in the channel 3 km down-glacier from the met station (t2), or the one in the channel 2 km down-glacier from the met station (t3) that ran simultaneously with the periphery station at t3. Difference is the change from the surface to the channel.

	Time Period	**Surface**	**Channel**	**Difference**
T (°C)	t1	-1.4	0.7	+2.1
	t2	-4.5	-2.8	+1.7
	t3	-6.6	-5.3	+1.3
			Average Difference	**+1.7**
WSp ($m\ s^{-1}$)	t1	3.5	1.2	-2.3
	t2	4.4	2.6	-1.8
	t3	3.5	0.4	-3.1
			Average Difference	**-2.4**
RH (%)	t1	63	58	-5
	t2	62	53	-9
	t3	65	70	+5
			Average Difference	**-3**
SWnet ($W\ m^{-2}$)	t1	120	143	+23
	t2	128	176	+48
	t3	109	80	-29
			Average Difference	**+14**

Lapse rate: ranges from -0.7 to -1.0°C/100 m. Average is -0.8°C/100 m and is consistent over the two field seasons studied.

3.5 Channel Morphology – A Working Hypothesis

Channels on Taylor Glacier develop from medial moraines that can be traced several kilometers up glacier (Figure 2.24). Unlike thick moraines common to temperate glaciers, these moraines are primarily composed of sporadically distributed boulders (Figure 2.25) interspersed with minor amounts of sand and cobble sized material. The shallow channels that contain the moraine (Figure 3.33) are formed by radiation absorbed by the finer-grained sediment and/or emitted in longwave form by the larger blocks. The blocks and sediment partially melt into the ice. However, winds are high and persistent, so the dominant mechanism of mass loss is sublimation.

Figure 3.33 - Representation of channel appearance as far back as can be traced.

The morphology of the South Channel changes little for several kilometers, maintaining a relatively narrow (width < 10 m) and shallow (depth < 3 m) state (Figure 3.34 a). I define this phase the *1st Steady-State*, during which time the channel widens at << 0.1 m yr^{-1}, deepens at <<0.01 myr^{-1} (Figure 3.34 b), and the width to depth ratio is relatively constant, at about 8. This state continues for roughly 7 km down-glacier, which is approximately equivalent to 1100 years. At ~ 7 km down-glacier, the channel enters the *Transition Phase* and it begins to widen much faster than it deepens. The rate at which the channel widens increases rapidly, to about

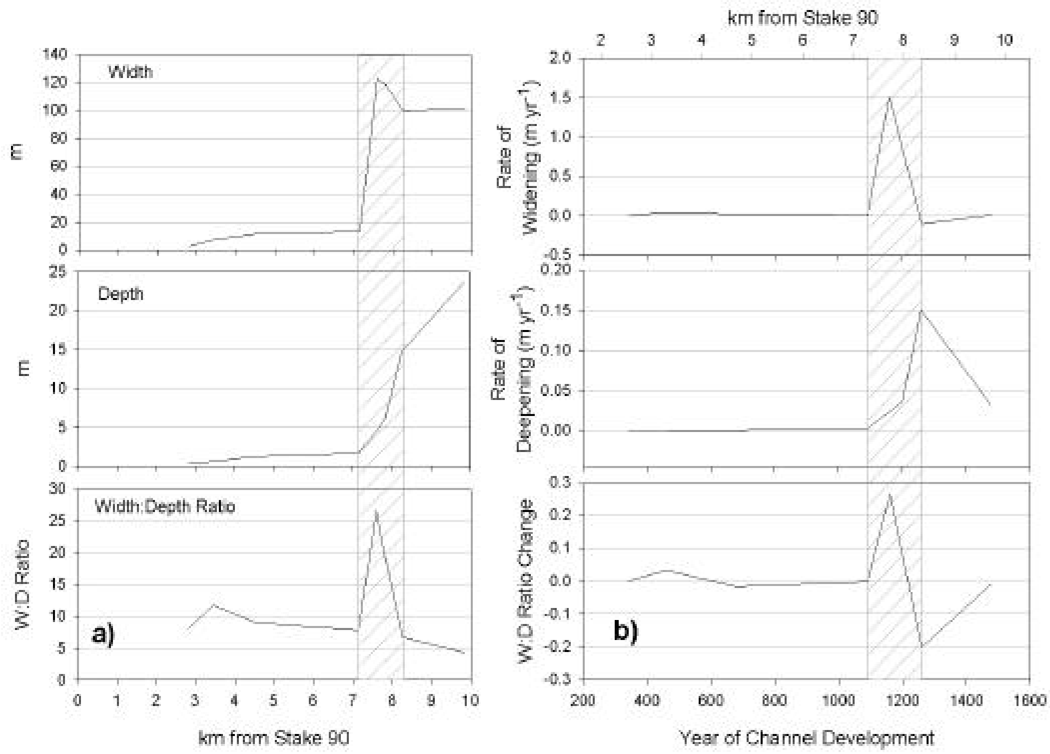

Figure 3.34 - a) Width, depth, and width to depth ratio of South Channel with distance down-glacier, and b) rate of change in width, depth, and width to depth ratio. The *Transition Phase* is hatched.

1.5 m yr^{-1}, then decreases toward a second relative steady-state condition. The rate of deepening in the channel also increases, but at a slower rate and a different spatial trend than the widening. The deepening rate increases throughout the *Transition Phase*, reaching a maximum of about 15 cm yr^{-1} at the down-glacier end of the transition (Figure 3.34 a and b). The width to depth ratio steadily and dramatically increases during the *Transition Phase*, by about 25% a year, to its maximum of 25. The *Transition Phase* covers a time span of about 160 years of channel development over a distance of about 1 kilometer, and the phase terminates when widening has ceased and the rate of deepening is at its maximum, about 8.25 km down-glacier (Figure 3.34 b). Following the *Transition Phase* is the *2nd Steady-State*, the final stage of channel development. This stage is the stage is characterized by a steady decrease in the rate of channel deepening and a return to a steady width to depth ratio. This stage lasts about 220 years over a distance of about 1.5 km. At the end of this stage (reflecting the end of the channel survey), the width to depth ratio is about 4.

What caused the *Transition Phase* of rapid channel growth? The onset of the *Transition Phase* coincides with a local air temperature of about –4.4°C (Figure 3.35), which may be the critical value for enhanced melt within the channel. Indeed, this air temperature also coincides with increased ablation at the glacier surface (Figure 3.35). In the presence of rock debris within the channel, melt should be enhanced due to the slow warming of the rock. Once the channel deepens sufficiently, a microclimate different from the glacier surface develops. The microclimate has reduced winds that reduce sublimation and sensible heat loss, making energy available for melt, which is a much more effective ablative process than sublimation (Chapter 4).

Another cause of channel widening is solar radiation, which supplies its greatest energy when it strikes a surface at a perpendicular angle (90°). The maximum solar angle in the dry valleys is about 36° (Figure 3.36). Thus, at this angle, it supplies the greatest energy to a surface that has a zenith angle of about 54° - or rather, in the case of the channel wall, a horizontal slope angle of 54°. As noted earlier, the average slope of the steeply-inclined, stepped regions along the north-facing wall of the

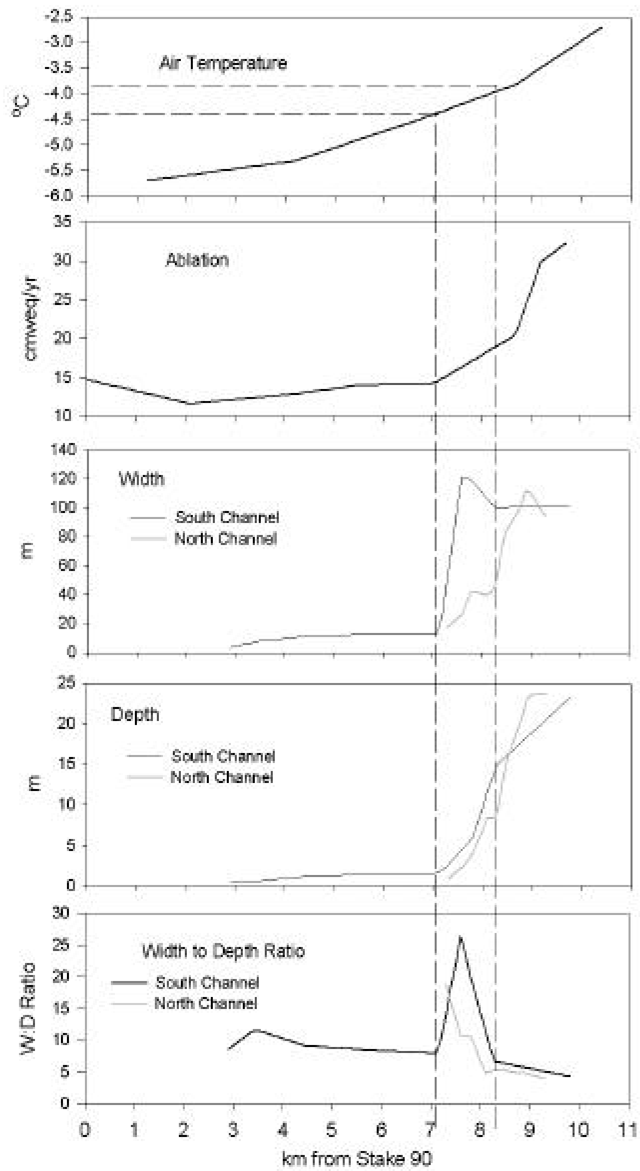

Figure 3.35 - Air temperature, ablation, channel width, depth, and width to depth ratio with distance down-glacier.

North Channel is 60° (Figure 3.8), yielding a solar incident angle of 84°. Therefore, these features might be a reflection of peak solar elevation in the valley.

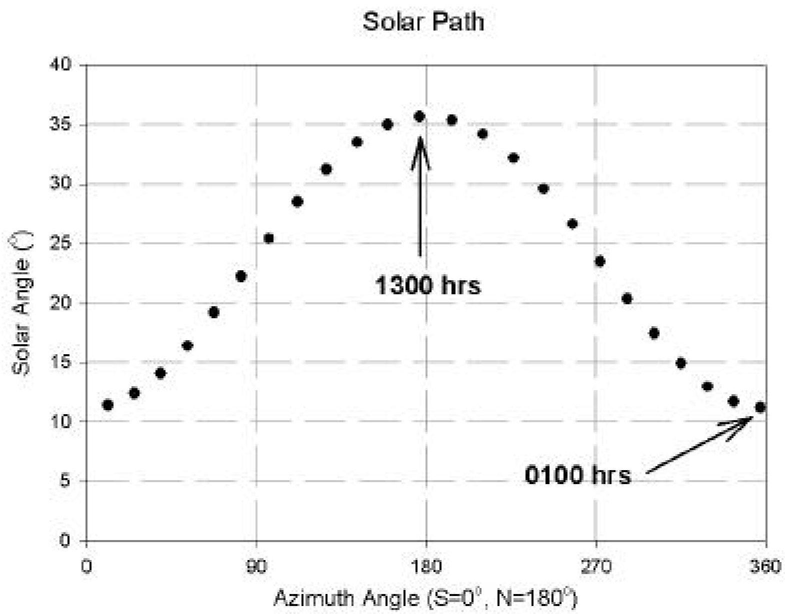

Figure 3.36 – A typical peak summer solar path over Taylor Glacier on December 25, 2000 at the met station.

The average solar angle of the sun when it is in the southern sky (20:00 – 07:00 hours) is about 15°; therefore, it supplies the greatest energy to a surface with a zenith angle of about 75°. In the well-developed down-glacier region of the North Channel, the average slope of the *south-facing* wall is about 25° from horizontal, corresponding to a zenith angle of about 65° and yielding a solar incident angle of 40°. The average solar angle of the sun when it is in the northern sky (08:00-19:00 hours) is about 31°; therefore, it supplies the greatest energy to a surface with a zenith angle of about 59° (Figure 3.37). The average slope of the *north-facing* wall is 30° from horizontal, corresponding to a zenith angle of about 60° and yielding a solar incident angle 61°.

Consequently, the north-facing walls receive more intense (northern sky) radiation at a higher incident angle, while the south-facing walls receive less intense radiation (southern sky) at a more oblique incident angle. Because of this relationship between average solar angles and average channel wall slopes, I believe that channels are in near equilibrium with the solar regime in the valley.

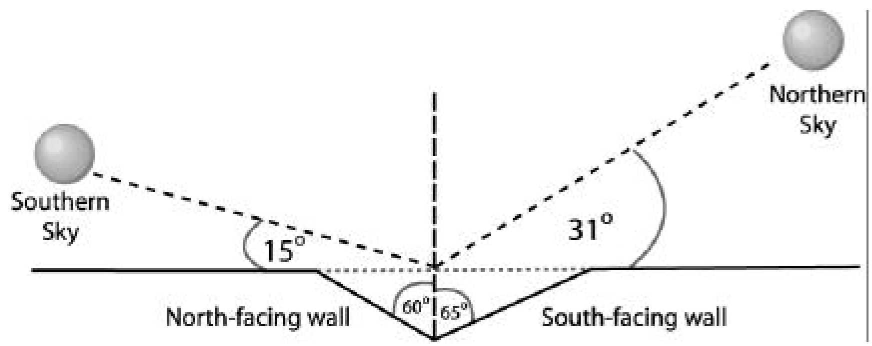

Figure 3.37 - Schematic of average wall angles and average incident solar angles on the channel walls.

As long as these channels continue to widen, cryoconite holes are scavenged as the walls ablate. This process releases sediment within the cryoconite holes to the channel walls and, ultimately, the channel floor. The holes cover about 3% of the glacier area. The average rate of channel widening during the *Transition Phase* is about 0.75 m yr^{-1} and the phase lasts for about 1 km, yielding an area of channel widening of 750 m^2 yr^{-1}. Sediment depth in cryoconite holes on glaciers in Taylor Valley averages 0.5 cm to 3 cm (Porazinska et al., 2003, Accepted; Fountain et al., Submitted February 2003). If I assume that 3% of the area is covered with cryoconite holes and those holes have, on average, 1.5 cm of sediment, then 22.5 m^2 yr^{-1} of cryoconite holes are cannibalized by the channel, yielding a sediment flux of 0.34 m^3 yr^{-1} during the *Transition Phase* of channel development. This is a conservative estimate since it excludes cryoconite holes that are scavenged outside of the *Transition Phase*. Any sediment flux to the system is a positive feedback mechanism, as it lowers albedo within the channel, which leads to increased melt in an already high melt environment.

4 ENERGY BALANCE

While glacier *mass balance* studies are used to track mass change over time, *energy balance* studies define the surplus or deficit of energy at the glacier surface. The energy balance includes short-and-longwave radiation, sensible heat (the transfer of heat energy), latent heat (the transfer of energy through sublimation/condensation and melt/freeze phase changes), subsurface heat conduction (the transfer of heat through the ice column), and melt energy. Energy balance calculations are useful for differentiating between sublimation and melt in the ablation record - they are a bridge between mass balance and regional hydrology.

Spatial and temporal patterns in solar irradiance throughout Taylor Valley show that Taylor Glacier receives more incoming solar radiation and net total radiation than the other glaciers in the valley (Dana et al., 1998). Reasons for this include the aspect of the glacier, minimal shadowing by surrounding terrain, reduced cloud cover, and lower surface albedo due to less snow cover.

Lewis et al. (1998) studied energy balance and ablation rates on Canada Glacier for the 1994-1995 and 1995-1996 summer seasons. The 1995-1996 season was warmer by ~2.3°C. Net radiation was the dominant energy source for both seasons. Latent heat was an important energy loss for both seasons and melt was a significant energy loss for the 1995-1996 season. Sensible and ice heat fluxes were small and both were a minor energy loss the first season only. Sublimation accounted for 80% and 42% of the surface ablation for the 1994-1995 and 1995-1996 seasons, respectively.

Chinn (1987) examined energy fluxes and ablation rates on the glacier surface and marginal cliff of Wright Lower Glacier, located at the eastern end of Wright Valley. He found that ablation rates on vertical faces of the glaciers were 2 to 4 times greater than rates at the nearly horizontal glacier surface. Along the glacier margin where radiation from nearby rock walls was a factor, ablation rates could be 8 times greater than the horizontal glacier surface.

Lewis et al. (1999) compared ablation on the horizontal surface and vertical terminus cliffs on Canada Glacier in Taylor Valley for the 1995-1996 and 1996-1997 summer seasons. Ablation stakes and meteorological stations were erected at the vertical terminus cliffs and compared to the same data collected at the horizontal glacier surface. Wind speeds on the cliff faces were nearly half those recorded on the glacier surface, which resulted in nearly half the sublimation at the cliff face. Ablation at cliff faces was found to be 3 to 6 times greater than on the horizontal surface. Over the period of record, net radiation was greater on the terminus cliff by 10 W m^{-2}, which corresponds to ~ 26 centimeters water equivalent (cm weq) if applied entirely to melt. This value was close to the measured ablation differences between the horizontal glacier surface and the terminus cliff.

4.1 Energy Balance Model

I developed an energy balance model to estimate the melt component of ablation. The model is developed for the glacier surface at the permanent meteorological station where ablation measurements are also taken. Then the model is applied to the channels where the temporary meteorological stations were located. The goal is determine the relative importance of the broad horizontal surfaces and the channels to meltwater generation, and to use this knowledge to estimate the meltwater flux from the channels on Taylor Glacier.

The model is one-dimensional and is based on Paterson's (1994) summary of energy balance equations. The energy balance at an ice surface can be expressed as

$$R + S + L + G + P + M = 0 \qquad (1)$$

where R = net radiation flux, S = sensible heat flux, L = latent heat flux, G = ice heat flux, P = energy supplied through precipitation, and M = energy of fusion (calculated as a residual). *P* is neglected because the rate of precipitation in the dry valleys is so low (<10 cm water equivalent per year (Keys, 1980)) and its temperature is probably close to the ice surface temperature. All the terms in equation (1) are in units of W m^{-2} and the sign convention (Figure 4.1) is positive for energy fluxes toward the glacier-air interface and negative for fluxes away from the interface.

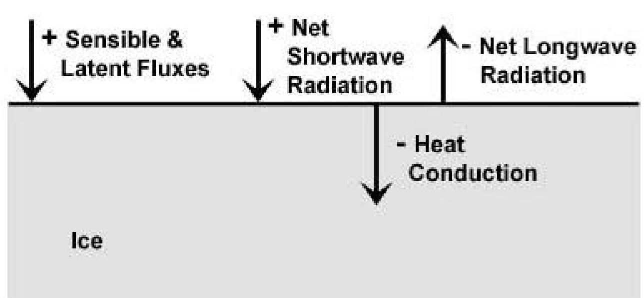

Figure 4.1 – Sign convention for the energy balance terms.

4.1.1 Radiative Heat Flux

Net radiation at the glacier surface is

$$R = SW_{net} + LW_{net} \qquad (2)$$

where SW_{net} and LW_{net} are net shortwave and longwave radiation, respectively. Net shortwave radiation (visible wavelengths, 400-760 nm) is often calculated as incoming minus outgoing radiation. However, this neglects the depth distribution of shortwave radiation in the glacier surface and can lead to overestimations of surface melt (Lewis, 1996). Therefore, I have formulated the net shortwave radiation calculation to take into account radiation absorbed in the surface layer of ice (Hobbs, 1974):

$$SW_{net} = \left[(1-a)SW\downarrow\right](1-e^{(-jz)}) \qquad (3)$$

where α is surface albedo, SW↓ is the incoming radiation flux, j is the absorption coefficient (m^{-1}), and z is the depth into the ice. The absorption coefficient I use, j = 1.6 m^{-1}, is a value adjusted, within reasonable limits, in calibrating the energy balance. The coefficient is a value that depends on several variables: wavelength, incident angle, and ice structure. Grenfell and Perovich (1981), Hobbs (1974), and Perovich (1996) provide comprehensive treatments of this topic, and it is discussed in more detail here in the section on error and sensitivity analysis. The maximum value of z I use is 1 m, consistent with Paterson (1994).

Net longwave radiation (LW_{net}) is the difference between incoming longwave radiation from the atmosphere and outgoing longwave radiation from the surface (LW↓ and LW↑, respectively):

$$LW_{net} = \quad LW\downarrow - LW\uparrow = e_a s\, T_a^4 - e_i s\, T_i^4 \qquad (4)$$

where ε_a and ε_i are air and ice emissivity, respectively (dimensionless), σ is the Stefan-Boltzman constant ($5.67\text{x}10^{-8}$ W m^{-2} K^{-4}), and T_a and T_i are air and ice temperature, respectively in Kelvin (K). The ice emissivity is taken to be 0.95, an average for ice (Arya, 2001). I calculated atmospheric emissivity based on empirically-derived formulas that use atmospheric vapor pressure and air temperature. Three possible formulations are

$$e_a = 0.605 + 0.048 * V_a^{0.5} \text{ (Brunt, 1932),} \qquad (5)$$

$$e_a = 1.08\left[1 - \exp\left(-V_a^{\frac{T_a}{2016}}\right)\right] \text{ (Satterlund, 1979),} \qquad (6)$$

and

$$e_a = 1.24\left(\frac{V_a}{T_a}\right)^{\frac{1}{7}} \text{ (Brutsaert, 1975)} \qquad (7)$$

where V_a is atmospheric vapor pressure in millibars (mb) and T_a is air temperature (K). Atmospheric vapor pressure is

$$V_a = \left[611.2\left(10^{X_a}\right)\right]\left(\frac{RH}{100}\right) \text{ (Goff and Gratch, 1946)} \qquad (8)$$

$$\text{where} \quad X_a = \left[-9.1\left(\frac{T_o}{T_a} - 1\right)\right] - \left[3.6\log_{10}\left(\frac{T_o}{T_a}\right)\right] + \left[0.88\left(1 - \frac{T_a}{T_o}\right)\right] \qquad (9)$$

and T_o is the triple point of water, 273.16 K at 611.2 Pascal (Pa). A fourth possibility is to solve for ε_a from measured incoming longwave radiation,

$$LW \downarrow = e_a s T_a^4 \quad \Rightarrow \quad e_a = \frac{LW \downarrow}{s T_a^4} \qquad (10)$$

Longwave radiation was only measured at the Taylor Glacier met station from 1995 to 1997. Therefore, to decide which of equations 5-7 to use, I calculated ε_a for 1995 to 1997 using equation 10 and compared it to values calculated from equations 5-7.

4.1.2 Turbulent Heat Fluxes

Turbulent heat fluxes include sensible and latent heat. Sensible heat, S (Eq. 11), is the vertical flux of heat through mechanical and natural convection (wind) and a temperature gradient between the ice and the air above it. For example, when the ice is warmer than the air above it, heat is transferred from the ice to the air, and S is negative.

$$S = (1.29x10^{-2}) APu(T_a - T_i) \qquad (11)$$

where A = 0.001 is the transfer coefficient, P = $9.74x10^4$ Pa is the atmospheric pressure, u is wind speed (m s^{-1}), and T_a and T_i are the air and ice temperatures (K), respectively.

The latent heat term, L (Eq. 12), represents the vertical transfer of heat through a phase change from solid or liquid to vapor, or the reverse. For example, when the vapor pressure at the surface is greater than in the air above it, evaporation or sublimation occurs, and L is negative.

$$L = 22.2\, Au\,(V_a - V_i) \qquad (12)$$

where V_a and V_i are the atmospheric and ice surface vapor pressures (Pa), respectively. V_i is calculated in the same way as V_a (Eq. 8), except that humidity at the ice surface is assumed to be saturated, and temperature is the ice temperature, T_i.

Transfer coefficients were used to calculate the turbulent fluxes rather than the more complex Monin-Obukhov similarity theory (Kraus, 1973). The latter accounts for stable and unstable atmospheric conditions but requires a broader set of atmospheric measurements than I have available. The main assumptions with the use of transfer coefficients are that the atmospheric conditions are neutrally buoyant and that the surface conditions are horizontally homogeneous.

4.1.3 Ice Heat Flux

A Note on Ice Temperatures

The energy balance is strongly dependent on ice surface temperature - it is a variable in the outgoing longwave radiation, sensible and latent heat, and ice heat fluxes. The only measured ice temperatures I have are at 0.20 m and 1.0 m depths for the established met station on Taylor Glacier. Ice temperature was not measured at the temporary stations erected during the 2000-2001 field season. Also, the depth of the temperature probes decreased due to ablation at the surface. These limitations are handled by correlating summer air temperatures with ice temperatures for the first year of installation and using the regression equation to estimate ice temperature in the 2000-01 season. Ice temperatures were presumed constant and equal to the average annual air temperature of –16.6°C at 15 m depth (Paterson, 1994). I use the 20 cm ice temperatures as surface temperatures.

The conduction of heat through the ice column is

$$G = -k\frac{\partial T}{\partial z} \qquad (13)$$

where k is the thermal conductivity (W $m^{-1}K^{-1}$) of ice and $\frac{\partial T}{\partial z}$ is the ice temperature gradient (K m^{-1}). The empirical formula for thermal conductivity of pure ice (Paterson, 1994) is

$$k = 9.828\, e^{\left(-5.7x10^{-3}\,T_i\right)} \qquad (14)$$

I calculated k for the first season meteorological data when the ice temperatures were correct and used it in the model. For the energy balance within the channel, I calculated k using ice temperatures predicted by the regression equation.

4.2 Energy Balance Model Results

None of the time-series of atmospheric emissivity calculated using equations 5-7 exhibit the short-term variability in values that were calculated from equation 10 using the measured radiation (Figure 4.2), but they do exhibit the same seasonal fluctuation. Equation 7 consistently underestimates emissivity (c) and equation 5 produces (a). Equation 6 appears to best replicate the variability in emissivity calculated using equation 10 for the 1995 to 1997 data (b). The correlation coefficients of the results from all three equations (5, 6, and 7) with the meteorological based emissivity are 0.41, 0.41,and 0.40, respectively, and although not highly correlated, the correlations are statistically significant at the 95% confidence level. The average atmospheric emissivity from equation 10, based on measured incoming longwave radiation, was 0.66. The average values for emissivity from equations 5, 6, and 7 were 0.67, 0.66, and 0.53, respectively. Therefore, I used use equation 6 for calculating ε_a in my energy balance models.

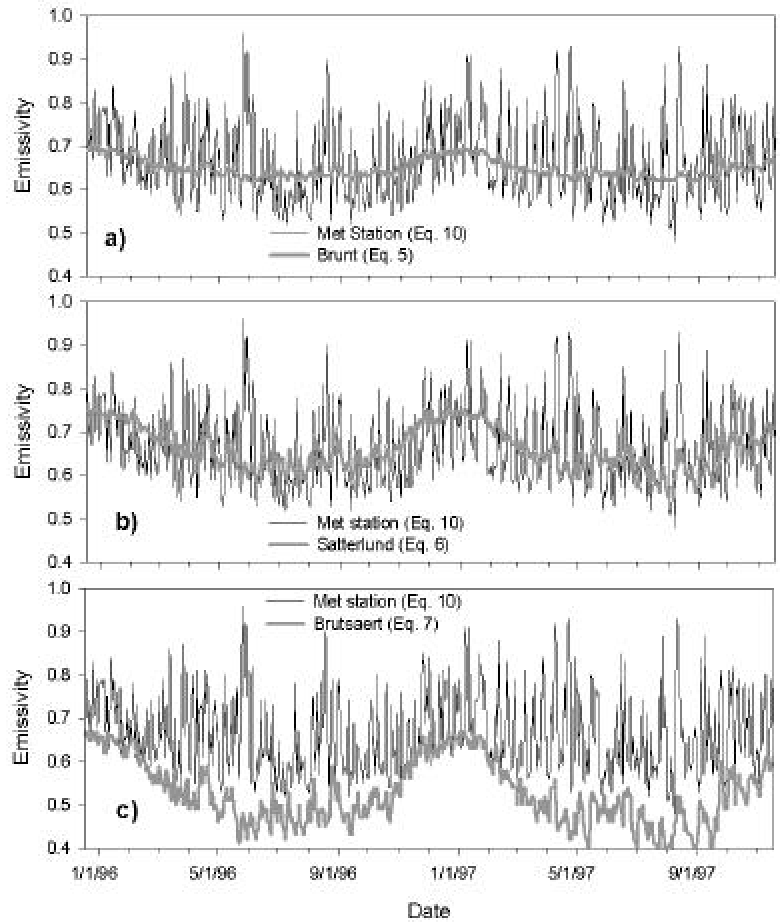

Figure 4.2 - Emissivity as calculated by Eq. 10 (hairline black) from measured meteorological data and the empirically-derived formulas of Eqs. 5, 6, and 7 (thick gray): a) Brunt, b) Satterlund, and c) Brustaert, respectively.

Air temperatures at the meteorological station on Taylor Glacier for the summer 1994-1995 season were better correlated with 0.2 m ice temperatures (r^2 = 0.79) than 1.0 m ice temperatures (r^2 = 0.58). Both correlations are statistically significant at the 95% confidence level (Figure 4.3). However, time-series plots of the air and ice temperatures at the meteorological station, and the ice temperatures resulting from linear regression for the temporary stations (Figure 4.4), illustrate the problems that arise when estimating ice temperatures in this way. Although the 20 cm ice temperatures do respond to air temperatures over the season (a), they don't respond quickly (b). Predictably, using linear regression to estimate ice temperatures results in a perfect correlation with air temperature and a constant difference in 20 cm and 1 m ice temperatures (c and d). This will affect energy balance calculations because many of the terms rely on ice temperature. However, because my model produces average energy balance terms, which I then apply to the season as a whole, this method of estimating ice temperature should suffice.

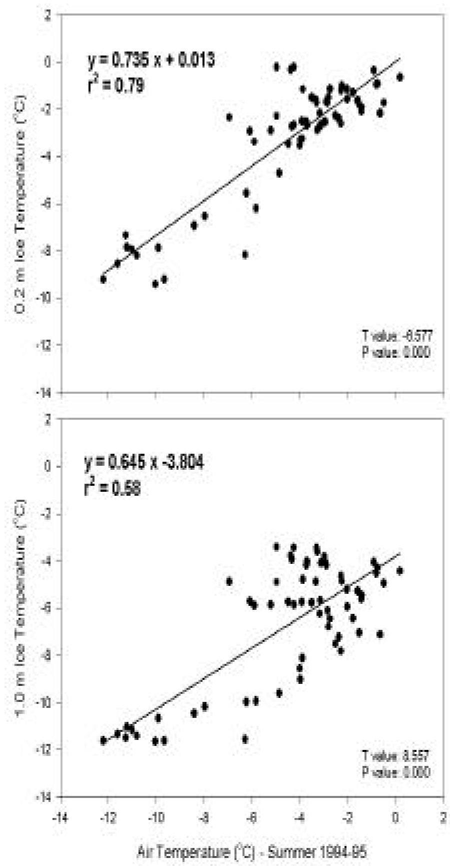

Figure 4.3 – Scatter plots and regression results for measured air and ice temperatures at the meteorological station on Taylor Glacier from 11/21/94 to 1/23/95.

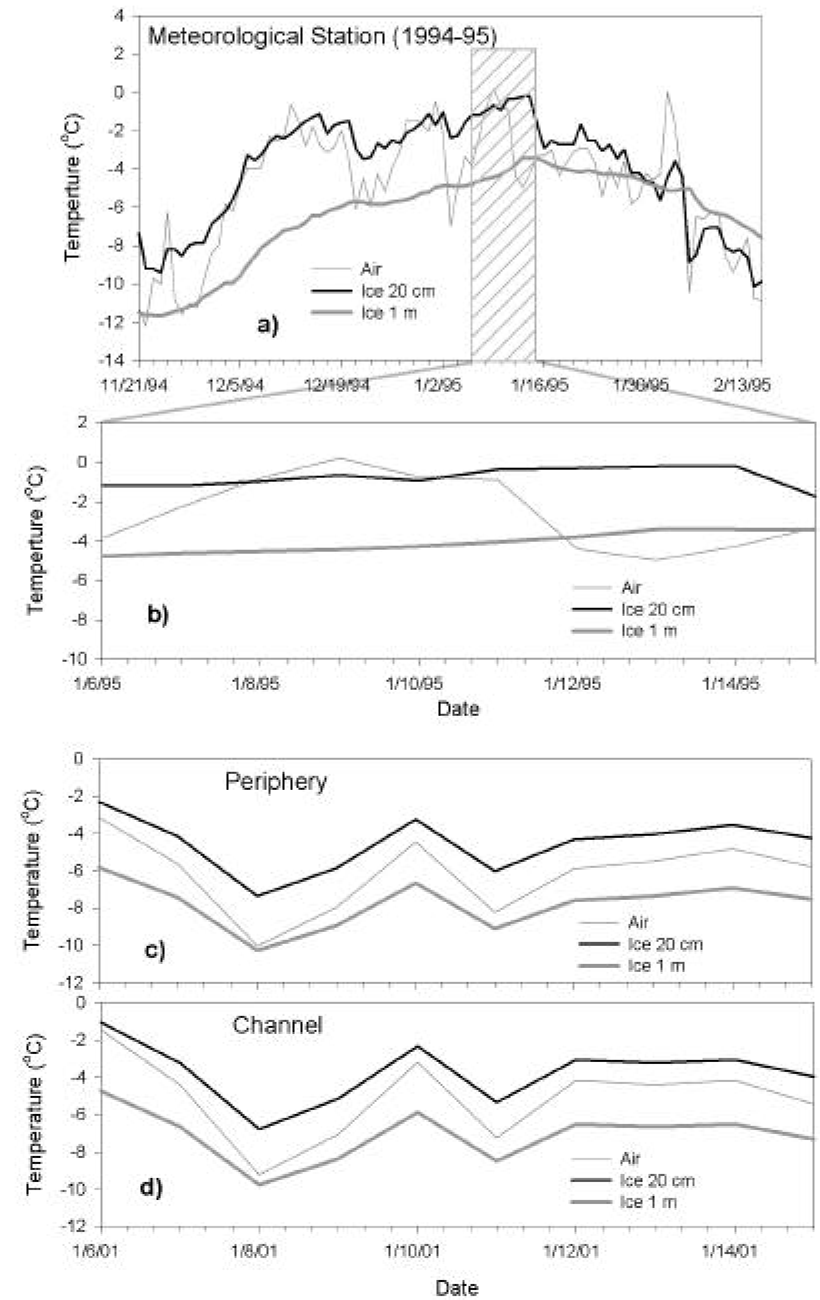

Figure 4.4 - Air and ice temperature time-series plots for the 1994-1995 season at the met station (a) and a 9-day inset of those data (b), and the ice temperatures resulting from regression at the periphery (c) and in the channel (d) for the 2001 field season.

4.2.1 Established Met Station: 1994-1995

The average daily values for sensible heat, S, and latent heat, L, for the summer 1994-95 season at the met station on Taylor Glacier are similar to those reported by Lewis (1996) at Canada Glacier (Table 4.1, Figure 4.5). Average net radiation, R, was greater by about 11 W m^{-2} at Taylor Glacier, which is consistent with a report of a higher overall solar flux in the upper reaches of Taylor Valley (Dana et al., 1998). Ice heat flux, G, at Taylor was greater than on Canada Glacier, possibly because calculations on Taylor Glacier were based on estimated ice temperatures that resulted in a constant temperature difference between 0.2 (surface) and 1 m depths or because of radiational heating of the thermistors on Canada Glacier.

Table 4.1 – Average daily value for energy balance terms for the 1994-95 summer season at Taylor and Canada glacier met stations. All terms are in W m^{-2}. R=net radiation, SWnet=net shortwave, LWnet=net longwave, S=sensible heat, L=latent heat, G=ice heat flux, and M=melt energy. Fluxes toward the surface are positive and fluxes from the surface are negative.

Energy Balance Term	**Taylor Glacier (W m^{-2}) Nov. 21, 1994 - Jan. 23, 1995**	**Canada Glacier (W m^{-2}) Dec. 21, 1994 – Jan. 21 1995**
SW_{net}	112.6	-
LW_{net}	-71.3	-
R	41.3	30.7
S	-6.4	-6.1
L	-22.1	-21.8
G	-10.8	-1.0
M	-2.0	-1.8
Mean Air T (°C)	-4.5	-4.2
Mean Wind Speed (m s^{-1})	4.1	2.9

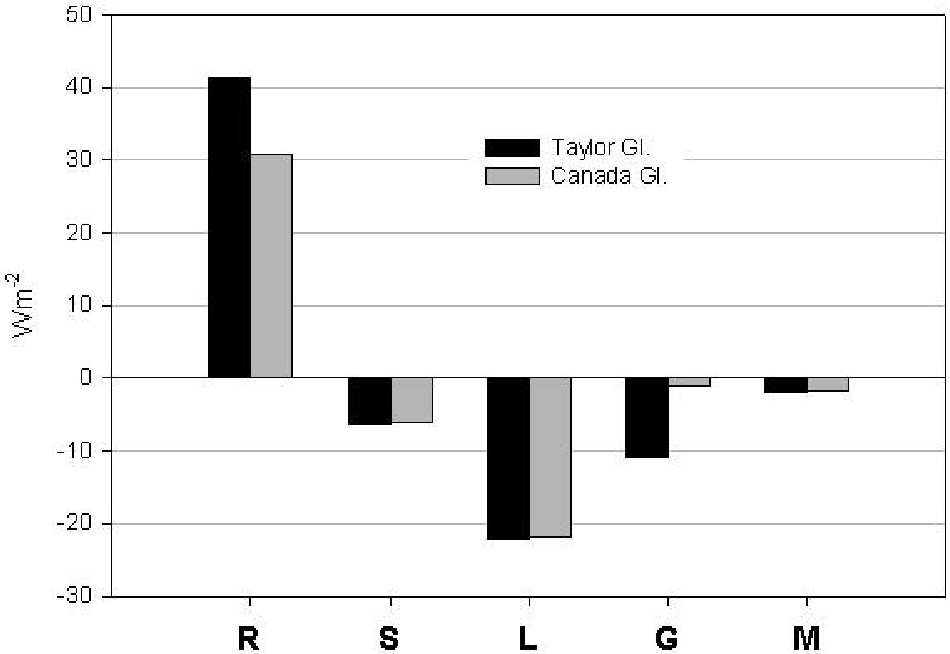

Figure 4.5 – Average energy balance terms for the summer 1994-1995 season at Taylor and Canada glaciers.

Results of the energy balance calculations are compared to measured ablation on Taylor Glacier to verify how well the energy balance model predicts ablation over the season. The measured ablation at stake 83 for the 1994-1995 summer season was –0.7 cm weq, but is believed to be an error (Nylen, 2002). A more accurate estimate is –7.0 cm weq, based on the average of stakes 81 and 85, those closest to stake 83. Average fluxes of -22.1 W m^{-2} for latent heat and –2.0 for melt, extrapolated over a season, correspond to -4.4 cm weq of sublimation (56%) and –3.4 cm weq of melt (44%), respectively, for a total ablation of –7.8 cm weq. Because ablation is measured in cm weq, I discuss the energy balance results in terms of cm weq. The conversion between energy (W m^{-2}) and ablation (cm) is given by Equation 15, where *Subl* is the sublimation rate in cm weq per day, L is latent heat in W m^{-2}, r_w is water density (1000 kgm^{-3}), L_v is the latent heat of vaporization (2.8x10^6 Jkg^{-1}), *Melt* is melt rate in cm weq per day, M is energy for melt in W m^{-2}, L_f is latent heat of fusion (3.34x10^5 Jkg^{-1}), and β (8.64x10^6) converts m s^{-1} to cm weq day^{-1}.

$$Subl = \frac{L}{r_w L_v}(b) \quad and \quad Melt = \frac{M}{r_w L_f}(b) \qquad (15)$$

Considering the errors in the measurements (discussed later), the comparison between the measured ablation value of –7.0 cm weq to the calculated –7.8 cm weq is quite good.

4.2.2 Channel Energy Balance

The slopes of the channel walls depart significantly from the horizontal as the channel develops. The slope of the north-facing wall in the North Channel averages 30.2° and the slope of south-facing wall averages 24.7°. Therefore, the incoming radiation, measured in the horizontal plane, was corrected by dividing by the cosine of the zenith angle of the sun. Additionally, I adjusted the value of the absorption coefficient, j, in the shortwave radiation term (discussed in the sensitivity analysis section). This is reasonable because j, as a function of wavelength, incident angle, and ice structure, varies over 4 orders of magnitude in the visible spectrum of solar radiation (0.01-10 m^{-1} in the 400-800 nm wavelengths) and I used values of j in the same order of magnitude as for the energy balance at the met station.

Net shortwave radiation was about 5 W m^{-2} higher in the channel than at the periphery, while the net longwave radiation was greater at the periphery by about 3 W m^{-2} (Table 4.2). Overall, net radiation was higher within the channel than at the periphery. These results are consistent with the findings of Lewis (2001) for a large basin on Canada Glacier. Both sensible and latent heat fluxes are much lower in the channel than at the periphery (Table 4.2, Figure 4.6 and 4.7), as expected with the reduced wind speed. Ice heat fluxes are similar at both locations. These conditions result in a much higher melt rate and reduced sublimation rate within the channel compared to the periphery. Melt energy was about 8 times greater in the channel than at the periphery.

Table 4.2 - Average daily value for energy balance terms for the 2001 summer season within the channel and at the channel periphery of Taylor Glacier. All terms are in W m^{-2}. R=net radiation, SWnet=net shortwave, LWnet=net longwave, S=sensible heat, L=latent heat, G=ice heat flux, and M=melt energy. Fluxes toward the surface are positive and fluxes from the surface are negative.

Energy Balance Term	**Periphery ($W m^{-2}$) Jan. 6-15, 2001**	**Channel ($W m^{-2}$) Jan. 6-15, 2001**
SW_{net}	106.4	113.3
LW_{net}	-70.6	-67.8
R	35.8	45.5
S	-7.3	-0.6
L	-13.6	-1.5
G	-10.1	-10.3
M	-4.9	-33.0
Mean Air T (°C)	-6.6	-5.3
Mean Wind Speed (ms^{-1})	3.5	0.4

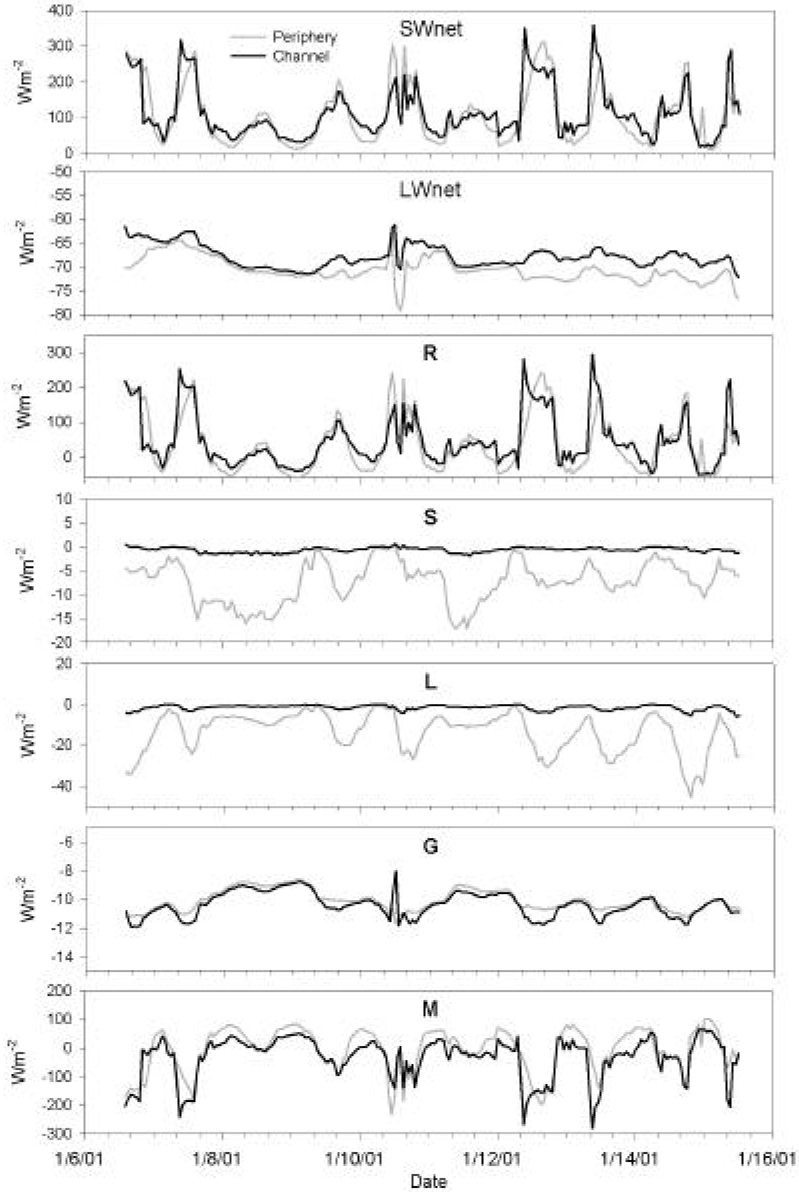

Figure 4.6 - Time series of energy balance terms for the temporary stations during the summer of 2000-2001 at the periphery (gray) and in the channel (black).

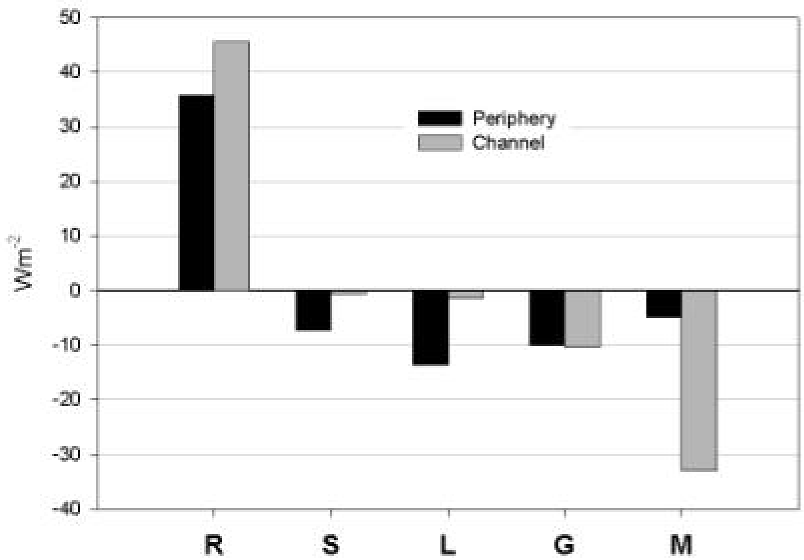

Figure 4.7 - Energy balance fluctuations within the channel and at the periphery for the 2000-2001 summer season. R = net radiation, S= sensible heat, L = latent heat, G = ice heat flux, and M = melt energy calculated as a residual.

The *measured* ablation at stake 79 (closest to the temporary met stations) for the 2000-2001 season (65 days) was -11.2 cm weq. To get the total *modeled* ablation at the periphery, I use Equation 15 for converting latent heat (L) and melt (M) energies to sublimation and melt, respectively, and multiply by 65 days (length of season). The *modeled* ablation at the periphery equates to –10.9 cm weq, with –2.7 cm weq (25%) sublimation and –8.2 cm weq (75%) melt (Table 4.3).

While ablation in the channel wasn't measured during the 2000-2001 field season, it *was* measured during the 2001-2002 field season through a series of stakes in the walls and at the channel floor. These measurements were compared to the measured surface ablation for the same year. On average, measured ablation in the channel was 4.5 times the measured surface ablation. Assuming this surface-to-channel ablation ratio applied to the 2000-2001 season, ablation in the channel would be about –50.4 cm weq (4.5 x -11.2 cm weq). The *modeled* ablation within the channel is about –55.9 cm weq, of which -0.3 cm weq (1%) is due to sublimation and –55.6 cm weq (99%) is due to melt.

Table 4.3 – Modeled and measured ablation in the channel and at the channel periphery. Measured ablation at the periphery is from Stake 79, the closest to the temporary met station.

	Ablation	cm weq
Periphery	Modeled Sublimation	-2.7
	Modeled Melt	-8.2
	Total Modeled Ablation	-10.9
	Measured Ablation	-11.2
Channel	Modeled Sublimation	-0.3
	Modeled Melt	-55.6
	Total Modeled Ablation	-55.9
	Estimated Ablation (4.5 x surface)	-49.3

4.2.3 Error and Sensitivity Analysis

Error associated with the meteorological instrumentation is listed in Table 3.1. These errors must be propagated through the energy balance equations in order to estimate error in the final result. This analysis was done using the general law of error propagation (Eq. 16, Baird, 1962),

$$\sigma_y = \sqrt{\sum \left(\frac{\partial y}{\partial x_i} \right)^2 \sigma_{xi}^{\ 2}} \qquad (16)$$

where σ_y is the error associated with the equation (y), $\partial y/\partial x_i$ is the change in equation y with respect to each variable x_i, i = 1,n where n is the number of variables in the equation, and σ_{xi} is the standard deviation associated with each variable.

The error associated with each term in the energy balance equation is listed in (Table 4.4). The very low error for net longwave radiation results from a ± 0.02°C error in temperature (Doran et al., 2002; Nylen, 2002). The error in the net radiation term is dominated by error in the shortwave radiation and generates an error of ± 14 cm weq in melt calculated over the season. Error in the sensible heat is small (± 8%) and equates to only ± 1 cm weq melt. Errors for latent heat (± 10%) and ice heat flux (± 1%) equate to cm weq melt of ± 2.7 and ± 0.2, respectively. The total error from Equation 16 is ± 8.7 W m^{-2} and equates to ± 14.8 cm weq melt, with the greatest error, with respect to melt equivalent, coming from the incoming shortwave radiation term.

Table 4.4 – Error associated with energy balance terms based on the 1994-95 season at the met station on Taylor Glacier.

Met Station (1994-1995)

Energy Balance Term	Ave. (W m^{-2})	Error (W m^{-2})	% Error	Seasonal Melt Equivalent (cm weq)
SW_{net}	112.6	± 8.5	± 7.6%	±14.3
LW_{net}	-71.3	± << 0.1	± << 1%	-
R	41.3	± 8.5	± 20.6%	±14.3
S	-6.4	± 0.5	± 8%	±0.8
L	-22.1	± 1.6	± 10%	±2.7
G	-10.8	± 0.1	± 1%	±0.2

Assuming that error estimates from the established meteorological station apply to the temporary met stations, error in the net radiation term is ±12.4 and ±15.8 cm weq melt over the season for the periphery and in the channel, respectively (Table

4.5). With the exception of the error in the latent heat term at the periphery station, errors associated with all other terms are relatively small.

Table 4.5 – Error associated with energy balance results from the temporary stations in the channel and at the channel periphery for the 2000-2001 season.

	Periphery 2000-2001			Channel 2000-2001		
Energy Balance Term	Ave. (W m^{-2})	Error (W m^{-2})	Seasonal Melt Equivalent (cm weq)	Ave. (W m^{-2})	Error (W m^{-2})	Seasonal Melt Equivalent (cm weq)
SW_{net}	106.4	± 8.0	±13.5	113.3	± 8.6	±14.4
LW_{net}	-70.6	± << 0.1	-	-67.8	± << 0.1	-
R	35.8	± 7.4	±12.4	45.5	± 9.39	±15.8
S	-7.3	± 0.6	±0.9	-0.6	± 0.05	±0.1
L	-13.6	± 1.0	±1.7	-1.5	± 0.1	±0.2
G	-10.1	± 0.1	±0.2	-10.3	±0.1	±0.2

Sensitivity Analysis

It is important to keep in mind that just 1 W m^{-2} of energy produces 0.20 cm weq sublimation or 1.68 cm weq of melt over a summer season. A simple example of this sensitivity as it applies to the energy balance: the error associated with incoming shortwave radiation instrumentation is ± 3%. The average incoming shortwave radiation for the summer of 1994-1995 was ~349 W m^{-2}, 3% of which is ~10 W m^{-2}. This amount of error alone amounts to ± 17 cm weq of melt over the season, more than double the measured ablation.

Shortwave radiation (Eq. 3) is the only term I adjusted in the energy balance equation. Values of j, the absorption coefficient in ice, range 4 orders of magnitude (0.01-10 m^{-1}) in the visible spectrum (Grenfell and Perovich, 1981; Hobbs, 1974; and

Perovich, 1996), varying with wavelength, incident angle, and ice conditions. I arrived at a value of 1.6 m^{-1} for j by tuning it so that the calculated total ablation (sublimation plus melt) was approximately equal to the measured ablation of –7.0 cm weq over the 1994-1995 season. The effect of changing j on the net shortwave radiation at the glacier surface is illustrated in Table 4.6. For the 1994-1995 summer season at the meteorological station, j had to be between 1.5 and 2 to actually produce melt.

Table 4.6 – Sensitivity analysis in the value of the absorption coefficient, j, and the effect it has on net shortwave radiation and resulting melt equivalent. Altering j has no affect on sublimation.

j (m^{-1}), with z = 1 m	**SWnet (W m^{-2})**	**Resulting Seasonal Melt Equivalent (cm weq)**
0.01	1.40	180.39
0.1	13.43	160.48
1	89.20	35.04
1.5	109.62	1.59
1.75	116.59	-9.94
3	134.08	-38.90
10	141.10	-50.90

Perhaps as a result of different meteorological and ice conditions for the 2000-2001 season, and to account for the incident radiation at the channel walls, I had to adjust j for the energy balance model in the channel and at the periphery. The modeled seasonal melt listed in Table 4.3 results from j values of 3.2 m^{-1} and 1.0 m^{-1} for the periphery and channel, respectively. These values are the same order of magnitude as the value of j used in calculating the energy balance at the met station during the 1994-1995 season.

4.2.4 Meltwater Contribution to Lake Bonney

Streamflow to Lake Bonney is monitored annually by the MCM-LTER at streams that enter the lake. However, water generated within the three large center channels (including the North Channel) at the terminus of Taylor Glacier is not monitored because it flows directly into the lake. I estimated the streamflow from these three channels using some of the results from this thesis: average surface and channel seasonal ablation, survey data to make a rough estimate of area of the North Channel, and fraction of melt from the energy balance within the channel.

The last complete gauging record for streams entering Lake Bonney is from January 1998 to January 1999. The volume change in Lake Bonney over that period was $6.1x10^5$ m^3 (taking into account winter sublimation at the lake surface) and the monitored stream input was $4.6x10^5$ m^3 (LTER, 2001). That leaves a residual volume change of $1.5x10^5$ m^3, which I assume to originate from the channels on Taylor Glacier (Figure 4.8).

The average surface ablation on Taylor Glacier for the summer 1998-1999 seasons was -9.0 cm weq. Ablation measurements in the channel made in 2001-2002 indicate that channel ablation is about 4.5 times the surface ablation. If this holds for the 1998-1999 season and I assume that about 99% of the ablation is attributable to melt (from energy balance model results in the channel), the estimated meltwater volume is $3.4\ x10^4$ m^3 from the North Channel for the 1998-1999 season. Tripling the above estimate to account for the other two (similarly-sized) channels produces

$1.0x10^5$ m^3, which underestimates of the residual volume in the lake by about 33% (Figure 4.8).

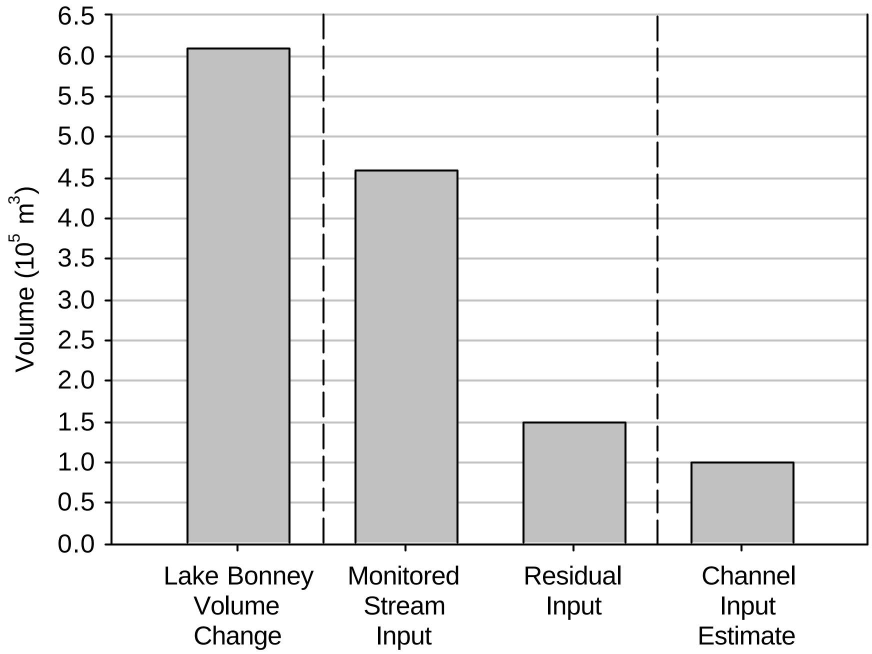

Figure 4.8 - Volume change in Lake Bonney, monitored stream input, and residual input for the 1998-99 summer seasons, as well as input estimate from channels on Taylor Glacier.

This is a very broad estimation of meltwater flow from the channels on Taylor Glacier to Lake Bonney, as it is based on average surface and channel ablation rates, rough estimates of channel area, and an energy balance model with substantial errors. Moreover, my results are relevant to the 2000-2001 season while Lake Bonney measurements were made in 1998-1999. Nevertheless, this study demonstrates the type of stream flow estimates that can be made using survey data and energy balance modeling. A better test of the methodology would make the comparison for a year in which both stream gauge data and energy balance modeling are available.

4.3 Energy Balance Discussion

Energy balance modeling based on the first year meteorological station data (summer 1994-1995) results in an estimated ablation of –7.7 cm weq compared to the measured ablation of –7.0 cm weq, with 44% attributed to melt and 56% to sublimation. The model relies on two estimated parameters - an absorption coefficient used to calculate radiation absorbed by the surface ice and the atmospheric emissivity in the incoming longwave radiation term. The former is tuned using observed and measured ablation at a met station and the latter was computed using observational data and a preferred empirical relationship. The results are similar to fraction of melt (41%) and sublimation (58%) calculated on Canada glacier for the same season (Lewis, 1996).

Energy balance modeling based on data from the temporary meteorological stations operated simultaneously in the channel and on the adjacently periphery from January 6-15, 2001 produces an ablation of –10.9 cm weq, compared to measured ablation of –11.2 cm weq, with –8.2 cm weq (75%) attributed to melt and –2.7 cm weq (25%) to sublimation. If ablation in the channel is indeed about 4.5 times that of surface ablation (as measured in the 2001-2002 summer season), then the modeled ablation of –55.9 cm weq is a reasonable result. Of that modeled ablation, –55.6 cm weq (99%) is attributable to melt and –0.3 cm weq (1%) to sublimation. This percentage may seem rather high, but it is justifiable, given that the average wind speed within the channel was only 0.4 m s^{-1}, and sublimation is strongly dependent on wind speed.

The greatest error in the energy balance equation lies in the net shortwave radiation term, at about $\pm$ 14 cm weq. While the modeled ablation at both the established meteorological station and the temporary periphery station closely resembled the measured ablation, the results fall within this error. This is one of the problems with energy balance models in regions of such low average ablation. However, understanding how sensitive the energy balance is to variables such as the absorption coefficient and atmospheric emissivity, as well as accounting for incident radiation on inclined surfaces, can help to reduce error.

Estimations of meltwater flow from the channels on Taylor Glacier are based on average surface and channel ablation rates, rough estimates of channel area, and spot energy balance results that have large errors. Therefore, these estimations are very broad and shouldn't be used as a substitute to more accurate results from comprehensive temporal and spatial energy balance modeling.

5 CONCLUSIONS

The deeply-incised features in the lower ablation zone of Taylor Glacier in Taylor Valley, Antarctica aren't unique in the valley. This type of feature exists on the lower reaches of Canada and Suess glaciers as well. They *are* unique in Taylor Valley, however, in that they are extensive (traced 10's of km up-glacier), initiate from medial moraines, cover a large region of the lower ablation zone (~ 40%), and are channel-like and aligned with the direction of flow. I hypothesized that as the glacier surface flows to lower elevations, and therefore to warmer air temperatures, the shallow channels rapidly enlarge due to a microclimate in the channels. My results support this hypothesis. Observations and calculations show that the channel microclimate is measurably different from the climate at the glacier surface. On average, the channels are warmer by 1.7°C, wind speed is reduced by 2.4 m s^{-1}, and the net shortwave radiation is greater by about 14 W m^{-2}. As a result, melt makes up a much higher percentage of the total ablation within the channels – energy balance modeling results indicate as much as 75% and perhaps up to 99% under extremely low wind regimes. Therefore, this study has demonstrated that the channels on Taylor Glacier actually produce the water they carry, rather than merely route water generated elsewhere. Reduced albedo within the channels, as a result of sediment cover, also plays a factor in increased melt rates in the channels. The more energy-efficient mass loss by melt versus sublimation also increases ablation.

In the well-developed down-glacier region of the North Channel, the average slope of the south-facing wall is about 25° from horizontal. The average horizontal solar angle in the southern sky is 15°, yielding an incident angle of 40° on the south-facing walls. The average slope of the north-facing wall is 30° from horizontal, and the average horizontal solar angle in the northern sky is 31°, yielding an incident angle of 61°. While the altered microclimate within the channels drives their rapid development during the *Transition Phase*, I believe that this relationship between average wall slopes and solar angles represents the channels coming into equilibrium with the solar regime in the valley. It is interesting to note that only the north-facing walls have a high number of steeply-inclined, stepped regions. These regions have an average slope of 60° that, at the maximum solar elevation of 36°, yields an incident angle of 84°.

The South Channel develops over roughly 1480 years (with respect to the farthest up-glacier fixed location) and goes through a series of stages in its development. The first stage, which I call the *1st Steady State*, is characterized by rather uniform development, where the channel widens and deepens slowly, maintaining a width to depth ratio of about 8. The channel widens at less than 0.1 m yr^{-1} and deepens less than 0.01 m yr^{-1}. The *1st Steady State* lasts for about 1100 years over a distance of about 7 km.

The second stage is the *Transition Phase*, which lasts for only about 160 years and covers a distance of about 1 km. During this stage the channels widen dramatically (from 10 to 110 m) and deepen (from 2 to 24 m). The rate of widening increases to about 1.5 m yr^{-1} in ~ 70 years, and then decreases again nearly as quickly. The rate of change in channel deepening during this stage is less dramatic, and continues to increase throughout the transition. During the height of this stage of channel development, the South Channel is about 25 times as wide as it is deep.

The third stage of channel development is the *2nd Steady State*, which is characterized by a steady decrease in the rate of channel deepening and a return to a steady width to depth ratio. The channel again reaches a near equilibrium state of continued uniform development where the width to depth ratio is about 4.

The *Transition Phase* may reflect a change in atmospheric conditions at the surface. At about the elevation where the *Transition Phase* begins, the surface ablation also begins to increase significantly. The increase in surface ablation coincides with an average air temperature of about –4.4°C. This may be a critical temperature for increased melt in the channels in conjunction with lower albedo sediment within the channels.

While energy balance modeling at the glacier surface and within the channels is a useful tool for differentiating between melt and sublimation in the ablation record, it is sensitive to variables such as the absorption coefficient and atmospheric emissivity, and dependent on accurate values of ice temperature. Over-estimations of melt can result if radiation absorption in the ice isn't accounted for in energy balance modeling. The value of the absorption coefficient can be tuned using observed and measured ablation at the glacier surface. Because of changing surface and channel conditions (meteorological, geometric, and radiative conditions) with distance down-glacier, more comprehensive spatial and temporal energy balance modeling would produce better modeling results than the ‘spot’ energy balance modeling undertaken in this study.

Future Work

Part of this work was based on comprehensive surveying of the channels on Taylor Glacier that produced a detailed picture of spatial and temporal changes in channel morphology. Readily available remote sensing data could be used in conjunction with this data to better define the total channel area. Future modeling of energy balance and meltwater production in the channels should be based on a more comprehensive network of temporary stations to alleviate problems that arise from the ‘spot’ energy balance conducted in this study. A station located at the inception of the *Transition Phase*, one at the glacier terminus, and one half way between the two would cover about 5 km of channel and provide some insight into spatial changes in the channel microclimate. In addition, ice temperature modeling may be a better method by which to estimate ice temperatures than the linear regression method based on air temperatures used in this study. While the errors associated with energy balance modeling in the dry valleys are relatively large, starting with the most accurate ice temperatures possible will help to reduce this error.

REFERENCES

Arya, S. P., 2001, Introduction to Micrometeorology, International Geophysics Series: San Diego, Academic Press, 420 p.

Baird, D. C., 1962, Experimentation: an introduction to measurement theory and experiment design: Englewood Cliffs, New Jersey, Prentice-Hall, Inc.

Benn, D. I., and Evans, D. J. A., 1998, Glaciers & Glaciation: New York, Arnold.

Bromley, A. M., 1985, Weather observations in Wright Valley, Antarctica. Information Publication No 11, New Zealand Meteorological Services, Wellington, 37 p.

Brunt, D., 1932, Notes on radiation in the atmosphere: Quarterly Journal of the Royal Meteorological Society, v. 58, p. 389-420.

Brutsaert, W., 1975, On a derivable formula for long-wave radiation from clear skies: Water Resources Research, v. 11, no. 5, p. 742-744.

Chinn, T. J. H., 1987, Accelerated ablation at a glacier ice-cliff margin, dry valleys, Antarctica: Arctic and Alpine Research, v. 19, no. 1, p. 71-80.

Dana, G. L., Wharton Jr., R. A., and Dubayah, R., 1998, Solar radiation in the McMurdo Dry Valleys, Antarctica: Ecosystem Dynamics in a Polar Desert: The McMurdo Dry Valleys, Antarctica. Antarctic Research Series, v. 72, p. 39-64.

Denton, G. H., Bockheim, J. G., Wilson, S. C., and Stuiver, M., 1989, Late Wisconsin and Early Holocene Glacial History, Inner Ross Embayment, Antarctica: Quaternary Research, v. 31, p. 151-182.

Doran, P. T., McKay, C. P., Clow, G. D., Dana, G. L., Fountain, A. G., Nylen, T., and Lyons, W. B., 2002, Valley floor climate observations from the McMurdo dry valleys, Antarctica, 1986-2000: Journal of Geophysical Research, v. 107, no. D24, p. 4772.

Drewry, D. J., Jordan, S. R., and Jankowski, E., 1982, Measured properties of the Antarctic ice sheet: surface configuration, ice thickness, volume and bedrock characteristics: Annals of Glaciology, v. 3, p. 83-91.

Fountain, A., G., Lyons, W. B., Burkins, M. B., Dana, G. L., Doran, P. T., Lewis, K. J., McKnight, D. M., Moorhead, D. L., Parsons, A. N., Priscu, J. C., Wall, D. H., Wharton Jr., R. A., and Virginia, R. A., 1999a, Physical Controls on the Taylor Valley Ecosystem, Antarctica: BioScience, v. 49, no. 12, p. 961-971.

Fountain, A. G., 2001, Velocity data on Taylor Glacier, unpublished data.

Fountain, A. G., Dana, G. L., Lewis, K. J., Vaughn, B. H., and McKnight, D. M., 1998, Glaciers of the McMurdo Dry Valleys, Southern Victoria Land, Antarctica: Ecosystem Dynamics in a Polar Desert: The McMurdo Dry Valleys, Antarctica. Antarctic Research Series., v. 72, p. 65-75.

Fountain, A. G., Lewis, K. J., and Doran, P. T., 1999b, Spatial climatic variation and its control on glacier equilibrium line altitude in Taylor Valley, Antarctica: Global and Planetary Change, v. 22, p. 1-10.

Fountain, A. G., Tranter, M., Nylen, T. H., Lewis, K. J., and Mueller, D., Submitted February 2003, Evolution of cryoconite holes and their contribution to meltwater runoff from glaciers in the McMurdo Dry Valleys, Antarctica: Journal of Glaciology.

Freckman, D. W., and Virginia, R. A., 1998, Soil biodiversity and community structure in the McMurdo Dry Valleys, Antarctica, *in* Priscu, J. C., ed., Ecosystem dynamics in a polar desert: The McMurdo Dry Valleys, Antarctica: Antarctic Research Series: Washington D.C., American Geophysical Union, p. 323-335.

Goff, J. A., and Gratch, S., 1946, Low-pressure properties of water from -160F to 212F: Transactions of the American Society of Heating and Ventilating Engineers, v. 52, p. 95-121.

Grenfell, T. C., and Perovich, D. K., 1981, Radiation absorption coefficients of polycrystalline ice from 400-1400 nm: Journal of Geophysical Research, v. 86, no. C8, p. 7447-7450.

Hall, B. L., Denton, G. H., Lux, D. R., and Bockheim, J. G., 1993, Late Tertiary Antarctic paleoclimate and ice-sheet dynamics inferred from surficial deposits in Wright Valley: Geografiska Annalar, no. 75A, p. 239-268.

Hendy, C. H., Healy, T. R., Rayner, E. M., Shaw, J., and Wilson, A. T., 1979, Late Pleistocene Glacial Chronology of the Taylor Valley, Antarctica, and the Global Climate: Quaternary Research, v. 11, p. 172-184.

Hobbs, P. V., 1974, Ice Physics: Oxford, Clarendon Press.

Keys, J. R., 1980, Air temperature, wind, precipitation and atmospheric humidity in the McMurdo region.: Department of Geology Publication No.17, Victoria University of Wellington, New Zealand. Antarctic Data Series No.9.

Kraus, H., 1973, Energy-exchange at air-ice interface: IAHS, v. 107, p. 128-162.

Langevin, P., 1998, Ice measurements from ground penetrating radar, unpublished data.

Lewis, K. J., 1996, Surface energy balance and meltwater production for a dry valley glacier, Taylor Valley, Antarctica: University of Colorado, 102 p.

-, 2001, Solar-forced roughening of Antarctic glaciers and the Martian icecaps: How surficial debris and roughness affect glacial melting in Taylor Valley, Antarctica and how this can be applied to the Martian icecaps [Dissertation thesis]: University of Colorado, 182 p.

Lewis, K. J., Fountain, A. G., and Dana, G. L., 1998, Surface energy balance and meltwater production for a Dry Valley glacier, Taylor Valley, Antarctica: Annals of Glaciology, v. 27, p. 603-609.

-, 1999, How important is cliff melt?: a study of the Canada Glacier terminus, Taylor Valley, Antarctica: Global and Planetary Change, v. 22, p. 105-115.

LTER, 2001, The US Long Term Ecological Research Network, http://lternet.edu/.

Marchant, D. R., Lewis, A., Phillips, W. C., Moore, E. J., Souchez, R., and Landis, G. P., 2002, Formation of patterned-ground and sublimation till over Miocene glacier ice in Beacon Valley, Antarctica: Geological Society of America Bulletin, v. In Press.

McIntyre, N. F., 1984, Cryoconite hole thermodynamics: Canadian Journal of Earth Sciences, v. 21, p. 152-156.

MCM-LTER, 2001, McMurdo Dry Valleys Long-Term Ecological Research (LTER), http://huey.colorado.edu/LTER/.

Meier, M. F., 1960, Mode of flow of Saskatchewan Glacier, Alberta, Canada: U.S. Geological Survey Professional Paper, v. 351.

Moorhead, D. L., and Priscu, J. C., 1998, The McMurdo Dry Valley ecosystem: organization, controls, and linkages, *in* Priscu, J. C., ed., Ecosystem dynamics in a polar desert: the McMurdo Dry Valleys, Antarctica: Antarctic Research Series: Washington, D.C., American Geophysical Union, p. 351-363.

Nakawo, M., Raymond, C. F., and Fountain, A., 2000, Debris-covered glaciers: Oxfordshire, IAHS, p. 288.

NSF, 1999, McMurdo Dry Valleys Long-Term Ecological Research (LTER) , Project Overview, http://huey.colorado.edu/LTER/project.html, Institute for Arctic and Alpine Research.

Nye, J. F., 1952, The mechanics of glacier flow: Journal of Glaciology, v. 2, p. 82-93.

-, 1958, A theory of wave formation on glaciers: IASH, v. 47, p. 139-154.

Nylen, T., 2002, Personal Communication: MCM-LTER mass balance and meteorological station coordinator in Taylor Valley since 1999.

Ostrem, G., 1959, Ice melting under a thin layer of moraine and the existence of ice in moraine ridges.: Geografiska Annaler, v. 41, p. 228-230.

Paterson, W. S. B., 1994, The Physics of Glaciers: Oxford, Pergamon.

Perovich, D. K., 1996, The optical properties of sea ice, CRREL Monograph.

Podgorny, I. A., and Grenfell, T. C., 1996, Absorption of solar energy in a cryoconite hole: Geophysical Research Letters, v. 23, no. 18, p. 2465-2468.

Porazinska, D. L., Fountain, A. G., Nylen, T. H., Tranter, M. L., and Virginia, R. A., 2003, Accepted, The biodiversity and biogeochemistry of cryoconite holes from McMurdo Dry Valley glaciers, Antarctica: Artic, Antarctic, and Alpine Research.

Satterlund, D. R., 1979, An improved equation for estimating long-wave radiation from the atmosphere: Water Resources Research, v. 15, no. 6, p. 1649-1650.

Schafer, J. M., Baur, H., Denton, G. H., Ivy-Ochs, S., Marchant, D. R., Schluchter, C., and Wieler, R., 2000, The oldest ice on Earth in Beacon Valley, Antarctica: new evidence from surface exposure dating: Earth and Planetary Science Letters, v. 179, p. 91-99.

Scott, C. R. F., 1905, The Voyage of the 'Discovery': London, John Murray, 556 p.

Taylor, G., 1916, With Scott: The Silver Lining: New York, Dodd, Mead and Company.

Waddington, E. D., 1986, Wave ogives: Journal of Glaciology, v. 32, p. 325-334.

Wharton Jr., R. A., McKay, C. P., Simmons Jr, G. M., and Parker, B. C., 1985, Cryoconite holes on glaciers: BioScience, v. 35, no. 8, p. 499-503.

Wilch, T. R., Denton, G. H., Lux, D. R., and McIntosh, W. C., 1993, Limited Pliocene glacier extent and surface uplift in Middle Taylor Valley, Antarctica: Geografiska Annalar, no. 75A, p. 331-351.

Appendix A – Survey Data Sample

Below is a small sample of the survey data from the cross-sections for the North Channel and South Channel (Appendix B) on Taylor Glacier. All points in the survey for each channel were reported with respect to northing and easting from the southern most point of the first cross-section. Therefore, all points in each cross-section were normalized to that particular cross-section to determine true distance across the channel. The columns numbered 1 through 5 are the raw survey data. The others are data created from the normalization.

Sample of survey data for cross-sections in the North and South channels. All survey points in the cross-sections were shot with respect to the control point 1A (last line) and were then normalized to obtain distance across channel. Columns numbered 1-5 are the data. The others are created from normalization.

	1	2			3				4	5
	POINT	EASTING	m E of 1A	E normed	NORTHING	m N of 1A	N normed	m across channel from A	ELEVATION	ALBEDO
XC 01	1B	1519.19	-4.81	-4.81	1542.61	18.61	18.61	19.22	262.81	62
	101	1519.82	-4.18	-4.18	1540.18	16.18	16.18	16.71	264.03	66
	102	1520.02	-3.98	-3.98	1539.40	15.40	15.40	15.91	263.96	55
	103	1520.14	-3.86	-3.86	1538.96	14.96	14.96	15.45	263.77	62
	104	1520.45	-3.55	-3.55	1537.75	13.75	13.75	14.20	263.63	59
	105	1520.75	-3.25	-3.25	1536.57	12.57	12.57	12.98	263.62	81
	106	1521.45	-2.55	-2.55	1533.89	9.89	9.89	10.21	263.67	61
	107	1522.40	-1.60	-1.60	1530.19	6.19	6.19	6.39	263.98	79
	108	1523.19	-0.81	-0.81	1527.15	3.15	3.15	3.25	264.22	61
	1A	1524.00	0.00	0.00	1524.00	0.00	0.00	0.00	264.50	63

Appendix B - South Channel Cross-Sections

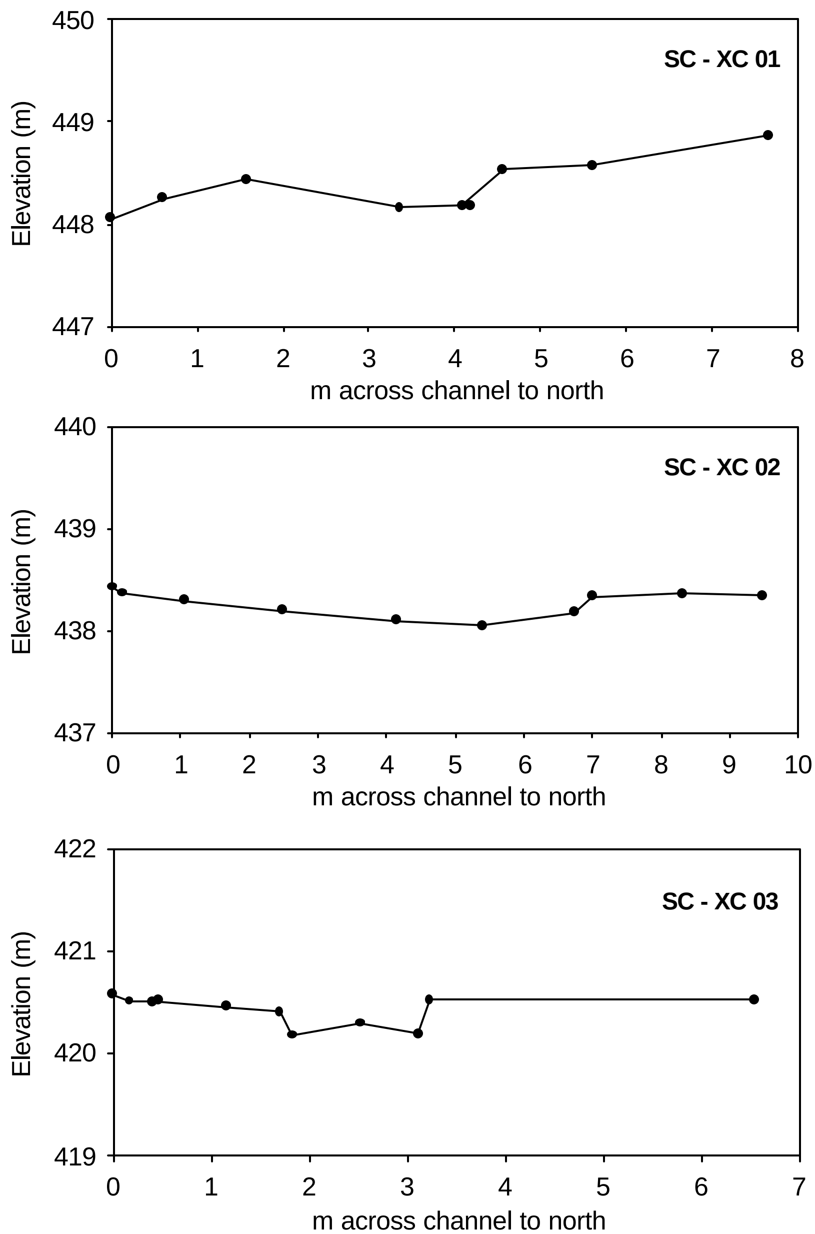

Cross-sections 1-3 of the South Channel (SC).

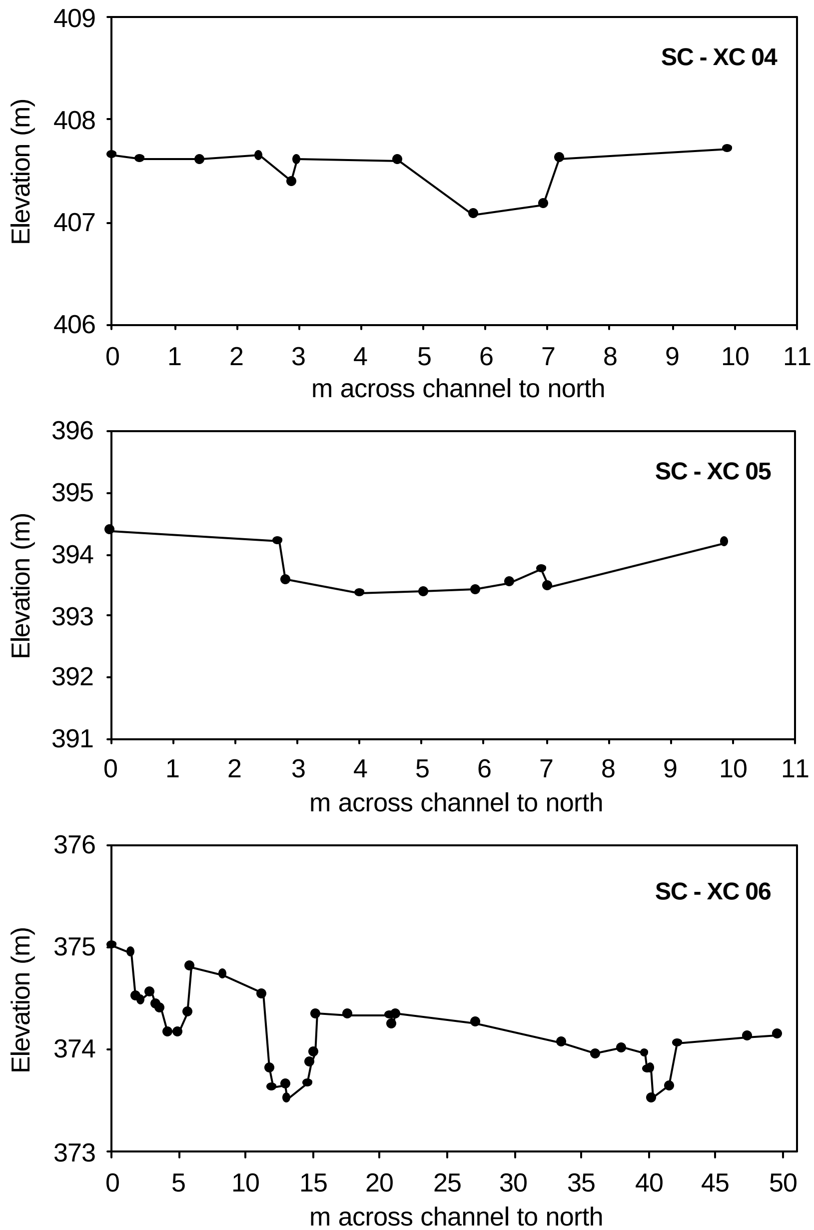

Cross-sections 4-6 of the South Channel (SC).

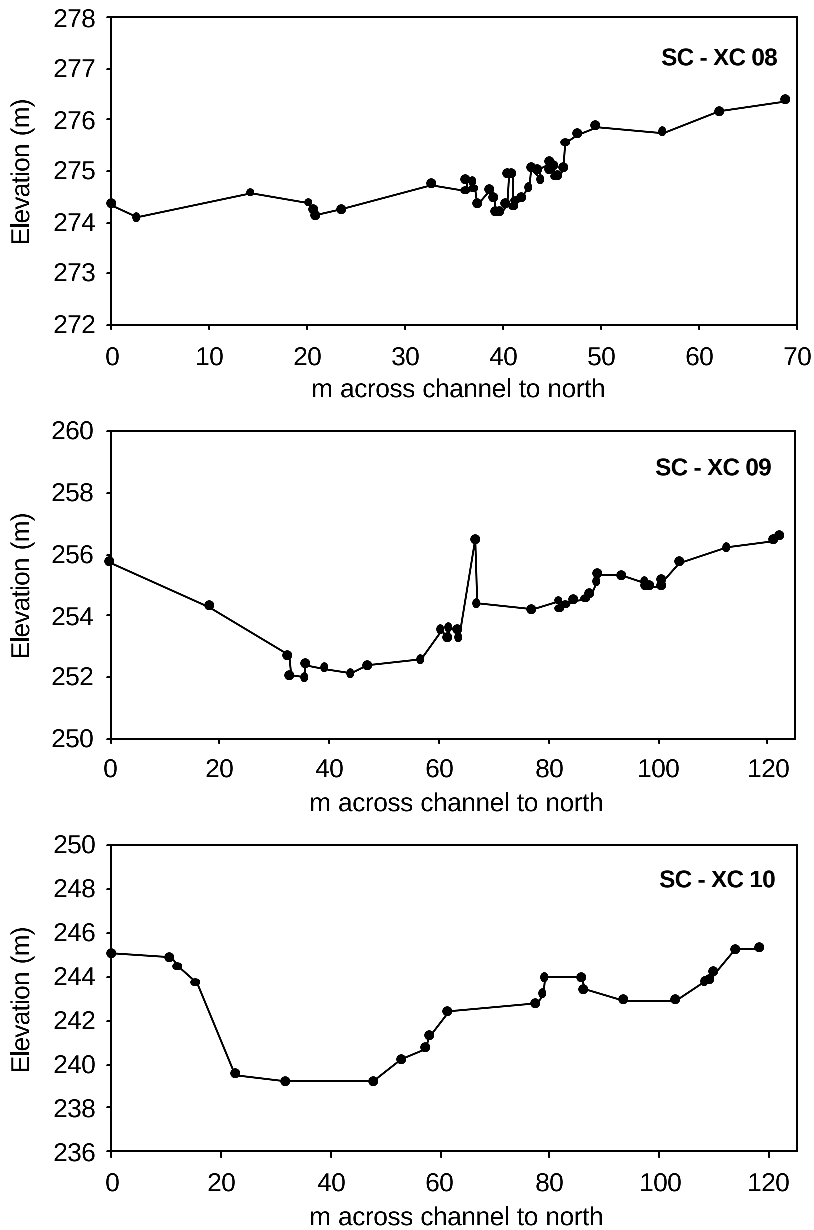

Cross-sections 8-10 of the South Channel (SC).

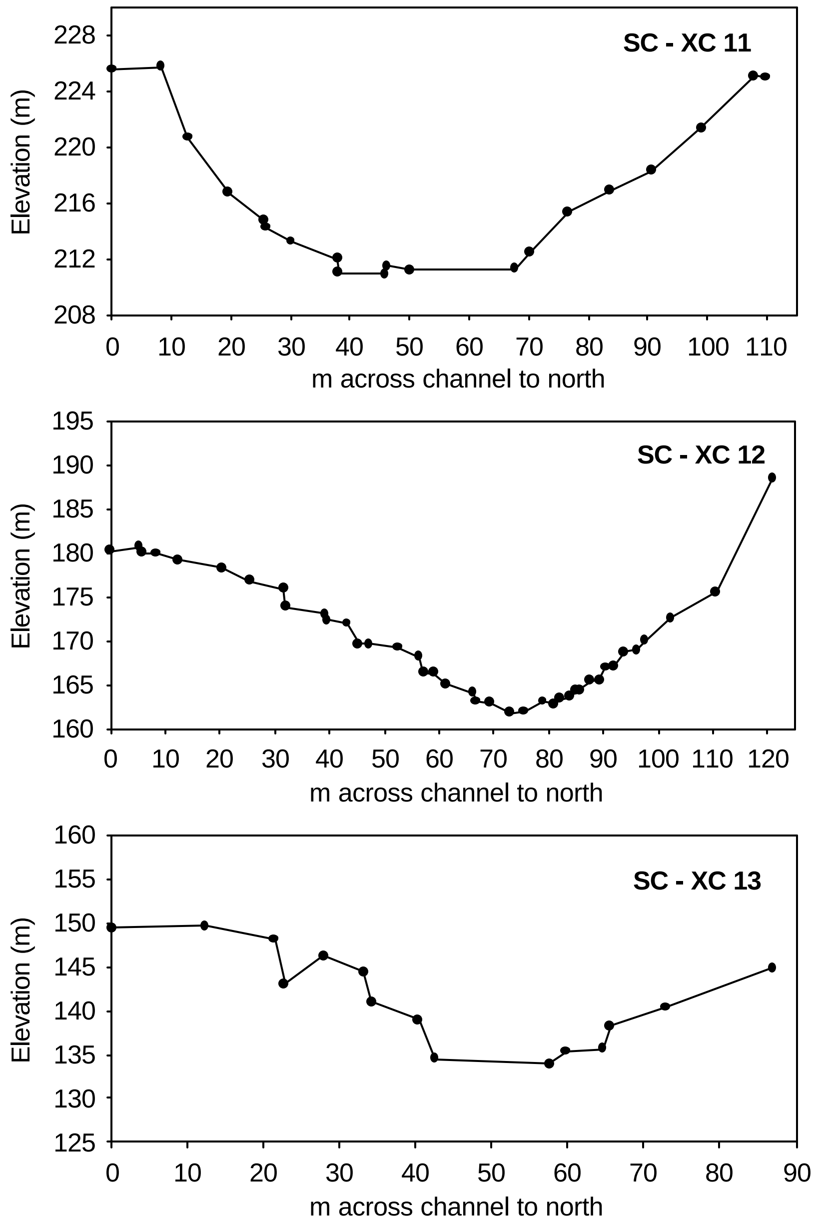

Cross-sections 11-13 of the South Channel (SC).

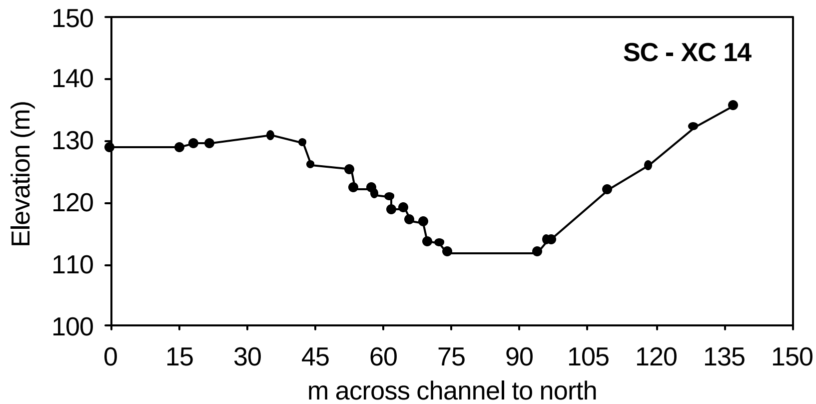

Cross-section 14 of the South Channel (SC).

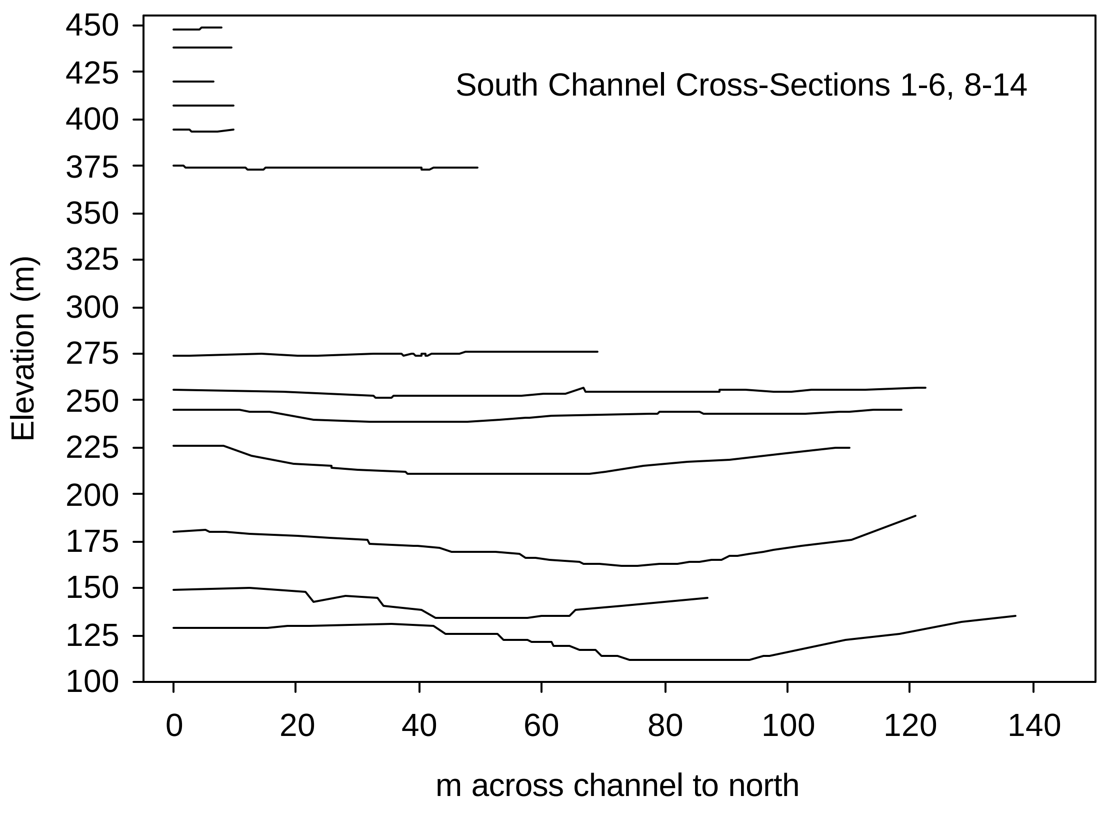

Cross-sections 1-6 and 8-14 of the South Channel, without any respect to distance down-glacier.

Appendix C - North Channel Cross-Sections

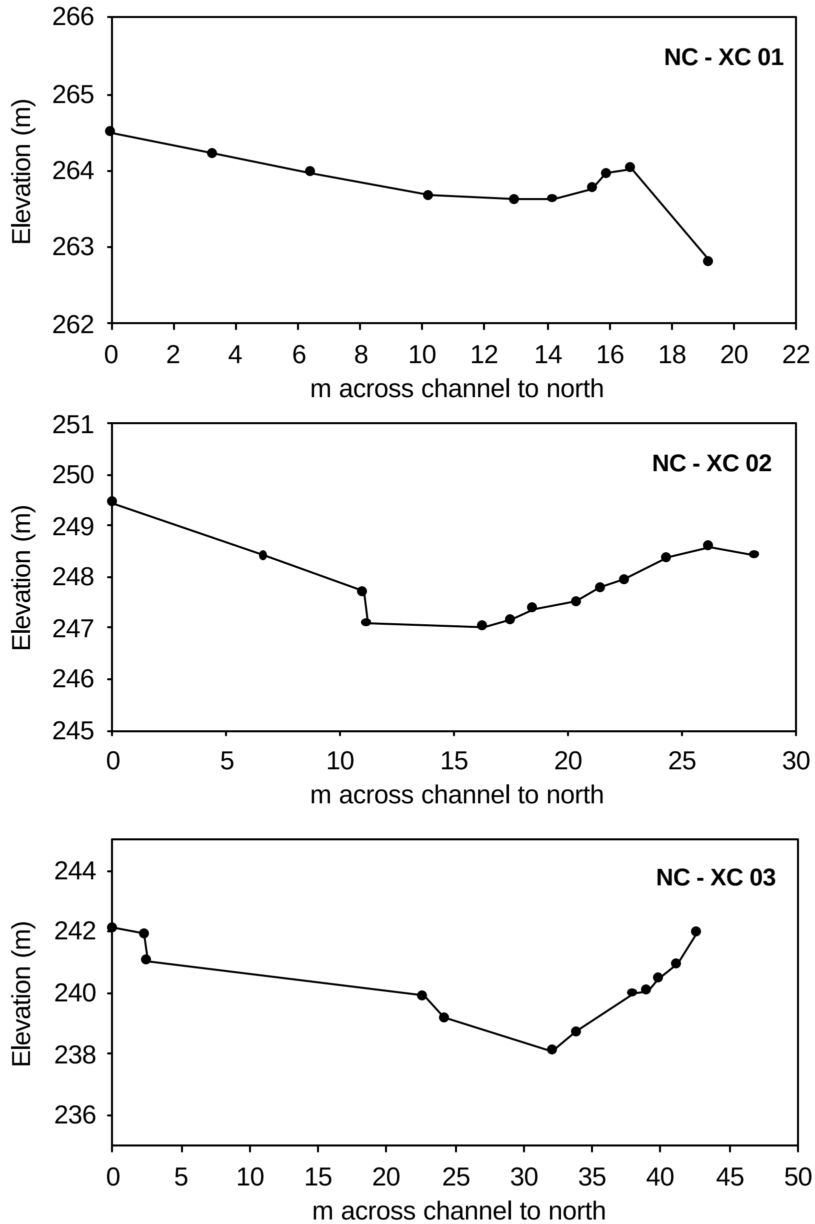

Cross-sections 1-3 of the North Channel (NC).

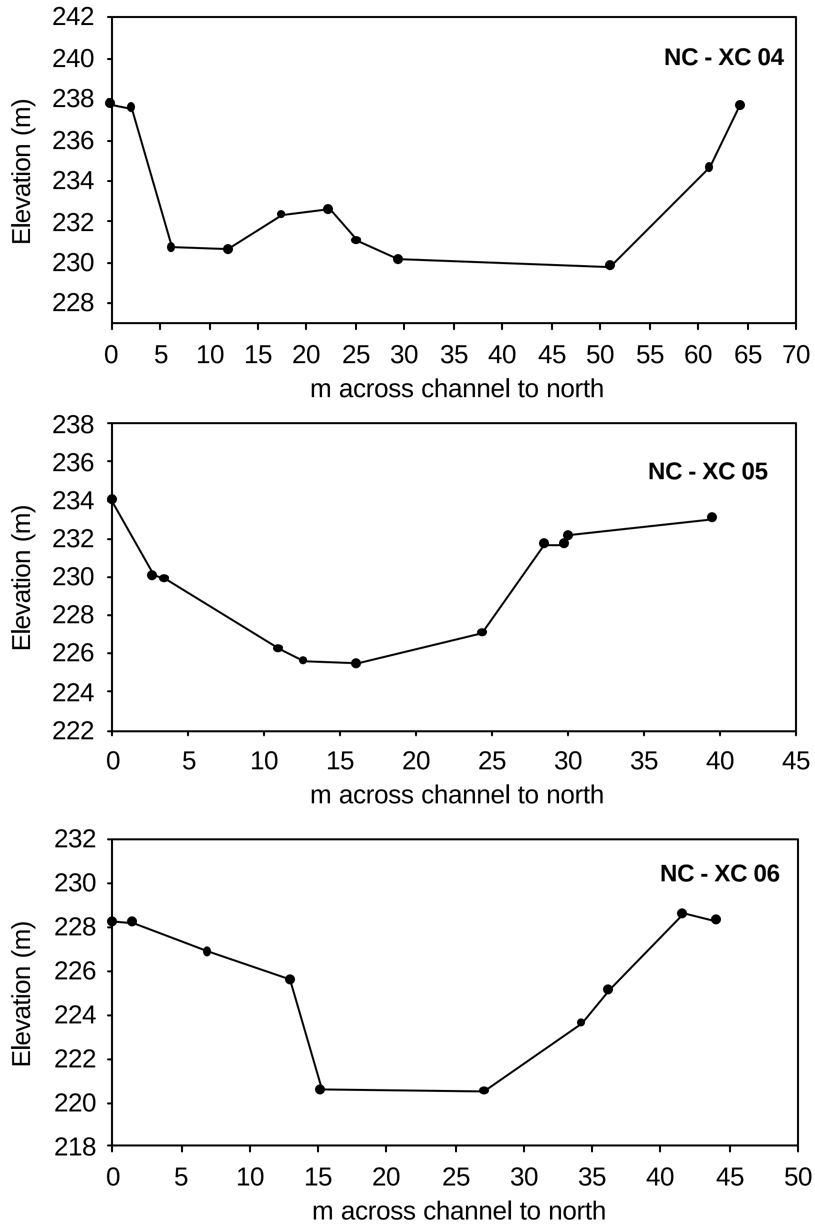

Cross-sections 4-6 of the North Channel (NC).

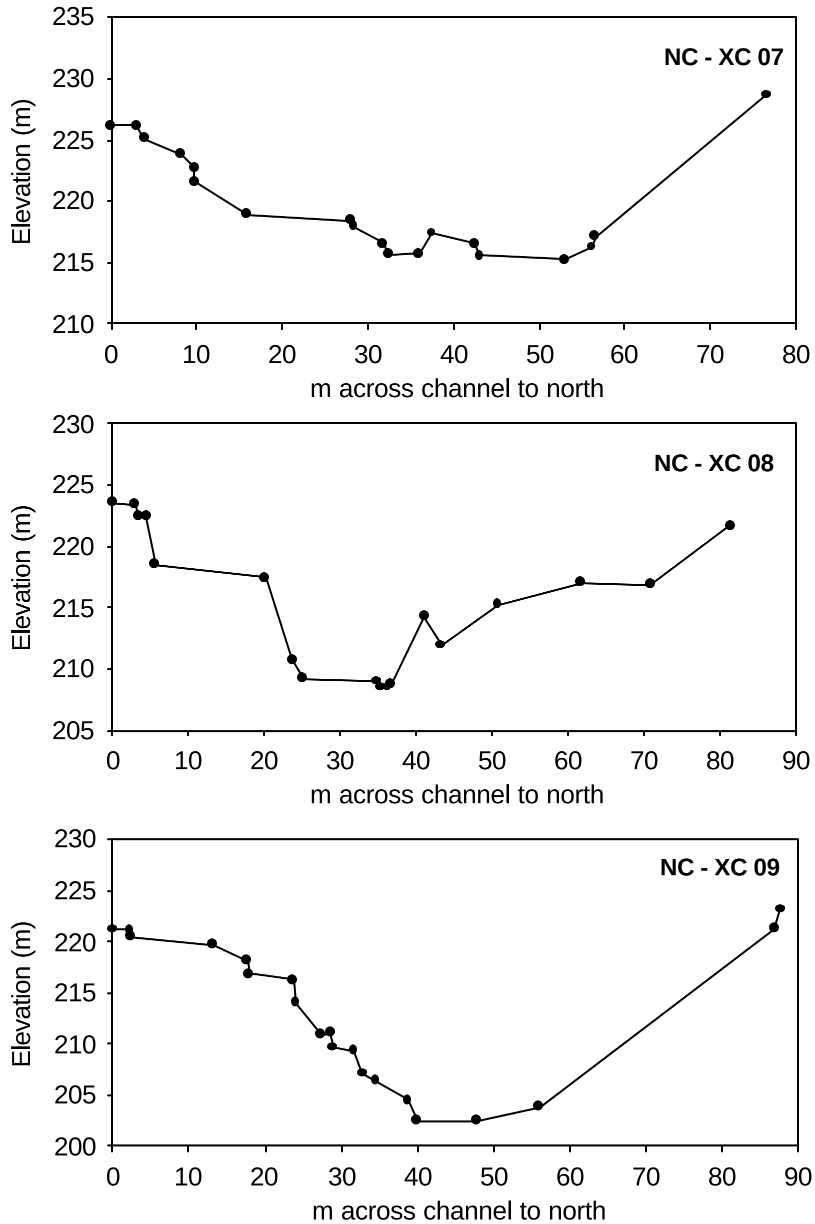

Cross-sections 7-9 of the North Channel (NC).

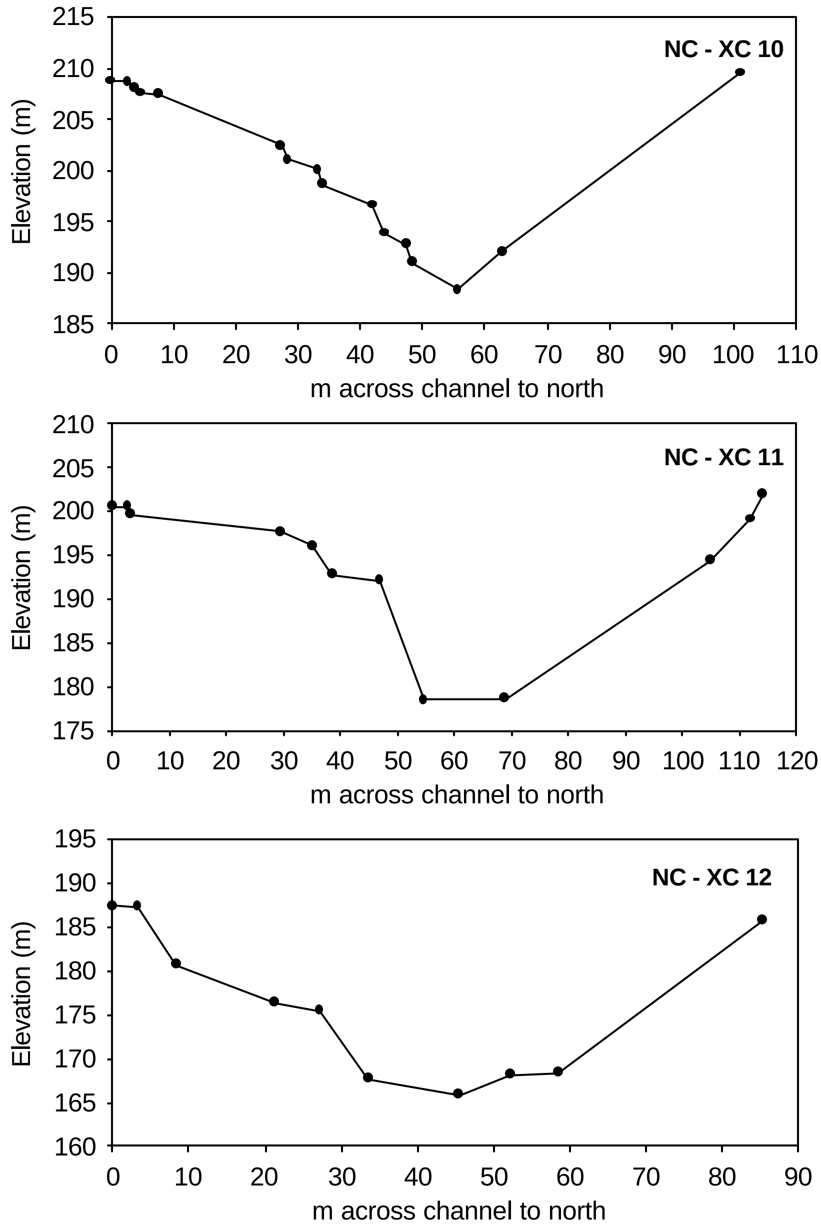

Cross-sections 10-12 of the North Channel (NC).

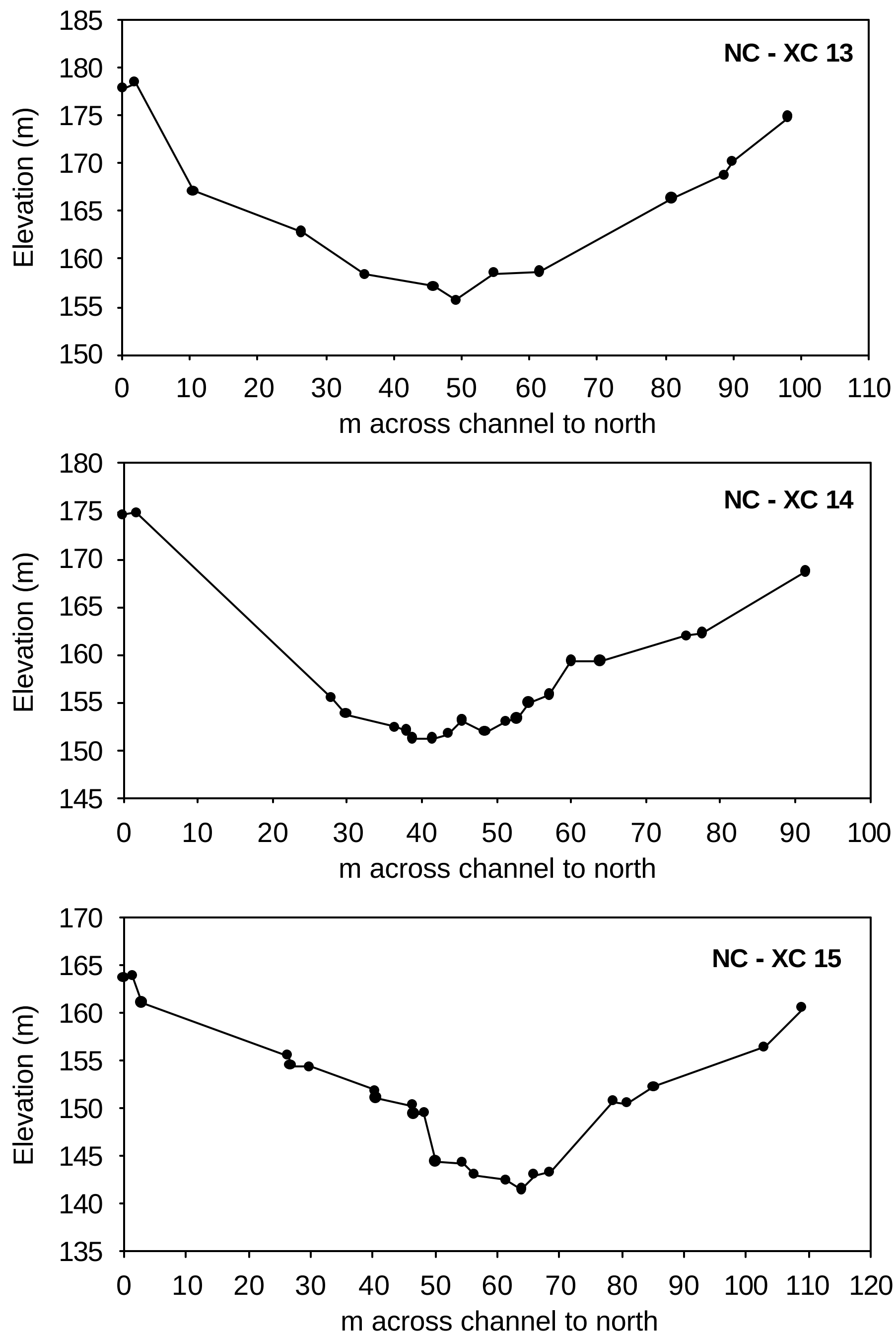

Cross-sections 13-15 of the North Channel (NC).

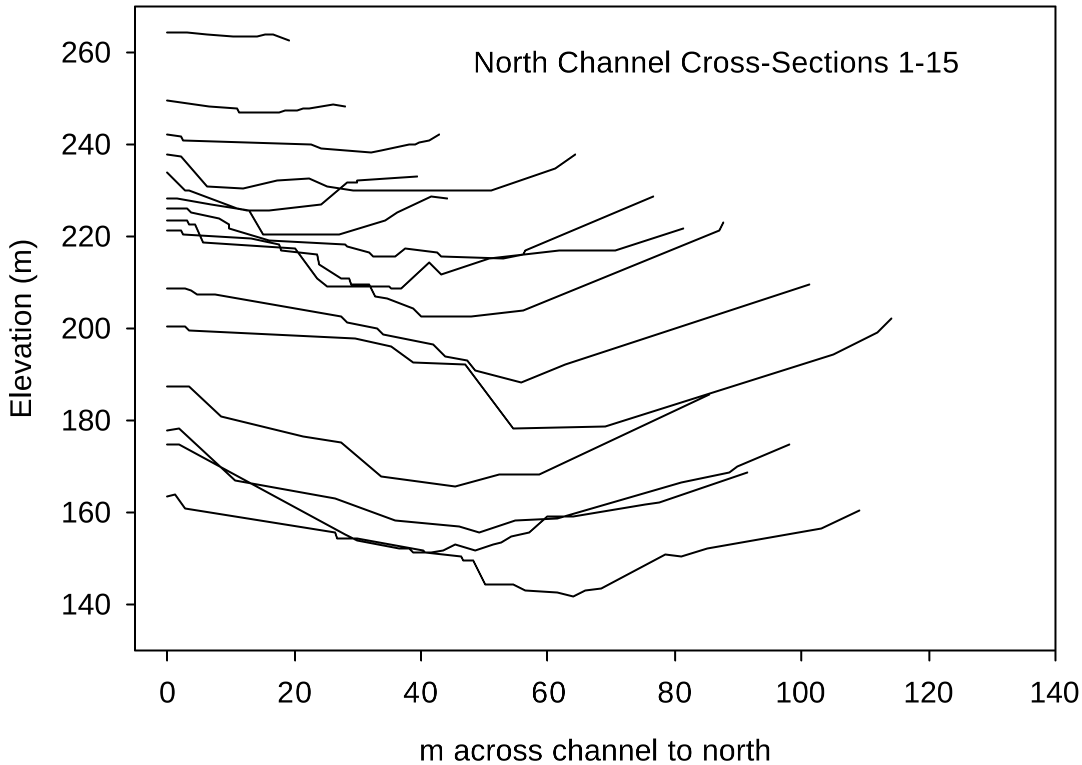

Cross-sections 1-15 of the North Channel, without any respect to distance down-glacier.

Appendix D - Ice Speed and Radar Data

Ice speed at the ablation stakes on Taylor Glacier calculated from data for November 1995 to January 1997 (LTER, 2001).

Stake	km from Stake 90	Speed (m yr^{-1})
90	0	5.28
89	1.14	5.06
88	2.10	5.56
87	3.17	4.56
86	4.21	3.44
85	5.42	7.00
84	6.95	1.50
83	7.03	6.67
82	7.19	6.86
81	7.88	7.26
80	8.68	7.16
79	9.20	6.99
91	9.79	6.37
92	10.41	4.92

Taylor Glacier bed and surface elevation data from ice radar in January 1998 (Langevin, 1998).

Stake	km from Stake 90	Bed Elevation (m)	Surface Elevation (m)
90	0		
89	1.14	278.5	503.8
88	2.10	284.0	489.1
87	3.17	272.8	467.8
86	4.21	270.5	452.0
85	5.42	185.2	393.7
84	6.95	320.9	245.1
83	7.03	69.3	335.1
82	7.19	322.5	87.1
81	7.88	-15.2	294.4
80	8.68	3.8	266.3
79	9.20	-2.9.	266.3
91	9.79	-8.9	234.2
92	10.41	66.2	148.9

Appendix E - Rate of Change in Width, Depth, and Width to Depth Ratio

The data in the following tables and graphs are from calculating the rates of change in width, depth, and the width to depth ratio of the South Channel. Rates were calculated in the South Channel because it was the more extensive survey. Rates are probably similar for the North Channel; however, the survey of that channel began much closer to the region where the channel begins to widen and deepen dramatically.

Rate of change of width in the South Channel. The stage numbers refer to the stages of development in the plot of channel width in the graphs below.

	Rate of Change in Widening						
	Width			Year			
Stage	Start (m)	Stop (m)	Difference (m)	Start (yr)	Stop (yr)	Difference (yr)	Rate (m yr^{-1})
1	3	7	4	340	450	110	0.036
2	7	12	5	450	680	230	0.022
3	12	14	2	680	1090	410	0.005
4	14	120	106	1090	1160	70	1.514
5	120	110	-10	1160	1260	100	-0.100
6	100	102	2	1260	1480	220	0.009

Rate of change of depth in the South Channel. The stage numbers refer to the stages of development in the plot of channel depth in graphs below.

	Rate of Change in Deepening						
	Width			Year			
Stage	Start (m)	Stop (m)	Difference (m)	Start (yr)	Stop (yr)	Difference (yr)	Rate (m yr^{-1})
1	0	2	2	340	1090	750	0.003
2	2	6	4	1090	1200	110	0.036
3	6	15	9	1200	1260	60	0.150
4	15	22	7	1260	1480	220	0.032

Rate of change of width to depth ratio in the South Channel. The stage numbers refer to the stages of development in the plot of channel width to depth ratio in the graphs below.

	Rate of Change in Width to Depth Ratio						
	Width:Depth			Year			
Stage	Start	Stop	Difference	Start (yr)	Stop (yr)	Difference (yr)	Rate (yr^{-1})
1	9	13	4	340	460	120	0.033
2	13	9	-4	460	680	220	-0.018
3	9	8	-1	680	1090	410	-0.002
4	8	26.5	18.5	1090	1160	70	0.264
5	26.5	6.5	-20	1160	1260	100	-0.200
6	6.5	4.5	-2	1260	1480	220	-0.009

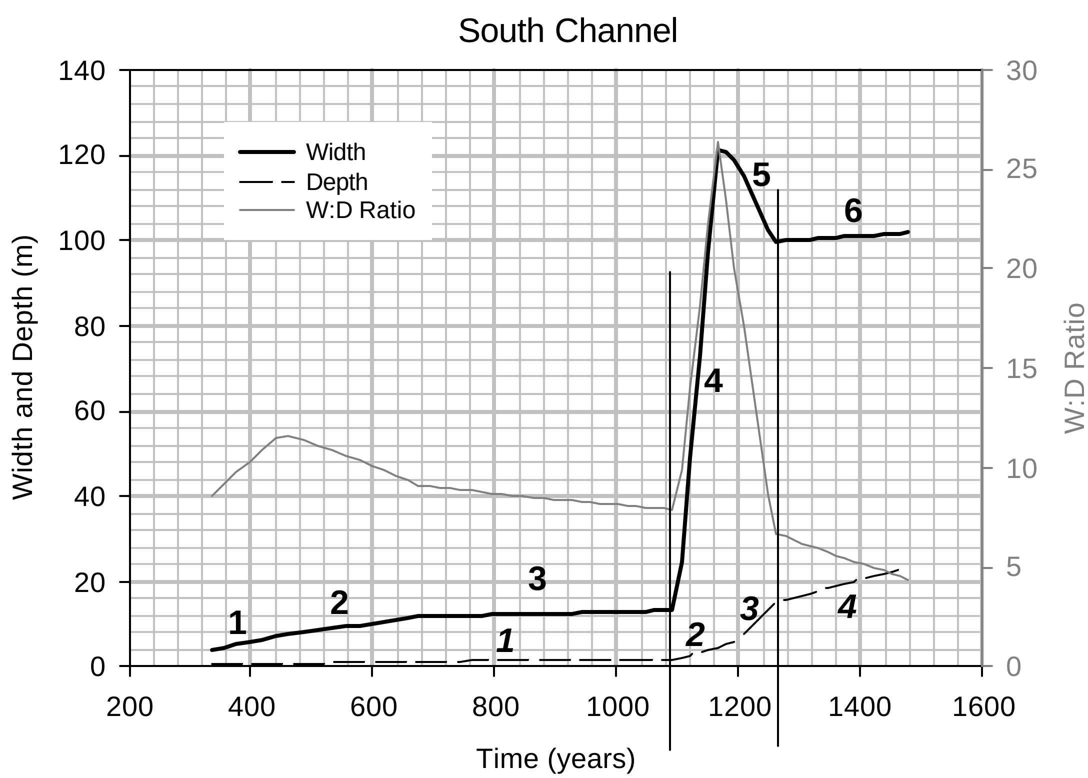

Width, depth, and width to depth ratio of the South Channel used to calculate rates of change in width and depth. The bold and italic numbers refer to stages in the tables above.

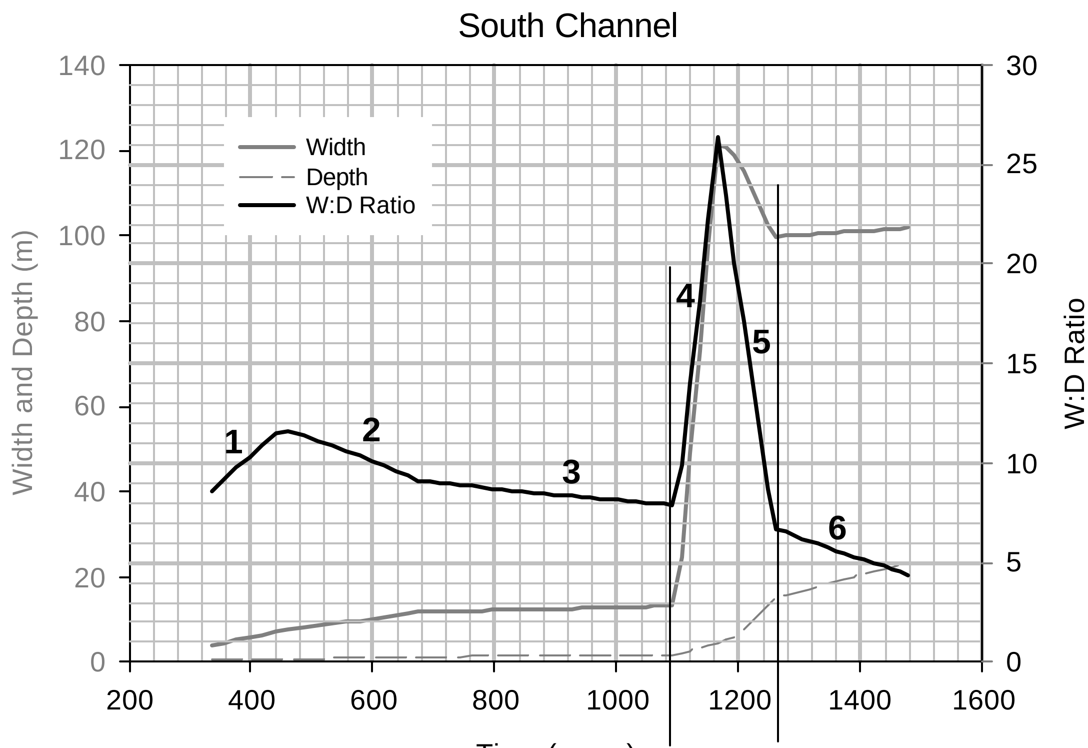

Width, depth, and width to depth ratio of the South Channel used to calculate rates of change in the width to depth ratio. The bold numbers refer to stages in the tables above.

Appendix F – Geographic Location of Stakes, Cross-Sections, and Met Station

Survey locations for ablation stakes, channel cross-sections, and the meteorological station on Taylor Glacier. Id example: 6-00 is cross-section 6 of the South Channel (surveyed in 2000) and 3-01 is cross-section 3 of the North Channel.

Id	Elevation (m)	Longitude (° E)	Longitude east from 90	Latitude (° S)	Latitude north from 90	Longitude Distance (m) from 90	Latitude. Distance (m) from 90	True Distance from 90 (m)
90	463.36	161.8416	0.0000	-77.7567	0.0000	0.00	0.00	0.00
89	450.47	161.8881	0.0465	-77.7539	0.0028	1098.92	312.67	1142.54
1-00	448.56	161.8892	0.0476	-77.7534	0.0033	1123.62	369.91	1182.94
2-00	438.43	161.9183	0.0767	-77.7519	0.0048	1811.82	535.07	1889.18
88	433.88	161.9274	0.0858	-77.7519	0.0048	2025.87	535.39	2095.42
3-00	420.58	161.9553	0.1137	-77.7490	0.0077	2684.75	857.34	2818.32
87	416.18	161.9725	0.1309	-77.7503	0.0064	3090.83	707.59	3170.79
4-00	407.66	161.9796	0.1380	-77.7466	0.0101	3260.18	1127.05	3449.50
5-00	394.38	161.9992	0.1576	-77.7447	0.0119	3724.39	1330.00	3954.74
86	400.14	162.0155	0.1739	-77.7487	0.0080	4108.65	895.12	4205.02
6-00	375.02	162.0211	0.1795	-77.7431	0.0136	4242.12	1517.58	4505.40
85	341.63	162.0608	0.2192	-77.7425	0.0142	5180.45	1585.61	5417.67
7-00	324.92	162.0761	0.2345	-77.7406	0.0161	5543.25	1796.24	5827.01
82	271.78	162.1219	0.2803	-77.7318	0.0249	6630.05	2771.24	7185.91
Met	334.13	162.1284	0.2868	-77.7402	0.0165	6778.96	1833.30	7022.48
83	278.79	162.1284	0.2868	-77.7401	0.0166	6780.36	1849.41	7028.06
84	269.02	162.1306	0.2890	-77.7452	0.0115	6828.46	1279.72	6947.34
8-00	274.81	162.1311	0.2895	-77.7381	0.0186	6844.78	2074.84	7152.34
1-01	264.50	162.1313	0.2897	-77.7342	0.0225	6850.96	2502.41	7293.67
2-01	249.46	162.1432	0.3016	-77.7331	0.0236	7133.84	2628.58	7602.70
9-00	255.72	162.1497	0.3081	-77.7371	0.0196	7284.22	2184.30	7604.67
3-01	242.12	162.1513	0.3096	-77.7324	0.0243	7324.26	2706.51	7808.33
81	243.81	162.1555	0.3139	-77.7331	0.0236	7423.52	2631.92	7876.27
10-00	245.03	162.1581	0.3165	-77.7364	0.0203	7484.26	2255.07	7816.61
4-01	237.76	162.1584	0.3168	-77.7319	0.0248	7493.30	2764.02	7986.83
5-01	233.99	162.1629	0.3213	-77.7313	0.0254	7600.90	2828.96	8110.28
6-01	228.23	162.1693	0.3277	-77.7307	0.0260	7751.87	2893.90	8274.43
7-01	226.19	162.1723	0.3307	-77.7306	0.0261	7824.07	2901.33	8344.68

Id	Elevation (m)	Longitude (° E)	Longitude east from 90	Latitude (° S)	Latitude north from 90	Longitude Distance (m) from 90	Latitude. Distance (m) from 90	True Distance from 90 (m)
11-00	225.60	162.1757	0.3341	-77.7349	0.0218	7901.89	2430.97	8267.38
8-01	223.57	162.1766	0.3350	-77.7300	0.0267	7925.04	2975.54	8465.23
9-01	221.25	162.1807	0.3391	-77.7297	0.0270	8022.59	3003.37	8566.34
80	211.58	162.1868	0.3452	-77.7304	0.0263	8166.38	2927.83	8675.37
10-01	208.75	162.1906	0.3490	-77.7290	0.0277	8258.11	3088.72	8816.84
11-01	200.54	162.1952	0.3536	-77.7288	0.0279	8366.24	3101.71	8922.70
12-01	187.41	162.2011	0.3595	-77.7281	0.0286	8505.94	3181.49	9081.46
79	180.06	162.2076	0.3660	-77.7288	0.0279	8660.54	3101.98	9199.31
13-01	177.86	162.2089	0.3673	-77.7278	0.0289	8691.91	3216.75	9268.05
12-00	180.29	162.2110	0.3694	-77.7324	0.0243	8738.47	2707.70	9148.36
14-01	174.64	162.2122	0.3706	-77.7276	0.0291	8768.58	3242.72	9348.97
15-01	163.63	162.2179	0.3763	-77.7272	0.0295	8904.91	3283.54	9491.00
13-00	149.44	162.2277	0.3861	-77.7317	0.0250	9132.60	2786.93	9548.37
91	142.82	162.2305	0.3889	-77.7266	0.0301	9204.05	3347.56	9793.91
14-00	131.32	162.2406	0.3990	-77.7307	0.0260	9439.10	2890.21	9871.67
92	95.17	162.2531	0.4115	-77.7238	0.0329	9740.37	3660.56	10405.50